The Dissertation Committee for Laurea Marie Diaz Certifies that this is the approved version of the following dissertation:

Dopamine and Ethanol Induced Trafficking of Viral Mediated eGFP Tagged Dopamine D1 Receptors in Parasagittal Explants

Committee:

Richard A. Morrisett, Supervisor

Christine L. Duvauchelle

Rueben A. Gonzales

Roy D. Mayfield

S. J. Mihic

Dopamine and Ethanol Induced Trafficking of Viral Mediated eGFP Tagged Dopamine D1 Receptors in Parasagittal Explants

by

Laurea Marie Diaz, B.S.

Dissertation

Presented to the Faculty of the Graduate School of Pharmacy

The University of Texas at Austin

in Partial Fulfillment

of the Requirements

for the Degree of

Doctor of Philosophy

The University of Texas at Austin

May 2005

Acknowledgements

I would like to acknowledge my dissertation committee members:
Dr. Richard Morrisett,
Dr. Christine Duvauchelle,
Dr. Rueben Gonzales,
Dr. R. Dayne Mayfield,
Dr. S. John Mihic

I would also like to acknowledge my fellow lab workers including but not limited to, and in no particular order:
Amanda Tang-Doyon, Billy Doyon, Donita Robinson, Jason Jaworski, Sheila Heater, Jennifer York, Rene Rodriguez, Judy Randall, Chris Olsen, Aiko Ikegami, Regina Maldve, Tao Zhang, Matthew Sullivan, Adam Hendricson, Paula Guerrero, Yunqing Han, Guadalupe Reyna, Jennifer Wilde, Jody Mayfield, Rajani Maiya, and David Galindo

I would also like to thank my family: Linda, John, Maria, Janet, Jonathan, Justin and MaKayla just to name a few, and all my friends.

My loving husband, Jason Norman, deserves more than an acknowledgment for more reasons than I can list

Dopamine and Ethanol Induced Trafficking of Viral Mediated eGFP Tagged Dopamine D1 Receptors in Parasagittal Explants

Publication No._____

Laurea Marie Diaz, Ph.D.

The University of Texas at Austin, 2005

Supervisor: Richard A. Morrisett

The mesolimbic pathway has been implicated in the rewarding effects of drugs of abuse, and an important component of this pathway is the D1 dopamine receptor (D1DR). D1DRs desensitize upon agonist stimulation by several mechanisms, including a process involving receptor clustering and internalization. This process removes post-synaptic D1DRs and may be a neuroadaptive mechanism associated with addiction to drugs of abuse, including ethanol. We measured localization of D1DRs in viable nucleus accumbens (NAcc) neurons from parasagittal explants. A sindbis RNA virus was used to mediate the expression of D1DRs containing an enhanced green fluorescent protein (eGFP) tag in these explants. The effects of dopamine and ethanol on D1DR localization were measured by changes in fluorescence intensity using two-photon laser scanning microscopy. Two-dimensional images from z-stacks of virally infected neurons displayed stable and homogenous fluorescence throughout the neuronal soma and processes. Dopamine (100 uM, 30 min) significantly enhanced the greatest increase of maximum

fluorescence intensity in distinct regions of interest (ROIs) by approximately 40% compared to control neurons in the absence of dopamine. Ethanol pretreatment significantly enhanced dopamine-induced clustering. Neurons exposed to dopamine (50 uM, 30 min) displayed receptor clustering only when pretreated with ethanol. Ethanol (50 and 100 mM, 30 min.) pretreatment followed by dopamine (50 uM, 30 min.) enhanced the greatest increase of maximum fluorescence intensity by 44±3 and 108±9%, respectively, while dopamine (50 uM, 30 min) in the absence of ethanol pretreatment showed no clustering with peak increases in maximum fluorescence intensity of only 3±2%. Ethanol (50 and 100 mM, 60 min) alone enhance the greatest increase of maximum fluorescence intensity by about 60% for both concentrations. Receptor clustering induced by dopamine, ethanol pretreatment of dopamine, or ethanol alone was partially blocked by the D1DR antagonist SCH 23390 (20 uM). These findings show that both dopamine and ethanol alter D1DR localization in NAcc neurons and suggest that a physical restructuring of D1DRs in this region may be involved in neuroadaptive mechanisms of ethanol action.

Table of Contents

List of Tables

List of Figures

Abbreviations

ACSF	artificial cerebral spinal fluid
AMP	ampicillin
AMPA	2-amino-3-hydroxy-5-methyl-4-isoxazole propionate
Avg	average
BHK	baby hamster kidney
BSA	bovine serum albumin
cAMP	cyclic adenosine 3', 5' -mono-phosphate
CHO	Chinese hamster ovary
ColE1	Colicin E1, Escherichia coli plasmid vector
D1DR	D1 dopamine receptor
DA	dopamine
DAB	3-3'-diaminobenzidine tetrahydrochloride
DEPC	diethylpyrocarbonate
DNA	deoxyribonucleic acid
EC_{50}	effective concentration of 50%
eGFP	enhanced green fluorescent protein
Etoh	ethanol
FBS	fetal bovine serum
GABA	gamma-amino butyric acid
GFP	green fluorescent protein
G-protein	guanine nucleotide protein
GPCR	G-protein coupled receptor
GRK	G-protein receptor kinase
HAD	high alcohol drinking
HC	hippocampus
HEK	human embryonic kidney
LB	luria base
Max	maximum

MEM	minimum essential medium
MPLSM	multi-photon laser scanning microscopy
NMDA	N-methyl-D-aspartate
NAcc	nucleus accumbens
nuc. free H_2O	nuclease-free water
nsP	nonstructural proteins
P	protocol
PBS	phosphate buffered saline
PFC	prefrontal cortex
PKA	protein kinase A
PKC	protein kinase C
PS	packaging signal
PSF	point spread function
P_{SG}	subgenomic promoter
R	recipe
RNA	ribonucleic acid
ROI	region of interest
SLM	single longitudinal mode
TEM_{00}	single transverse mode
TH	tyrosine hydroxylase
VTA	ventral tegmental area

Chapter 1. Introduction and Literature Review

1-1. General Introduction

Addiction is a poorly understood disorder defined as compulsive use and subsequent loss of control of drug self-administration even in the face of negative consequences (American Psychiatric Association, 1987; World Health Association, 1975). One widely accepted theory concerning the development of addiction is that drug exposure disrupts homeostasis by development of adaptive changes in neural systems which progress to a permanently altered state or allostasis of brain reward and stress responses (Koob and Le Moal, 2001). The reward threshold of addicts is, thus, altered caused by adaptations in reward and stress circuits of the addicted brain that fail to return to a homeostatic level. Many of the neural adaptations associated with addiction have not been discovered or characterized; clearly, a better understanding of these neural adaptations may lead to more effective treatments of addiction.

The mesolimbic pathway has been implicated in the rewarding actions of drugs of abuse (Wise, 1996; Koob et al., 1998). Since addiction is associated with adaptations in reward circuits, this pathway is a candidate for alterations that may lead to addiction. The mesolimbic pathway originates in the ventral tegmental area (VTA) where dopaminergic neurons project to the NAcc as well as other areas (Ungerstedt, 1971; Oades and Halliday, 1987; Van Bockstaele and Pickel, 1995; Feldman et al., 1997). Medium spiny neurons make up approximately 90% of the neurons in the NAcc (Meredith, 1999; Gonzales et al., 2004) and project back to the VTA (Walaas and Fonnum, 1980; Heimer

et al., 1991). The VTA is subdivided into anterior and posterior regions that have different cell types and neuronal connections. The posterior VTA is implicated in reward based on effects of ethanol self-administration (Rodd-Henricks et al., 2000) while the anterior VTA is involved in mediating reward through pharmacological alterations of GABA receptors (Ikemoto et al., 1997; Boehm et al., 2002). The NAcc is subdivided (Zaborszky et al., 1985) into shell and core regions with different neuronal connections (Heimer et al., 1991; Usuda et al., 1998; O'Donnell et al., 1999). The shell and core are both implicated in different aspects of addiction; however, the precise roles of either region are still unknown (for review see Gonzales et al., 2004). Another important brain region that is intertwined with the mesolimbic pathway is the prefrontal cortex. It receives dopaminergic innervation from the VTA (Albanese and Bentivoglio, 1982; Carr et al., 1999) and delivers glutamatergic input to the NAcc (Carr et al., 1999; Groenewegen et al., 1999). The prefrontal cortex is also affected by drugs of abuse; for example, the morphology of neurons in both the prefrontal cortex and NAcc has been altered by drugs of abuse (Robinson and Kolb, 1997).

In addition to morphological changes in the NAcc, drugs of abuse increased extracellular dopamine levels, and this increase in dopamine is believed to be associated with the rewarding effects of these drugs (Wise, 1996; Koob et al., 1998). The increased dopamine levels occurred by multiple mechanisms depending on the drug of abuse. For example, cocaine blocked the reuptake of dopamine into pre-synaptic terminals, thereby increasing the synaptic concentration of dopamine in the NAcc (for review see Wise, 1984). In contrast, opiates increased dopamine in the NAcc by a disinhibition of GABA-

ergic inter-neurons in the VTA (for review see Shippenberg, 1998). Ethanol may directly excite dopaminergic neurons in the VTA, resulting in an increased firing rate which then leads to enhanced dopamine release in the NAcc (Brodie et al., 1999). Also, ethanol injection enhanced extracellular dopamine levels in the NAcc (Imperato and Di Chiara, 1986), and ethanol perfusion elevated dopamine levels in rat striatum (Yim et al., 1997). Thus, drugs of abuse increased extracellular dopamine levels in the NAcc albeit by different mechanisms. Understanding adaptations that occur following enhanced dopamine levels may lead to a better understanding of drug-induced neuronal mechanisms.

Ethanol has also been shown to modulate other neurotransmitters. Extensive literature exists on the inhibition of excitatory N-methyl-D-aspartate (NMDA) receptors by ethanol (Dildy and Leslie, 1989; Hoffman et al., 1989; Lovinger et al., 1989; for review see Chandler et al., 1998). There is also extensive literature on the potentiation of gamma-amino-butyric acid (GABA) and glycine receptor function by ethanol (Celentano et al., 1988; for review see Chandler et al., 1998, for review see Mihic, 1999; for review see Davies, 2003). Ethanol has been shown to inhibit voltage-gated calcium channels (Wang et al., 1994; Widmer et al., 1998; Hendricson et al., 2003). Furthermore, ethanol alters cyclic adenosine 3',5'-mono-phosphate (cAMP)-mediated cascades via changes in adenylyl cyclase activity or other components in this cascade (Tabakoff and Hoffman, 1979; Hynie et al., 1980; Lucchi et al., 1983; Gordon et al., 1986; Maldve et al., 2002). Thus, ethanol appears to have several sites of action in the central nervous system.

The rewarding effects of ethanol are thought to be mediated by the mesolimbic dopamine pathway. In several studies, ethanol was self-administered directly into discrete areas of the VTA, demonstrating that ethanol produced rewarding effects (Gatto et al., 1994; Rodd-Henricks et al., 2000; Rodd et al., 2004). Additionally, increased dopamine levels were observed in the NAcc of rats which orally self-administered ethanol (Weiss et al., 1993). This indicates that ethanol-induced increases in dopamine levels in NAcc may underlie its rewarding effects. A consequence of increases in extracellular dopamine in the NAcc would likely be activation of native D1DRs because of the localization of these receptors in the NAcc (Hersch et al., 1995; Caille et al., 1996). Additional studies have suggested that mesolimbic D1DRs play a role in ethanol self-administration. Mice that have been genetically modified to lack D1DRs drank markedly less alcohol than their heterozygous and wild-type counterparts (El-Ghundi et al., 1998). In addition, D1DR agonists and antagonists reduced ethanol intake in rats (Dyr et al., 1993; Hodge et al., 1997). Collectively, these studies suggest that the D1DRs in the mesolimbic pathway are mediating, at least in part, the rewarding effects of ethanol.

Continued activation of D1DRs could lead to receptor desensitization, a type of neural adaptation that may be involved in addiction (Wise, 1996). Receptor desensitization is characterized by a reduced response despite continued presence of the receptor agonist (Sibley and Housley, 1994; Kallal and Benovic, 2000). The D1DR is a G-protein coupled receptor (GPCR); this family of receptors desensitize upon agonist stimulation in several ways, including internalization of the receptor (Kallal and Benovic, 2000). Interestingly, ethanol has been shown to produce changes in the surface expression of some receptors.

For example, internalization of the α1 subunit of the $GABA_A$ receptor in the cerebral cortex has been reported after chronic ethanol exposure (Kumar et al., 2003). Furthermore, hippocampal cultures exposed to ethanol for 4 days showed clustering of the NR1 subunit of the NMDA receptor with the pre-synaptic protein marker synapsin (Carpenter-Hyland et al., 2004). Internalization of receptors following chronic ethanol treatment may constitute a cellular mechanism for acute tolerance to ethanol.

Ethanol's effects on D1DR desensitization are not as well understood. Expression of D1DRs in response to chronic ethanol has been examined in several studies with varied results (Hruska, 1988; Hietala et al., 1990; Djouma and Lawrence, 2002; Quadros et al., 2002; Vasconcelos et al., 2003). A better understanding of how D1DRs desensitize after ethanol administration is needed to determine if ethanol-induced D1DR trafficking could be a mechanism involved in the acute or chronic actions of ethanol.

1-2. TWO FAMILIES OF DOPAMINE RECEPTORS

Two families of dopamine receptors (D1 and D2) were originally defined by their opposite effects on adenylyl cyclase activity (for review see Huang et al., 2001). D1DRs stimulate adenylyl cyclase and were cloned by several labs (Dearry et al., 1990; Monsma et al., 1990; Sunahara et al., 1990; Zhou et al., 1990) while D2 dopamine receptors (D2DRs) inhibit adenylyl cyclase and were also cloned by several labs (Bunzow et al., 1988; Dal Toso et al., 1989; Grandy et al., 1989b; Selbie et al., 1989; Todd et al., 1989). The human D1DR gene is located on chromosome 5 (Sunahara et al., 1990), and the human D2DR gene is located on chromosome 11 (Grandy et al., 1989a). Although these

receptors are encoded by different genes, it is hypothesized that they have a similar GPCR structure of seven hydrophobic transmembrane alpha-helices with an extracellular amino-terminal, a cytoplasmic carboxyl-terminal, and an intracellular third loop (Suryanarayana et al., 1992; for review see Bockaert and Pin, 1999). The seven transmembrane regions of D1DRs form binding sites for ligands on the extracellular side of the cellular membrane (for review see Bockaert and Pin, 1999).

The dopamine D1 family of receptors, including the human D_1 and D_5 receptor subtypes, is commonly associated with the stimulatory guanine protein (G-protein, $G_{s\alpha}$) which, acting through adenylyl cyclase, increases the synthesis of the second messenger molecule cAMP (for reviews see Kebabian and Calne, 1979; Huang et al., 2001). D1DRs may also couple to other G-proteins such as $G_{o\alpha}$ (for review see Sidhu, 1998) and $G_{z\alpha}$ (for review see Huang et al., 2001) as well as stimulate additional second-messenger pathways. For example, there is evidence of D1DR stimulated nitric oxide production (Chen et al., 2003), intracellular calcium release (Lezcano and Bergson, 2002), and arachidonic acid release (Piomelli et al., 1991). Despite these other actions, cAMP is the gold standard for characterizing D1DRs (for review see Feldman et al., 1997; Huang et al., 2001).

1-2.1. D1DR Desensitization

Since drugs of abuse, including ethanol, increase dopamine levels in the NAcc, it is likely that D1DR activation will increase as a consequence of elevated dopamine. GPCRs, including D1DRs, desensitize upon agonist stimulation in three, possibly sequential,

ways (Kallal and Benovic, 2000). Specifically, D1DRs have been shown to desensitize upon agonist stimulation by 1.) uncoupling from the G-protein (Memo et al., 1982; Ng et al., 1994), 2.) internalization of the receptor (Ng et al., 1995; Dumartin, 1998; Martin-Negrier et al., 2000) and 3.) down regulation of expression of the D1DR itself (Barton and Sibley, 1990; Gupta and Mishra, 1993). Agonist-induced desensitization is a decreased receptor-mediated response in the presence of continued agonist stimulation (for review see Sibley and Housley, 1994).

1-2.1.1. D1DR Uncoupling from the G-Protein & Desensitization

Initially, D1DR desensitization is indicated by a decrease in adenylyl cyclase activity or a decrease in cAMP production following agonist stimulation. There are many studies that support this type of desensitization. Adenylyl cyclase activity or cAMP production decreased during dopamine receptor stimulation in rat striatal slices (Memo et al., 1982), D384 cells derived from the human astrocytoma cell line G-CCM, (Balmforth et al., 1990), NS20Y neuroblastoma cells (Barton and Sibley, 1990), striatal neurons (Chneiweiss et al., 1990), COS-1 monkey cells (Steffey et al., 1991), SK-N-MC neuroblastoma cells (Zhou et al., 1991), opossum kidney cells (Bates et al., 1993), Sf9 insect cells (Ng et al., 1994) and in human embryonic kidney (HEK) cells (Tiberi et al., 1996). These decreases were associated with an uncoupling of the receptor from the G-protein.

1-2.1.2. D1DR Phosphorylation & Desensitization

Phosphorylation of GPCRs may be involved in desensitization resulting from uncoupling of the receptor with the G-protein (Anderson and Jaworski, 1979). Agonist-induced phosphorylation of D1DRs expressed in insect Sf9 cells was associated with desensitization of cAMP production (Ng et al., 1994). Similarly, phosphorylation of D1DRs preceded desensitization of cAMP production in C6 glioma cells (Gardner et al., 2001). Although cAMP desensitization has not been linked temporally with loss of D1DRs on the cell surface (Barton and Sibley, 1990; Bates et al., 1993), decreased high affinity receptor binding has been detected (Barton and Sibley, 1990). A decrease in high affinity binding is associated with receptor:G-protein uncoupling. High affinity binding is observed when the D1DR is coupled to the G-protein, and upon uncoupling, the D1DR undergoes a conformational change which reduces agonist affinity. Thus, D1DR phosphorylation decreased cAMP production which is linked to decreased high affinity binding which in turn is associated with G-protein uncoupling. The end result of phosphorylation may be uncoupling of the D1DR from the G-protein, thus beginning the desensitization process.

If D1DR phosphorylation is a mechanism for receptor:G-protein uncoupling, controversy exists concerning the kinase(s) responsible for D1DR desensitization. The particular D1DR or cell model used may contribute to this confusion, since D1DRs of different mammalian species likely possess slight differences in phosphorylation sites and different cell systems may express different kinases. Cyclic AMP-dependent protein kinases and possibly Ca^{+2} –calmodulin protein kinases were first implicated in D1DR:G-protein

uncoupling (Memo et al., 1984). The desensitization of D1DR-mediated cAMP production was shown to be protein kinase A- (PKA, a cAMP-dependent kinase) dependent in permeabilized SK-N-MC neurotumor cells (Zhou et al., 1991). However, cAMP-dependent kinases were not required for D1DR phosphorylation in subsequent studies. Opossum kidney cells transfected with the cDNA of cAMP phosphodiesterase (an enzyme that catalyzes the hydrolysis of phosphodiester bonds in cAMP) surprisingly had no effect on the desensitization of cAMP production, suggesting that the accumulation of cAMP and thereby activation of cAMP-dependent kinases did not affect desensitization of cAMP production (Bates et al., 1993). PKA or protein kinase C (PKC) did not appear to mediate the phosphorylation of D1DRs in C6 cells, as activators of these enzymes had no effect on D1DR phosphorylation (Gardner et al., 2001). G-protein-coupled receptor kinases (GRKs) caused direct phosphorylation of the D1DRs in HEK cells as the overexpression of both D1DRs and GRKs led to rapid desensitization of cAMP production (Tiberi et al., 1996).

Additional studies involving mutations of the D1DR phosphorylation sites have aided in clarifying the role of phosphorylation in desensitization of cAMP production. PKA is at least partially responsible for D1DR desensitization, since a point mutation in the third cytoplasmic loop (T268), a phosphorylation site for PKA, reduced agonist-induced desensitization (Jiang and Sibley, 1999). Phosphorylation of the D1DR by GRK also appears to be important for desensitization, since a mutation of the GRK phosphorylation site on the carboxyl tail (T360) abolished agonist-induced desensitization (Lamey et al.,

2002). Mutation studies also indicate that phosphorylation may be required for D1DR internalization, another form of GPCR desensitization, discussed in the next section.

1-2.1.3. D1DR Internalization & Desensitization

D1DR internalization, a cellular mechanism of desensitization (Kallal and Benovic, 2000), is caused by endocytosis from the cell membrane and results in clustering of receptors away from the cell surface (Ariano et al., 1997). The localization of receptor clusters can indicate different states. For example, receptors clustered on the cell surface usually indicate sensitization. Conversely, if receptors cluster away from the cell surface, inaccessible to ligands, this often indicates desensitization.

Internalization of D1DRs can be investigated by immunohistochemical techniques and binding studies of carefully prepared membrane preparations. Immunohistochemical detection of receptors has proven to be a valuable method for receptor localization studies; this technique gives an additional method for observing changes in receptor localization rather than relying solely on binding experiments which may not conclusively demonstrate which form of desensitization is occurring (internalization versus down-regulation of expression). Ng and colleagues (1994) reported that diffuse staining of immunohistochemically detected D1DRs became more punctate following dopamine stimulation in Sf9 cells. The punctate nature of staining, or clustering, was thought to represent the sequestration of receptors from the cell surface by endocytosis. This sequestration was blocked by the D1DR antagonist SCH 23390 (Ng et al., 1994). In another study, these investigators reported that internalization of the D1DR, but not

adenylyl cyclase activity desensitization, was blocked by concanavalin A or sucrose pretreatment (Ng et al., 1995). Others have demonstrated that similar treatments inhibit the internalization of the archetype GPCR, the β-adrenergic receptor (Yu et al., 1993). Blocking the internalization of D1DRs in C6 glioma cells by sucrose or concanavalin A did not inhibit dephosphorylation, suggesting that internalization is not required for dephosphorylation of the receptor (Gardner et al., 2001). Ariano et al. (1997) demonstrated a loss of D1DR immunofluorescence after dopamine stimulation in CHO cells, primary striatal cell cultures, and striatal slice preparations which was blocked by the dopamine receptor antagonists butaclamol or SCH 23390. In the same study, direct evidence of membrane endocytosis was observed by FM1-43 incorporation of the lipid bilayer into endocytosed vesicles following dopamine stimulation, suggesting D1DR internalization. A redistribution of immunostained D1DRs upon the dopamine agonist SKF 82958 stimulation for 1 hour was observed in fixed primary dissociated striatal cells by Martin-Negrier and colleagues (2000). That study indicated that dendritic D1DRs internalized, and this process was reversed 7 hours after agonist removal and was blocked by the D1DR antagonist SCH 23390. Conversely, D1DRs expressed in axons may have shown clustering on the cell surface upon activation by SKF 82958 (Martin-Negrier et al., 2000). Another lab assessed *in vivo* treatment with SKF 82958 or amphetamine and observed internalization of D1DRs in cell bodies and dendrites of striatal neurons, and injections of SCH 23390 blocked this internalization as detected by electron microscopy (Dumartin et al., 1998). Finally, D1DR internalization was observed after application of the dopamine precursor, L-Dopa, by immunocytochemistry; however, ropinirole, a dopamine partial agonist, did not cause internalization (Muriel et al., 2002). Therefore,

multiple labs have demonstrated that D1DRs undergo internalization, and this process can be inhibited with D1DR antagonists or by inhibition of endocytosis.

The role of phosphorylation in D1DR desensitization by internalization was clarified recently when a model for a step-wise phosphorylation of the D1DR was proposed (Kim et al., 2004a). In HEK cells, phosphorylation appears to occur first in the carboxyl terminus and then in the third cytoplasmic loop. This step-wise phosphorylation allows for conformational changes of the D1DR, allowing arrestin to bind to the receptor, thereby causing endocytosis or internalization of the receptor (Kim et al., 2004a). Arrestin functions as a scaffolding protein associated with endocytosis of GPCRs (Zhang et al., 1996b). Other studies have supported this model. Truncation of the D1DR carboxyl tail at amino acid 351 resulted in a loss of dopamine-induced internalization to a perinuclear membrane of HEK cells; however, this mutation still desensitized the activation of adenylyl cyclase (Jackson et al., 2002). Mutations in the distal carboxyl tail failed to induce internalization of the D1DR but did decrease cAMP levels upon agonist exposure in CHO cells (Lamey et al., 2002). These studies demonstrate a requirement for phosphorylations at different locations on the D1DR as a mechanism for internalization as proposed in the model from the Sibley lab, whereas multiple phosphorylations are not required for desensitization associated with receptor:G-protein uncoupling.

Numerous radioligand binding studies have sought to determine the types of dopaminergic agonists required for D1DR desensitization. In NS20Y cells, the maximum loss of dopamine receptors on the cell surface, determined by [^{3}H] SCH 23390 binding

on membrane preparations, was observed after 3 hours of stimulation by the agonist dopamine (Barton and Sibley, 1990). Similarly, more than 1 hour exposure of either dopamine or the full D1DR agonist, SKF 82958, resulted in equivalent losses of antagonist binding in SK-N-MC cells, while the partial D1DR agonist, SKF 38393, resulted in less desensitization than a full agonist in these cells (Zhou et al., 1991). The D1DR antagonist, SCH 23390 had no effect on D1DR binding but blocked the effects of dopamine (Zhou et al., 1991). Therefore, it appears that maximal loss of D1DR binding from plasma membranes depended on receptor activation by full agonists, while partial agonists were less effective and antagonists were ineffective at causing a loss of receptor binding on the cell surface. Depending on the type of membrane preparation studied, it can be difficult to differentiate between internalization of the receptor vs. down-regulation of its expression since both forms of desensitization result in a decrease in surface binding.

Other forms of stimulation not involving direct receptor activation also appear to induce D1DR desensitization measured by loss of plasma membrane binding. Pretreatment of NS20Y cells with CPT-cAMP, a membrane permeable analog of cAMP, decreased receptor binding on plasma membranes in a dose-dependent manner, while the cAMP antagonist, RP-cAMPS, blocked this effect (Black et al., 1994). Sibley and colleagues have also shown that CPT-cAMP desensitization of adenylyl cyclase activity was maximally and temporally different from the CPT-cAMP induced decrease in D1DR binding. Furthermore, a decrease in high affinity D1DR binding closely matched that of reduced adenylyl cyclase activity. These findings demonstrate that direct receptor

activation is not required for D1DR desensitization and provide further evidence that the uncoupling of receptor and G-protein, and not D1DR internalization. is the cause of decreased cAMP production (Black et al., 1994).

1-2.1.4. D1DR Down-regulation & Desensitization

A long-term form of desensitization is down-regulation of protein expression (Kallal and Benovic, 2000). As discussed previously, it is often difficult to distinguish down-regulation of expression from internalization in binding studies since both mechanisms result in decreased cell surface binding. Internalization may thus be mistaken as down-regulation.

There appears to be a time factor in agonist stimulation that determines whether the form of desensitization is internalization of the receptor or down-regulation of receptor expression. If protein synthesis was required, as observed with longer duration (3 hour) of receptor activation, new receptors were likely synthesized, thereby suggesting an initial down-regulation of receptor expression. If protein synthesis was not required, as observed with shorter periods (30 minutes) of stimulation, internalization of receptors likely occurred, and receptors will return to basal levels by re-insertion into the plasma membrane. Thus, a return to basal receptor levels and the requirement of protein synthesis clarifies which form of desensitization has taken place (Barton and Sibley, 1990). Long exposure (72 hours) to dopamine or SKF 38393 decreased D1DRs as measured by homogenated tissue binding and also decreased a portion of the heterotrimeric stimulatory G-protein, $G_{s\alpha}$ as measured by Western blot analysis (Gupta

and Mishra, 1993). These studies indicate that prolonged D1DR activation may produce down regulation not only in receptor expression, but also in the stimulatory G-protein subunit associated with transduction of the D1DR.

In summary, stimulation of D1DRs by the naturally occurring agonist dopamine and other dopaminergic agonists such as SKF 82958 results in desensitization of the receptor. Different mechanisms of desensitization are possible, including uncoupling of the receptor from the G-protein, internalization of the receptor, or down-regulation of receptor expression. I propose that dopamine and ethanol will induce desensitization of D1DRs via the mechanism of receptor internalization. The D1DR is an important component in the mesolimbic pathway (Hersch et al., 1995; Caille et al., 1996), and this pathway is associated with the rewarding actions of ethanol (Wise, 1996; Koob et al., 1998). Therefore, desensitization of D1DRs may be involved in the cellular mechanisms of ethanol abuse and addiction.

1-3. VIRAL MEDIATED GENE TRANSFER

I hypothesize that D1DR desensitization by internalization is a neural adaptation that occurs in ethanol abuse. To test this hypothesis, I will use viral-mediated gene transfer of the D1DR containing a fluorescent marker, eGFP (eGFP-D1DR), to provide a method for monitoring D1DR trafficking in intact neurons of the NAcc. The sindbis virus has been used successfully to transfect neural preparations with proteins of interest (D'Apuzzo et al., 2001; Diaz et al., 2004; Ehrengruber et al., 1999; Jeromin et al., 2003; Kim et al., 2004a; Shi et al., 1999; Xiong et al., 1989). The sindbis pseudovirus has been used to

induce expression of eGFP-D1DR in several neuronal preparations, including dissociated cells, explants, and *in vivo* (Diaz et al., 2004).

The transfection of post-mitotic neurons has been accomplished using a variety of viral expression systems, including adenovirus (Le Gal La Salle et al., 1993), adeno-associated virus (Xiao et al., 1997), and herpes simplex virus (Casaccia-Bonnefil et al., 1993; Neumaier et al., 2002). However, the sindbis virus was chosen for these experiments since the viral constructs are quite selective for neurons compared to glia (Gwag et al., 1998). Additionally, the time course of infection is rapid, with significant transfection levels in one to three days.

1-3.1. Naturally Occurring Sindbis Virus

Sindbis is considered an arbovirus, or arthropod-borne virus. The World Health Organization in 1967 defined arboviruses as

> "viruses which are maintained in nature principally, or to an important extent, through biological transmission between susceptible vertebrate hosts by haematophagous arthropods; they multiply and produce viremia in the vertebrates, multiply in the tissues of arthropods, and are passed on to new vertebrates by the bites of arthropods after a period of intrinsic incubation."

Virus-infected vertebrates have varying responses from no significant infection to encephalitis and death (Schlesinger and Schlesinger, 2001).

The sindbis virus belongs in the genus alphavirus of the family of *Togaviridae* (Schlesinger and Schlesinger, 2001). The sindbis virus is closely related to another

alphavirus in structure and infectivity, the semliki forest viruses. The original strain, AR339, of the sindbis virus was collected from mosquitoes near Sindbis, Egypt in 1952 (Taylor et al., 1955). The alphavirus genome is comprised of a single strand (Strauss et al., 1968) of positive-sense RNA, capped at the 5' terminus and polyadenylated at the 3' terminus (Schlesinger and Schlesinger, 2001). The RNA strand is encapsulated by an icosahedral (20-sided) homomeric assembly of 240 molecules of capsid protein which is enveloped upon host cell budding by a lipid bilayer, producing a virion of a total diameter of approximately 70 nm (Schlesinger and Schlesinger, 2001; Ehrengruber, 2002). The viral RNA products are differentiated on the basis of the sedimentation coefficient of two resulting RNA strands: the 49S RNA (which is the total genomic RNA) and the subgenomic 26S RNA fraction (which encodes the structural genes of the virus).

Projecting through the lipid bilayer of the virus are glycoprotein spikes made of 80 trimers consisting of three heterodimers of E1and E2 glycoproteins (Schlesinger and Schlesinger, 2001; Ehrengruber, 2002). These glycoprotein spikes participate in infection as well as viral budding. Alphaviruses infect cells through binding of cell surface receptors in the major histocompatibility class I molecules such as laminin (for review see Marsh and Helenius, 1989). The glycoprotein E2 is most likely the protein which attaches the virus to the host cell by interactions with laminin. Evidence for this is based on mutations in the E2 protein, which were defective in binding to chicken embryo fibroblasts yet showed normal assembly and release (Dubuisson and Rice, 1993). Endocytosis is the general method of host cell entry by alphaviruses (for review see Marsh and Helenius, 1989).

Upon entry into the host cell, the genomic RNA acts both as messenger RNA for the nonstructural proteins and also as a template for both negative stranded RNA for structural proteins as well as additional positive stranded RNA(Schlesinger and Schlesinger, 2001). The messenger RNA is translated as a single polyprotein for the first two-thirds of the genome. This polyprotein is cleaved to give rise to the nonstructural genes nsP1, nsP2, nsP3 and nsP4. The final one-third of the genome is also translated into a structural polyprotein consisting of capsid-P62-6K-E1.

The nonstructural protein genes (nsP1-4) act as replication enzymes. nsP1 plays a role in the synthesis of negative stranded RNA (Wang et al., 1991) and is also important in the methylation of the 5' terminal cap structure on genomic RNA (Mi et al., 1989; Ahola and Kaariainen, 1995). nsP2, found in high concentrations in the nucleus (Peranen et al., 1990), is implicated in the regulation of negative stranded RNA (Sawicki and Sawicki, 1993), in subgenomic RNA synthesis (Suopanki et al., 1998), and proteolytic processes of the nsPs (Ding and Schlesinger, 1989). nsP3, acting as a phosphoprotein, is implicated in positive stranded RNA synthesis and as a negative stranded RNA replicase (De et al., 2003). nsP4 is believed to be important for RNA polymerase (Li and Stollar, 2004).

There is a proposed model for the RNA synthesis mechanism through nonstructural proteins and polyproteins (Lemm et al., 1994). The nsPs are translated as polyproteins nsP1234 and nsP123. These polyproteins include all 4 proteins sequentially or nsP1-3 depending on an in-frame opal codon better known as the UGA stop codon. nsP1234 is

cleaved to nsP123 and nsP4. These two proteins then form a complex which is implicated in initiating negative-strand RNA synthesis. A positive-strand RNA is also synthesized with an nsP123-nsP4 complex, although inefficiently. nsP123 is later cleaved to nsP1, nsP2 and nsP3. The cleavage halts negative strand RNA synthesis, although in conjunction with host cell factors the four separated nonstructural proteins can synthesize positive strand RNA and subgenomic or structural gene RNA. This model explains the low level of negative strand RNA because nsP123 does not recombine to make more negative strand RNA; therefore new protein synthesis is required for more negative strand RNA synthesis.

Structural proteins, encoded in subgenomic 26S RNA, are produced quickly within 2-3 hours after infection (Schlesinger and Schlesinger, 2001). A polyprotein that includes the capsid- p62- 6K- E1 is translated; however, the capsid is cleaved early in synthesis. Once the capsid is removed, the remaining polyprotein, p62- 6K- E1, is shuttled by the host cell to the endoplasmic reticulum where oligosaccharides are attached. The polyprotein then continues through to an intermediate compartment where palmitoylation occurs. In the Golgi complex, host oligosaccharides are further altered. These oligosaccharides are important for glycoprotein spike formation. p62 is cleaved to form E2 (Schlesinger and Schlesinger, 1972) and E3 in the trans-Golgi vesicle. The rest of the polyprotein is cleaved by host cell enzymes at differing areas along the path to the cell membrane, depending on the host cell.

The virion assembles after structural protein synthesis (Schlesinger and Schlesinger, 2001). Initially, a portion of the nsP1 RNA binds to the capsid protein (Weiss et al., 1994). Pre-formed nucleocapsids then interact with the host cell plasma membrane where viral glycoproteins are present. Additional viral glycoproteins then diffuse to the plasma membrane, bind to the capsid, and induce the membrane to round, forming the capsid with the membrane and finally fusing, thus releasing the newly formed virion. The 6K protein appears to be important but not required in virion budding since mutations of this gene only result in a decreased amount of released virus from BHK cells (Schlesinger et al., 1993).

1-3.2. Sindbis Expression Vector System

The sindbis two-vector expression system was originally commercially available from Invitrogen (Carlsbad, CA cat # K750-01). One vector encodes the same non-structural replicase genes (nsP1-4) as well as a gene of interest, and another vector encodes the structural genes (capsid- p62- 6K- E1) for the virus (Liljestrom and Garoff, 1991; Bredenbeek et al., 1993). The sindbis pseudo-virus expression system results in a similar virion as the naturally occurring sindbis virus with a lipid bilayer and capsid. Naturally occurring sindbis is different in that a single RNA strand encodes for the nonstructural genes and for the subgenomic structural genes. The separation of the genomic information into two vectors allows a gene of interest to be included into the subgenomic pseudo-virus system, thus enabling synthesis of high levels of the protein of interest and better control of infectivity. The infectivity is controlled because the structural gene RNA is not repackaged into the virion. The helper vector, which encodes the structural genes,

does not have a packing signal (PS), thus constituting a pseudoviral system that ensures no new structural genes are made after the first infection.

Naturally Occurring Sindbis

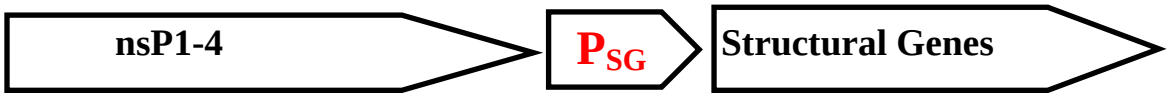

pSinRep5 Sindbis Expression System Vector

DH(26)S Sindbis Expression System Vector

Figure 1-1. Illustration of genetic information in naturally occurring sindbis as well as the vectors used in the sindbis expression system pSinRep5 and DH(26)S. Non-structural protein genes 1-4 (nsP1-4) are encoded in naturally occurring sindbis and in the pSinRep5 vector. Structural Genes are encoded in naturally occurring sindbis and in DH(26)S. All three vectors encode a subgenomic promoter (P_{SG}). pSinRep5 and DH(26)S both encode ampicillin (AMP) resistance, bacterial uptake information (ColE1), and the Sp6 promoter. pSinRep5 only encodes the packaging signal needed for virions made by the sindbis expression system to include this vector so that a gene of interest can be expressed. See Tables 1-1. through 1-3. for further description of genetic information.

1-3.2.1. pSinRep5 Vector

The vector for sindbis that encodes the nonstructural genes and the gene of interest is designated pSinRep5 (Bredenbeek et al., 1993); it contains 9951 nucleotides without the gene of interest. This vector has several important genetic areas as indicated in Table 1-1:

Table 1-1. pSinRep5 Genetic Information

Genetic Area	**Approximate bp Encoding the Genetic Area**	**Purpose of Genetic Area**
Packaging signal (PS)	(1-60)	allows for packaging into the capsid to form pseudo-virions
nonstructural protein genes 1- 4 (nsP1-4)	(60-7598)	encodes replicase proteins used for *in vivo* replication of recombinant and subgenomic RNA
subgenomic promoter (P_{SG})	(7580-7603)	allows the transcription of the gene of interest
Cloning sites (6)	(7647-7689)	where insertion of a gene of interest is designed after the subgenomic promoter
poly-A sequence	(7997-8033)	stabilizes the RNA
linear restriction sites (3)	(8047-8067)	cleavage sites present where the vector is linearized for *in vitro* transcription; the enzyme used should cut the vector only in this position
Ampicillin resistance gene (AMP)	(8227-9085)	gene so that the vector can be *selectively* mass produced in bacteria
ColE1	(9232-9861)	origin for high copy replication in bacteria
Sp6 promoter region (Sp6)	(9933-9951)	promoter allows for the transcription of the linearized vector

1-3.2.2. Helper Vectors

DH(26)S is a defective helper vector that encodes for structural proteins (Bredenbeek et al., 1993). This vector is 8189 nucleotides. The E1 and E2 glycoproteins of the defective helper DH(26)S are derived from a neurovirulent form of sindbis and are more selective for neurons than glia (Gwag et al., 1998). This helper vector also has several important genetic areas similar to pSinRep5 but is different in that it encodes structural proteins but not a packaging signal or any non-structural proteins.

Table 1-2. DH(26)S Genetic Information

Genetic Area	**Approximate bp Encoding the Genetic Area**
subgenomic promoter (P_{SG})	(2073-2096)
structural genes 1-4 capsid p62 (E2 & E3) 6K hydrophobic 6kD protein E1 glycoproteins	(2140-5874) (2140-2931) (2932-3123) (4393-4557) (4558-5874)
poly-A sequence	(6197-6233)
Ampicillin resistance gene (AMP)	(6465-7323)
Co1E1	(7470-8099)
Sp6 promoter (Sp6)	(8171-8189)

DH-BB is another helper vector encoding structural genes that form the capsid and other structural elements of the virion (Bredenbeek et al., 1993). DH-BB is so named because it is a defective helper made using restriction enzymes BspMII and Bam HI. This vector contains 6729 nucleotides. It does not contain packaging signals (unlike pSinRep5), so structural genes are not packaged to form a second round of virions. This ensures only one round of infection since there will theoretically be no capsids, glycoproteins, or any other structural genes present after the initial infection.

Table 1-3. DH-BB Genetic Information.

Genetic Area	**Approximate bp Encoding the Genetic Area**
subgenomic promoter (P_{SG})	(671-694)
structural genes 1-4	(738-4472)
capsid	(738-1528)
p62 (E2 & E3)	(1530-2990)
6K a hydrophobic membrane protein	(2991-3155)
E1	(3456-4472)
poly-A sequence	(4795-4831)
ampicillin resistance gene (AMP)	(5005-5863)
Co1E1	(6010-6639)
Sp6 promoter (Sp6)	(6711-6729)

1-4. MULTI-PHOTON LASER SCANNING MICROSCOPY

For this project, the eGFP-tagged D1DR that is transfected using the sindbis pseudovirus was localized by multi-photon laser scanning microscopy (MPLSM). This technique allows for live-cell, real-time imaging of native neurons which is critical for localizing proteins such as receptors for trafficking (Denk and Svododa, 1997). MPLSM offers an advantageous method for detecting D1DR desensitization by clustering and internalization in the presence of dopamine and ethanol stimulation.

Other forms of microscopy, such as light, electron and confocal, have limitations (Denk and Svododa, 1997) that make these techniques inadequate for testing the hypothesis of this dissertation. Although light microscopy can be used on living tissue with little photo-damage, light scattering caused by tissue inhomogeneities degrades the resolution and contrast of light detection. Additionally, the methods used to mark proteins of interest, such as the D1DR, often require fixation of the tissue, leaving the tissue no longer viable when using light microscopy. Electron microscopy, although ideal for definitive protein localization, requires fixation of the tissue, thereby live cell, real-time imaging cannot be completed. Confocal microscopy has higher depth of tissue penetration compared to light microscopy, but light scattering is still an issue. In fact, light scattering for confocal microscopy leads to additional photo-damage of not only the tissue but the fluorophore, referred to as photo-bleaching. Photo-damage is a significant problem in confocal microscopy; excitation outside of the detection focal plane is not only wasteful but causes photo-damage of both the fluorophore and tissue.

There are several major advantages to multi-photon laser scanning microscopy, in particular when compared to its single-photon excitation counterpart, confocal laser scanning microscopy (Nakamura, 1999). First, the volume of excitation is very small in multi-photon excitation since the probability of two photon absorption is proportional to the quadratic of the intensity of the excitation field. The decreased volume of excitation allows not only for decreased bleaching of fluorophores but also an optical sectioning effect when coupled with raster scanning. Second, there is a reduction of light scattering within a sample with multi-photon excitation since the wavelength of the pulsed laser is approximately twice as long as the single photon wavelength, thereby decreasing Rayleigh scattering effects, resulting in more efficient excitation, and also causing less photo-damage. Third, a deeper penetration of the laser into biological samples is possible due to the near-infrared laser wavelength (which has decreased electron transition and molecular vibration absorption) and greater peak power levels.

There are few disadvantages to multi-photon versus confocal microscopy. One major concern is the price of multi-photon lasers; although with more market competition spurred by scientific demand, price may not be a problem in the future. Another concern is the difficulty to scan multiple wavelengths in the same specimen. This makes MPLSM not useful for imaging double-labeled tissue. Not only are the excitation spectra wider for multi-photon excitation (causing spectral overlap for many fluorophores) but sequential, repeated retuning of the laser is difficult if the same laser properties are to be maintained. Finally, despite the fact that there is less out-of-focus emission in multi-photon excitation, the resolution is not greater than confocal microscopy (Nakamura, 1999). Resolution is

often defined through the point spread function (PSF) which is inversely proportional to the wavelength of excitation. Therefore, the shorter the wavelength, the better the resolution, and multi-photon excitation utilizes longer wavelengths than confocal excitation.

The use of two-photon laser scanning microscopy has been more than 50 years in the making. This technique is only recently made possible by advances in technology though it has long been hypothesized. The theory for multi-photon excitation was first described in the dissertation of Maria Göppert-Mayer in 1931 (for review see Masters and So, 2004). Interestingly, in 1963 Maria Göppert-Mayer would receive a Nobel Prize in a different field for the development of the nuclear shell model. In her dissertation Dr. Göppert-Mayer described two-photon absorption and emission (Masters and So, 2004). In one-photon excitation, as shown in the Jablonski Energy diagram in Figure 1-2, a photon excites an electron from the ground state to an excited state. This electron then relaxes to a lower energy state, releasing the energy received from the incident photon as a different photon of fluorescence. In one-photon excitation the excitation wavelength is always longer then the emission wavelength because there is energy lost between electronic vibrational states as indicated by the small dashed lines in Figure 1-2. For two-photon absorption the first photon excites an electron from the ground state to a virtual state. The second photon must excite the electron from that virtual state to the excited state before the electron returns to the ground state. Absorption by the second photon must therefore happen on the order of femto-seconds. With the low probability of two photons completing this excitation, a high intensity light is required. In fact, Dr. Göppert-

Mayer derived that the probability of two-photon absorption is quadratically related to the excitation light intensity; therefore, multi-photon fluorescence is a nonlinear optical process.

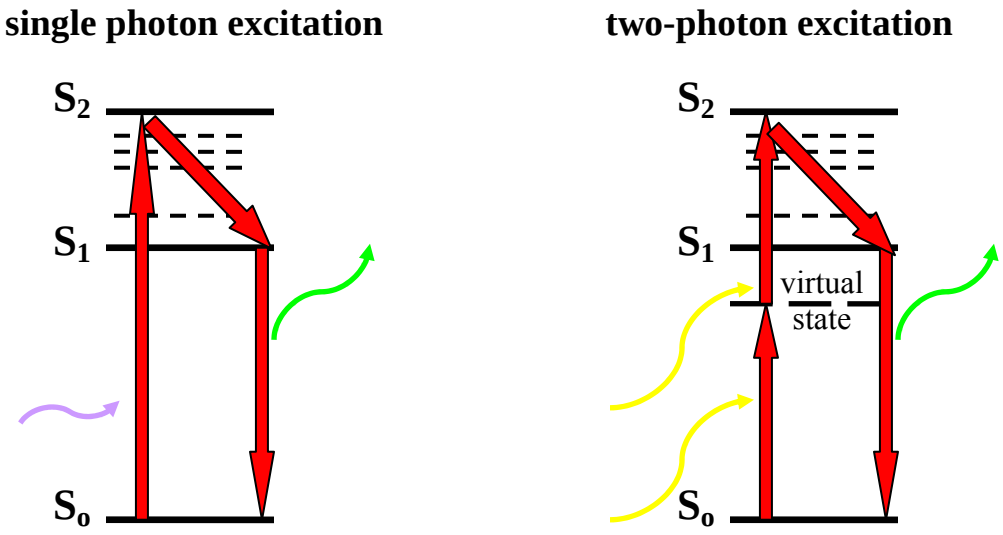

Figure 1-2. Jablonski energy diagram for single photon excitation and two-photon excitation. Curved arrows are photons, different colors represent different wavelengths. The red arrows are changes in electron energy state, S_0 is the ground state while S_1 and S_2 are excited singlet states. The small dashed lines in between singlet states are electron excited vibrational states. Excited rotational energy states are not pictured. A virtual state is reached before a second photon can excite the electron in the two-photon scheme.

Lasers are an intrinsic element of multi-photon excitation, particularly with the requirement for a high intensity light. Laser is an acronym for light amplification by the stimulated emission of radiation (Maiman, 1960; Hitz et al., 2001). All lasers have three things in common, they are: 1) monochromatic, 2) collimated and 3) coherent (Hitz et al., 2001). Monochromatic refers to the fact that all the lasing photons have the same wavelength and are thus the same color. Collimation describes the directional nature of the beam due to the low rate of expansion. Finally, coherence, which requires the laser to be both monochromatic and collimated, refers to phase matching of all photons, the alignment of the crests and troughs of the waves.

Several basic components make up the laser itself, which can also be considered an optical oscillator or an optical amplifier with partial positive feedback (Hitz et al., 2001). The most important component is the lasing material. This material must undergo population inversion which is the change in the electronic energy state in the lasing medium. When a photon of the proper frequency passes near an electron in the excited state contained within the lasing medium, this photon induces the electron to drop from a higher excited state to emit a photon. The emitted photon induces the same energy drop of an additional electron causing a cascade of electron drops and photon emissions. The device that provides the energy source that initiates this process is the pump, another key component of a laser. The pump excites the lasing medium causing a population inversion. Mirrors, a third key component of the laser, are placed on either side of the lasing cavity, allowing this cascade of photons and electrons to continue. The final

component of a laser is an output coupler. This component is usually a mirror, modified to allow a small portion of the emission to exit the lasing cavity.

The first laser was built in 1960 by Maiman (Maiman, 1960). His short two page report would impact many fields, from electronics to medicine. Maiman has been nominated twice for the Nobel Prize and has also won the Asian equivalent to the Nobel Prize, the Japan Prize, in 1987. Maiman made a laser using ruby as the lasing medium, which had been silvered, effectively creating mirrors on two parallel faces. The ruby was then irradiated by a high power flash lamp which acted as a simple pump.

Once functioning lasers had been achieved, the further development of non-linear optical processes such as laser pulsing for multi-photon excitation proceeded. The first experimental two-photon excitation fluorescence was observed in 1961 by Kaiser and Garrett of Bell Telephone Laboratories. Crystals of $CaF_2:Eu^{2+}$ were excited with a reported wavelength of 694 nm from a ruby optical maser which resulted in blue fluorescent light with a reported wavelength of 425 nm from Eu^{2+} relaxing from the excited state. A log-log plot of fluorescence intensity vs. excitation intensity resulted in a slope of 2 indicating two-photon nonlinear excitation.

Another important development for two-photon laser scanning microscopy was made with the self-mode-locked titanium:sapphire ($Ti:Al_2O_3$) laser (Spence et al., 1991). These lasers have a large working range of 700-1,100 nm as well as mode locking capabilities causing pulse widths in the femto-second range optimal for multi-photon excitation. An

advantage of the titanium-sapphire laser is the tunability of the laser, with a pulsing wavelength slightly less than the working range of ~770-950 nm. In order for lasers to be tunable the laser medium must have a broad gain profile so that different wavelengths can be selected. Lasing must then be restricted to a single transverse mode (TEM_{00}) using an intracavity aperture (Hitz et al., 2001). For many titanium:sapphire lasers, the aperture is a metal slit. The emission is then finally limited to a single longitudinal mode (SLM) by a dispersive element such as a prism. The combination of the lasing medium, a metal aperture and prism provide tuning, while the ability to make the laser pulse in the femto- to pico-second range allow multi-photon excitation.

Another significant advancement in the development of MPLSM occurred with the development of nonlinear scanning optical microscopes based on second-harmonic generation in 1977 (Sheppard and Kompfner, 1978). This microscope utilizes excitation light focused to a small volume, and then either the light or the specimen can be raster scanned to form an image. Sheppard and Kompfner theorized the ability for added resolution (including three-dimensional imaging) since excitation occurs in such a small volume, also limiting heating of the specimen, making this technique optimal for biological sampling. Additionally, nonlinear optical techniques are optimal since such a pulsed laser as required for MPLSM would result in an overall decrease in sustained power but much greater peak power. Confocal microscopy, the single photon excitation equivalent of multi-photon laser scanning microscopy, was also introduced by the same group (Sheppard and Choudhury, 1977).

In 1990 all the pieces were finally available to produce a multi-photon laser scanning microscope in the lab of Watt Webb at Cornell University (Denk et al., 1990). The resultant two-photon laser scanning microscope revolutionized the field. A colliding-pulse mode-locked dye laser was used as the now standard titanium:sapphire was not yet available with proper pulsing. This combination of laser scanning microscopy complimented by a mode-locked laser pulsed in the near infrared wavelength allowed for the fluorescent microscope detection of two-photon excitation of molecules.

MPLSM provides optimal characteristics (viability of tissue, real-time imaging, resolution in heterogeneous tissue) and therefore encompasses the best technique for localizing eGFP-D1DRs in viable cells growing in slice cultures for real time analyses. Several antecedents to MPLSM have been described including lasers and nonlinear scanning optical microscopes. These fundamental developments help to clarify the technical aspects of the techniques used in this dissertation.

1-5. SPECIFIC AIMS

Mesolimbic dopamine neurons project from the VTA to the NAcc. This pathway is believed to be important in establishing the rewarding effects of drugs of abuse including alcohol (Wise, 1996; Koob et al., 1998). One potential molecular mechanism underlying reward and addiction involves alterations in D1DR localization. Cellular mechanisms of desensitization include internalization of the receptor through complex receptor dynamics. The overall hypothesis for this dissertation was that dopamine and acute ethanol exposure will cause the internalization of D1DRs. This hypothesis was tested

using virally transfected D1DRs tagged with eGFP which were localized using MPLSM in explants containing the mesolimbic pathway. The aims of this dissertation included:

1. Development of virally transfection of eGFP tagged D1DRs. This specific aim was designed for the subcloning of a pseudovirus to induce the expression of eGFP-D1DRs. Briefly, the virus was produced through several steps with the major steps listed herein. The DNA encoding the eGFP-D1DR was obtained from Dr. Zhou (University of California, Irvine). This construct was inserted into the sindbis virus vector. RNA from two vectors, one encoding the sindbis nonstructural proteins (and gene of interest) and a second vector encoding viral structural proteins, were electroporated into baby hamster kidney (BHK) cells to produce sindbis pseudovirions.
2. Characterization and expression of eGFP-D1DR through viral infection of parasagittal explants imaged using multi-photon excitation. This aim was designed to characterize the pseudovirus infectivity as well as the function of the virally transfected receptor. Additionally, the characterization of parasagittal explants and multi-photon excitation of eGFP in these explants was accomplished. eGFP-D1DR function was tested using cAMP production upon agonist and antagonist application. The development of a novel parasagittal explant containing the mesolimbic pathway required characterization to ascertain that dopaminergic neurons were present. Tyrosine hydroxylase (TH) staining confirmed dopaminergic cells were present in the appropriate areas. The methodology for viral delivery into

explants was established as well. In addition, optimal multi-photon excitation parameters for explant imaging were established.

3. Test the hypothesis that dopamine and ethanol induce virally transfected eGFP-D1DR clustering and internalization detected in viable neurons of parasagittal explant using MPLSM. This aim was designed to investigate the localization of eGFP-D1DR by two-photon fluorescence excitation in viable neurons in the NAcc. D1DRs have been shown to internalize upon agonist-induced stimulation, but such internalization has never been shown in viable mammalian neurons. D1DRs are also hypothesized but have never been shown to internalize in response to ethanol. Therefore, dopamine and ethanol were used to stimulate eGFP-D1DRs, expressed by viral infection of cells in a parasagittal explants to test our hypothesis that D1DRs will cluster and internalize in response to these stimulations.

Chapter 2: Subcloning eGFP- D1DR into the Sindbis Expression System

2-1. OVERVIEW

The production of the eGFP-D1DR sindbis virus is described in this section. Additional details (such as recipes) and commonly used protocols are provided in Appendix I and II, respectively; however, enzymatic reactions that were required are included in this chapter. The DNA containing eGFP-D1DR was ligated into the pSinRep5 vector. Both the subcloned pSinRep5 vector and the defective helper DH(26)S vector (which encodes the structural proteins of the virus) were linearized and transcribed into RNA by *in vitro* transcription. These RNA preparations were then electroporated into baby hamster kidney (BHK) cells, used as hosts to make virions. The virions were then collected from the media and concentrated by discontinuous gradient ultracentrifugation.

2-2. Vector Propagation

A kanamycin resistant DNA vector (based in the pEGFP-N1 vector, Clontech, Palo Alto, CA, exact sequence unknown) containing the eGFP-D1DR sequence (the *Rattus norvegicus* dopamine-1A receptor with eGFP fused to the carboxyl tail) was provided by the lab of Dr. Q. Zhou at the University of California at Irvine (Bermak et al., 2002). The sindbis vectors (pSinRep5 and DH(26)S) are both ampicillin resistant (see Table 1-1,2 for more information on vectors). Separate kanamycin- and ampicillin-containing agarose plates were prepared for the purposes of quick transformation (Recipe R1 in Appendices). A quick transformation utilized heat shock so that bacteria would endocytose the DNA vectors; bacterial colonies that have incorporated these vectors were

propagated on antibiotic agarose plates since these vectors contain the appropriate antibiotic resistant gene.

2-2.1. Quick Transformation

Approximately 10 ng of each vector was transformed at 40 °C for one minute into 10 uL Epicurean coli XL-1 Blue cells (Stratagene, La Jolla, CA). Media (100 uL SOC media) was added to transformed bacteria. Aliquots (25 uL and 75 uL) of transformed bacteria were plated on kanamycin or ampicillin/luria broth base (LB) plates which were incubated overnight at 37 °C. A single colony from each plate was propagated in LB broth containing kanamycin or ampicillin (depending on the vector) at 37 °C with shaking at 225 rpm overnight; the resultant plasmid DNA was then extracted as described below.

2-2.2. Plasmid DNA-Purification

Plasmid DNA from the overnight culture was extracted using a Qiagen Plasmid Maxi Kit (Qiagen, Valencia, CA). The broth from the overnight culture was poured into a 50 mL conical centrifuge tube and the cells pelleted by centrifugation (6,000 x g for 15 minutes at 4 °C). The supernatant was discarded and the pellet was fully re-suspended in 10 mL of P1, the cell resuspension buffer (with RNase added). The cells were lysed by adding 10 mL of P2 lysis buffer and the container was gently inverted five times and incubated for 5 minutes at room temperature. At this step the bacteria were lysed and the fluid was handled gently to avoid shearing genomic DNA. Then, chilled P3 neutralizing buffer (10 mL) was added and gently mixed by inverting the container five times, causing the

precipitation of the genomic material. This mixture was immediately transferred into a QIA filter cartridge and incubated for 10 minutes at room temperature. During the incubation, the Qiagentip was prepared with 10 mL of QBT buffer. The Qiagentip and the Qiagen filter cartridge were than assembled and the genomic material was applied to the column (assisted by a plunger). Once the genomic material had fully entered the column, 60 mL of QC wash buffer was added. The DNA was eluted with 15 mL of QF buffer and collected in a 30 mL tube. The DNA was next precipitated by adding 10.5 mL of room temperature isopropanol to the 30 mL tube, which was immediately mixed and centrifuged at 15,000 x *g* for 30 minutes at 4 °C. A small transparent pellet formed, and the supernatant was carefully discarded. This pellet was washed with 70% ethanol by rolling it over the pellet in the tube, and the mixture was centrifuged again at 15,000 x *g* for 10 minutes followed by pellet isolation. The tube was inverted and the pellet was air dried for 10 minutes. The pellet was fully dissolved in 0.5-1.0 mL of nuclease-free H_2O. A nanodrop UV spectrometer (Nanodrop Technologies, Wilmington, DE) was used to analyze 1 uL of the resulting DNA solution for concentration and quality measurements.

2-3. PREPARATION OF EGFP-D1DR DNA FOR PSINREP5 LIGATION

2-3.1. Obtaining the Appropriate DNA for Ligation

The DNA needed for ligation was excised from the Zhou vector and subcloned into the pSinRep5 vector. The pSinRep5 vector was linearized by cleaving the vector with the restriction enzyme Pml I, a ligation point located near the middle of the insertion of the

gene of interest sites. The Zhou vector was cleaved using both restriction enzymes Not I and Hind III to release an insert containing eGFP-D1DR.

The following reactions were incubated for 3 hours at 37 °C:

pSinRep5		Zhou vector	
DNA:	5 ug	DNA:	5 ug
BSA:	1 uL	BSA:	1 uL
Buffer 1:	10 uL	Buffer C:	10 uL
Pml I:	4 uL	Not I:	4 uL
		Hind III:	4 uL
Nuc. free H_20:	balance	Nuc. free H_20:	balance
	100 uL		100 uL

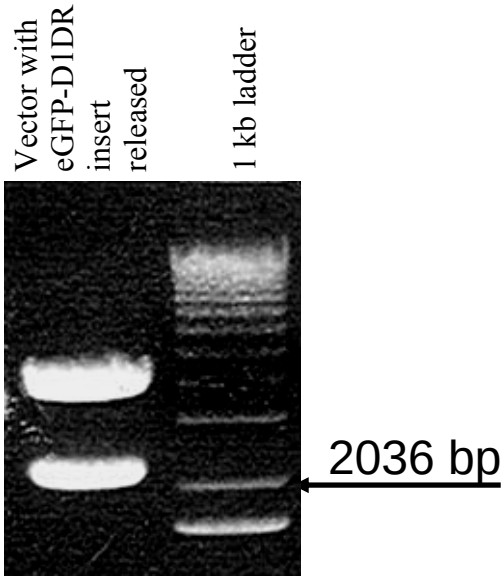

Figure 2-1. Gel displaying release of the insert of eGFP-D1DR to be ligated into pSinRep5. The vector received form Dr. Zhou was cleaved with the restriction enzymes Not I and Hind III. The eGFP-D1DR insert is approximately 2100 bp.

Large portions (80 uL) of these reactions were subjected to agarose electrophoresis at 80 V for 45 minutes on a 1% gel made of clean agarose (see Recipes in Appendices for further electrophoresis conditions). The bands associated with the linearized pSinRep5

vector and the eGFP-D1DR insert (Figure 2-1) were excised from the gel, placed in 1.5 mL tubes and weighed. Using the "rapid gel extraction" protocol (from Gibco BRL Life Technologies Concert Rapid PCR Extraction System, Invitrogen, Carlsbad, CA), the DNA of appropriate size was extracted from the gel. For every 10 mg of gel, 30 uL of gel solubilizing buffer (L1) was added and the preparation then incubated at 50 °C. Every 3 minutes the tube was shaken, and after the gel was dissolved, a final 5 minute incubation was performed. This mixture was pipetted into a spin cartridge, placed in a 2 mL wash tube, and centrifuged at 12,000 x g for 1 minute at room temperature. The supernatant was discarded. The cartridge, which contained the DNA of appropriate size bound to the column, was returned to the wash tube and 700 uL of wash solution (H2) was added and incubated for 5 minutes at room temperature. The cartridge and tube were centrifuged for 12,000 x g for 1 minute at room temperature. The supernatant was discarded, and an additional 1 minute spin was conducted to clear all the supernatant. The spin cartridge was then placed in a 1.5 mL tube, and DNA was eluted with 30 uL of 50 °C nuclease-free H_2O and incubated at room temperature for 5 minutes. The cartridge and tube were then centrifuged at 12,000 x g for 2 minutes.

2-3.2. Preparation of Appropriate DNA for Ligation

The DNA of both the insert and the pSinRep5 vector were treated for better ligation probability. The linearized pSinRep5 was dephosphorylated to reduce the probability of recombination of the vector without the eGFP-D1DR insert. The cleaved ends of pSinRep5 were dephosphorylated by treatment with alkaline phosphatase from calf

intestine. The eGFP-D1DR was prepared with an end-filling polymerase (klenow DNA polymerase) in order that the insert had blunt ends for ligation with the pSinRep5 vector.

linearized pSinRep5 DNA:	30 uL
10X CIP Buffer:	5 uL
Nuc. free H_20	10 uL
CIP enzyme	5 uL

37 °C 15 minutes
added 1 uL CIP enzyme
55 °C 45 minutes
0.5 uL of 500 mM EDTA
75 °C 10 minutes

insert eGFP-D1DR DNA:	15 uL
10X Klenow Buffer :	5 uL
Nuc. free H_20	26 uL
Klenow enzyme	1 uL
10X dATP	1 uL
10X dGTP	1 uL
10X dCTP	1 uL
10X d TTP	1 uL

37 °C 15 minutes
75 °C 10 minutes

2-3.3. DNA Isolation

Phenol/chloroform extraction was used to isolate DNA for ligation. Both reactions from the previous section had 50 uL of nuclease-free H_20 added so that each reaction had a total volume of 100 uL. Phenol was added in equal volumes to each reaction (100 uL). These samples were mixed and centrifuged at 12,000 x *g* for 1 min. The DNA in the upper aqueous layer was carefully transferred to a fresh tube, and the organic lower layer containing protein was discarded. The aqueous layer was again extracted from an equal volume of chloroform after the sample was centrifuged at 12,000 x *g* for 1 minute. The DNA was precipitated by adding one tenth the volume (1/10x) of 3M sodium acetate (~10 uL) and twice the volume (2x) of 100% ethanol (~200 uL). These samples were placed in a -80 °C freezer for 2 hours and were then centrifuged at 12,000 x *g* for 15 minutes at 4 °C. The supernatant was discarded, the pellets allowed to air dry, and 15 uL

of nuclease-free H_20 was used to resuspend the pellets and incubated at room temperature for 10 minutes.

2-3.4. Ligation

The eGFP-D1DR insert and the linearized pSinRep5 vector were ligated in a 1:1 molar ratio with T4 DNA ligase in an overnight reaction at 4 °C. The pSinRep5 vector was twice the concentration of the insert at this step since twice the volume was used to dephosphorylate vector DNA than was used for end filling of the insert DNA.

pSinRep5 vector DNA:	2 uL
eGFP-D1DR insert DNA:	1 uL
2x ligase buffer:	2.5 uL
T4 DNA ligase	1 uL
Nuc. free H2O	1 uL

4 °C overnight

2-3.5. Slow Transformation of Ligation

After ligation, a slow transformation was performed as the DNA was fragile at this juncture. The DNA of the ligated vector (5 uL) was mixed with 50 uL of Epicurean coli XL1-Blue (never thawed) and incubated on ice for 30 minutes. The DNA was transformed with a heat shock at 42 °C for one minute. Media (450 uL SOC) was added and the resulting mixture incubated for 45 minutes at 37 °C. An aliquot of 100 uL was plated on an ampicillin/LB plate. The remaining cell mixture was centrifuged at 12,000 x *g* for 1 minute. Supernatant (200 uL) was discarded and the remaining supernatant and resulting pellet were re-suspended and plated on an ampicillin/LB plate and incubated overnight at 37 °C.

Individual colonies (8) were selected from the ampicillin/LB plates and mass produced in broth media. This number was chosen to ensure several colonies of the proper orientation of eGFP-D1DR in pSinRep5. Approximately half of those colonies should represent the proper orientation of the eGFP-D1DR insert in pSinRep5 while the other half will have the insert in the reverse orientation in pSinRep5. There was also a third possibility, that no insert may be present in some colonies as self-ligation of the pSinRep5 vector was possible even with dephosphorylation of the vector. LB broth (3 mL) and ampicillin (3 uL) were put into 8 tubes and inoculated with a 20 uL pipette tip that had touched an individual colony. Of these 8 tubes, 7 grew bacteria. DNA was harvested from those 7 tubes by Qiagen Plasmid Miniprep.

2-3.6. Plasmid DNA Purification

Qiagen spin Minipreps were used for smaller volume and quantity of bacterial production. The seven tubes were spun at 12,000 x *g* for 5 minutes at 4 °C. The supernatant was discarded and the pellet was re-suspended in 250 uL of P1 buffer. This solution was then transferred into a 1.5 mL microfuge tube. Buffer P2 (250 uL) was added and the tubes inverted gently 5 times. Next Buffer N3 (350 uL) was added and the tubes inverted gently 5 times. These tubes were then centrifuged at 12,000 x *g* for 10 minutes. During centrifugation a QIAprep spin column was placed in a 2 mL collection tube. The supernatant was then applied to the QIAprep spin column by decanting. The supernatant was centrifuged for 1 minute at 12,000 x *g*, and flow through of the column discarded. The column was washed with 0.75 mL of PE buffer and centrifuged for 1 minute at 12,000 x *g*, and the wash through was discarded. An additional 1 minute at

12,000 x *g* centrifugation was done to remove all wash buffer. The QIAprep spin column was then placed into a clean 1.5 mL tube. The DNA was eluted with 50 uL of nuclease-free H_2O by pipetting into the center of each column and incubating for 2 minutes at room temperature. The column and tube were centrifuged for 1 minute at 12,000 x *g*. These solutions were analyzed with a nanodrop UV spectrometer to determine quality and quantity of genomic material.

2-3.7. Verification of the Correct Orientation of eGFP-D1DR in pSinRep5

The restriction enzyme Cla I was used to cleave each harvested transformation to identify the ligation orientation. DNA (1 ug) was incubated with 2 uL of Cla I, 1 uL of BSA, and 2.5 uL of Cla I buffer in a final volume of 25 uL for 1 hour at 37 °C. The ligations were also compared to pSinRep5 (without eGFP-D1DR) cleaved with Cla I, and the cleaved fragments were analyzed by gel electrophoresis.

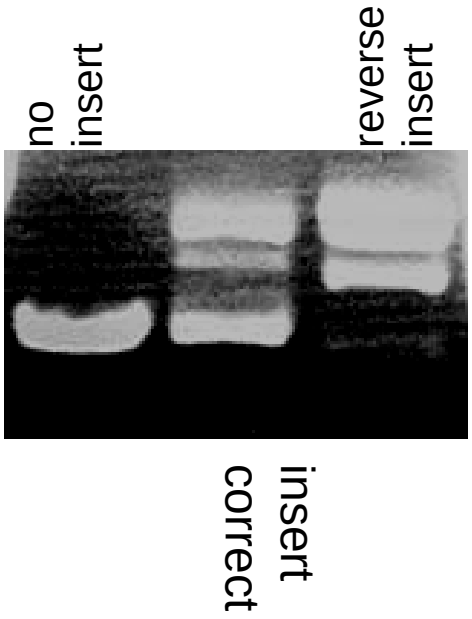

Figure 2-2. Cla I digestions of ligations of pSinRep5 and eGFP-D1DR. The proper orientation was determined by sequencing. The ligations with resulting fragments that were similar to the middle well had a sequence corresponding to a dopamine receptor.

The resulting cleavage differences were grouped as two unknown insert orientation groups and one no insert group (Figure 2-2). Two examples from the unknown orientation group were sequenced using primers directed at the ligation area of pSinRep5. Primers were ordered from IDT (Coralsville, IA): (pSinRep5 primer forward: 5'AGCATAG TACATTTCAT CTG-3'). The primer tubes were centrifuged briefly before opening and 100 uL of nuclease-free H_2O was added. This was further diluted 1:10, and 1 uL of this diluted primer was used for sequencing. For the sequencing reaction, 700-1000 ng of the DNA was added to about 6 pmol of primer in nuclease-free H_2O with a final volume of 11-12 uL. These samples were then analyzed by the DNA

Sequencing Core Facility at the University of Texas at Austin Institute for Cellular and Molecular Biology. The resultant sequence (shown following) showed a significant match with "*Rattus norvegicus* Dopamine-1A receptor (Drd1a)," a D1DR as authenticated by the National Center for Biotechnology Information website http://www.ncbi.nlm.nih.gov/. The sequence match was verified by performing a nucleotide-nucleotide BLAST search.

CACACCACCACCTCTAGACGCGTAGATCTCACAGCTTGATTCGAGCTCGCCCC
GCCCCCAGCCAGTGCGCTTACCTGCCAGACTGCGCGCCATGAAGACGATCAT
CGCCCTGAGCTACATCTTCTGCCTGGTGTTCGCCGACTACAAGGACGATGATG
ACGCCATGGATGAGGCCGGGCTGCCAGCGGAGAGGGATTTCTCCTTTCGCAT
CCTCACGGCCTGTTTCCTGTCACTGCTCATCCTGTCCACTCTCCTGGGCAATA
CCCTTGTCTGTGCGGCCGTCATCCGGTTTCGACACCTGAGGTCCAAGGTGACC
AACTTCTTTGTCATCTCTTTAGCTGTGTCAGATCTCTTGGTGGCTGTCCTGGTC
ATGCCCTGGAAAGCTGTGGCCGAGATTGCTGGCTTTTGGCCCTTTGGGTCCTT
TTGTAACATCTGGGTAGCCTTTGACATCATGTGCTCTACGGCGTCCATTCTGA
ACCTCTGCGTGATCAGCGTGGACAGGTACTGGGCTATCTCCAGCCCTTTCCAG
TATGAGAGGAAGATGACCCCCAAAGCAGCCTTCATCCTGATTAGCGTAGCAT
GGACTCTGTCTGTCCTTATATCCTTCATCCCAGTACAGCTAAGCTGGCACAAG
GCAAAGCCCACATGGCCCTTGGATGGCAATTTTACCTCCCTGGAGGACACCG
AGGATGACAACTGTGACACAAGGTTGAGCAGGACGTATGCCATTTCATCGTC
CCTCATCAGCTTTTACATCCCCGTAGCCATTATGATCGTCACCTACACCAGTA
TCTACAGGATTGCCCAGAAGCAAATCCCGGCGCATCTCAGCCTTGGAGAAGG
GCAGCANNTCCATGCCAAGAATTGCCAGACCACCGCAGGNTAACNGGAAAC
CCCGTCNAATGCCCCCAGNTCTGAAAGTTCCCTTTAANATGT

2-4. PRODUCTION OF SINDBIS EGFP-D1DR

2-4.1. Propagation of New eGFP-D1DR Containing pSinRep5 Vectors

The ligations containing eGFP-D1DR were propagated as described above with quick transformations and purified with Qiagen maxi-preps.

2-4.2. *in vitro* Transcription of Sindbis eGFP-D1DR viral DNA

Both DH(26)S, the viral structural gene vector, and pSinRep5 containing the eGFP-D1DR construct were linearized using the restriction enzyme Xho I. DNA (5.0 ng) was added to 1 uL of BSA, 10 uL of Xho I buffer, and 5 uL of XhoI enzyme with nuclease-free H_2O making up the balance for a final volume of 100 uL and incubated at 37 °C for

3 hours. These reactions were checked for complete cleavage by agarose gel electrophoresis using uncut vectors as a control.

Protease K (1 uL) was added to inactivate any remaining restriction enzymes (37 °C for 30 minutes). Then a phenol:chloroform extraction was completed to isolate the DNA as described previously. The precipitated DNA was dissolved in 4 uL of DEPC-treated H_2O. The tube was incubated at room temperature for 10 minutes for full resolubilization. The following reactions then were completed in small PCR tubes (all solutions were included in the Ambion SP6 *in vitro* transcription kit (Ambion, Austin, TX):

4 uL of DNA in DEPC H_2O
10 uL of 2x NTP/Cap
2 uL 10x Reaction Buffer
2 uL Enzyme Mix
1 uL GTP

Reactions were incubated at 37 °C for 1 hour. Then an additional 1 uL of enzyme mix was added followed by one additional hour incubation at 37 °C. RNA was isolated by phenol:chloroform extraction as previously described for DNA, and the RNA pellets were dissolved in 20 uL of DEPC H_2O (see Protocol P1 in Appendices for step by step instruction).

2-4.3. Analysis of Sindbis RNA

Gel electrophoresis of the RNA was performed (Figure 2-3) and analyzed by ultraviolet spectrometry using the nanodrop UV spectrometer for quality and quantity measurements. Great care was taken to avoid contamination by RNases. The gel box and

attachments were soaked in ~3N HCl for 15-30 minutes and then rinsed with RNase-free TBE. All RNase-free solutions were prepared using DEPC H_2O. A 0.7% agarose gel in TBE with 90 ug/uL of ethidium bromide was prepared. Gel electrophoresis was performed using RNase-free TBE running buffer.

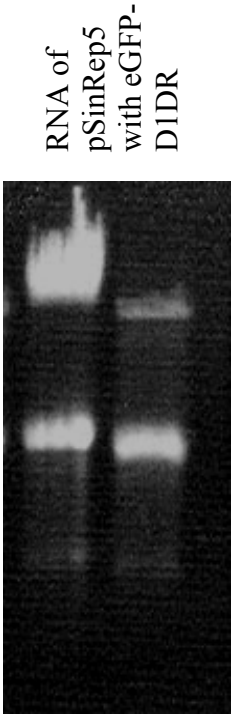

Figure 2-3. Gel displaying two samples of RNA made by *in vitro* transcription from pSinRep5 ligated with eGFP-D1DR.

2-4.4. Electroporation of Sindbis RNA

BHK cells were grown in five 175 cm^2 flasks at a passage cycle below 75. The media was removed and the cells washed with 10 mL RNase-free PBS without cations at room temperature. Each flask was treated individually with 3 mL of 0.25% trypsin until cells were freely floating without forming clumps. Trypsinization was halted with 5 mL of

10% fetal bovine serum (FBS) in minimum essential medium (MEM). This mixture was transferred to 15 mL sterile tubes and centrifuged for 5 minutes at 500 rpm at room temperature. Cells were washed by re-suspending in 5 mL ice cold RNase-free PBS without cations. Re-suspension was by gentle inversion repeated fifty times. The re-suspension was then centrifuged for 5 minutes at 500 rpm at room temperature. This wash was repeated by gently re-suspending the cells in 5 mL ice cold RNase-free PBS without cations and centrifuged for 5 minutes at 500 rpm at room temperature. A small aliquot of the cells was taken and the total number of cells was determined by using the Hemacytometer equation:

(Hemacytometer average) x (10^4) x (volume of cells) = total number of cells.

A third RNase-free PBS wash and centrifugation was followed by the re-suspension of cells at a density of 1.5 x10^7 cells/mL in ice cold RNase-free PBS without cations. The final electroporation mixture contained in ice cold 1.5 mL eppendorf tubes was: 500 uL of BHK cells and 10-15 ug each of RNA for both the DH(26)S and pSinRep5 eGFP-D1DR. This mixture was transferred to ice cold cuvettes and electroporated twice as follows:

BioradGene Pulsar with Pulse Controller
0.2 mm electrode gap cuvettes from biorad
1.5 kV, 25 uFD, resistance=infinity
time constant should result in 0.7 msec

After electroporation the cuvettes were incubated at room temperature for 10 min. With a sterile glass pipette the solution was removed and 9.5 mL of MEM with 10% FBS was gently mixed with electroporated BHK cells by inversion. Then 2 mL of combined media

and electroporated cells were placed into five 35 mm dishes and incubated at 37 °C in a standard cell culture incubator containing 5% CO_2. Successful electroporation of BHK cells was verified by fluorescence detection after 24-60 hours. Media was collected daily for as long as fluorescence was observed (Figure 2-4) (see Protocol P2 in Appendices).

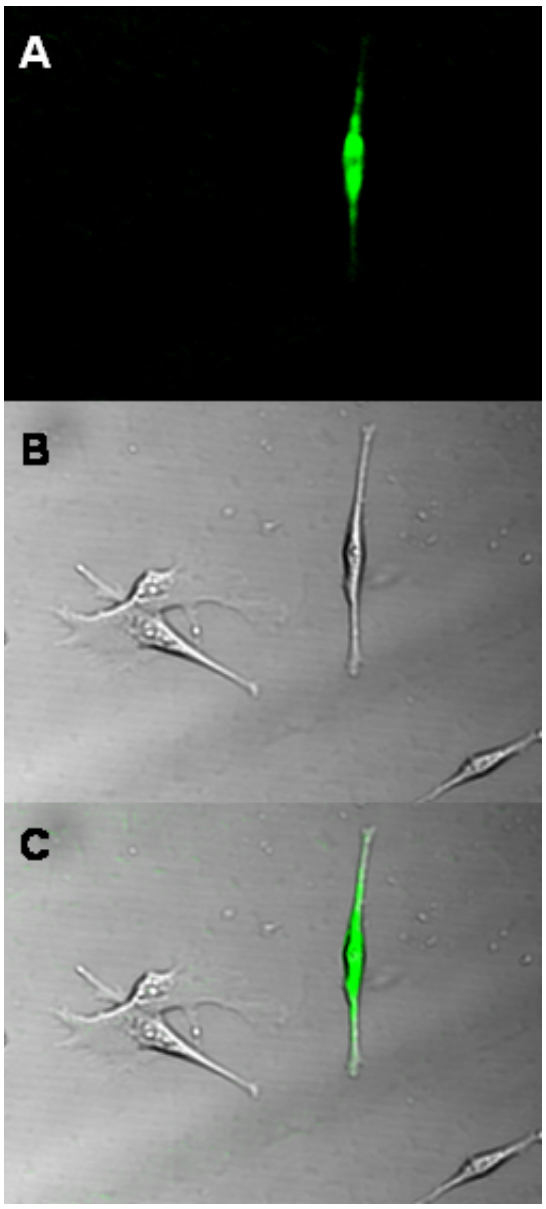

Figure 2-4. Electroporated baby hamster kidney cells. A) Fluorescent image illustrating the production of eGFP. B) Light image showing cells present after electroporation. C) Overlay of A and B showing that the vertically positioned cell is expressing eGFP.

2-4.5. Sindbis Viral Stock Concentration

The media collected from electroporated BHK cells was concentrated by ultracentrifugation through a discontinuous sucrose gradient. All solutions were kept sterile for later infection of sterile cells. In ultracentrifuge tubes 1 mL of 55% sucrose in TNE buffer (see Recipes R6 and R7 in Appendix I) formed the gradient base. A 3 mL layer of 20% sucrose in TNE buffer was placed over the 55% sucrose layer. Finally 6 mL of culture media from electroporated BHK cells was layered over the 20% sucrose. These tubes were carefully balanced with the swinging portions of an ultracentrifuge rotor (CA SW-41Ti, Beckman Coulter, Inc, Fullerton) and were ultracentrifuged (Optima XL-100K Ultracentrifuge, Beckman Coulter, Inc, Fullerton, CA) for 90 minutes at 30,000 rpm (160,000 x *g*). The top layer (8 mL) was carefully aspirated and discarded (after autoclaving in case of virion contamination). The 1 mL layer above the interface, which contained purified virions, was collected, aliquoted and stored at -80 °C. The final 1 mL fraction was also discarded after autoclaving in case of viral contamination.

Chapter 3: Sindbis Viral Mediated Expression of eGFP-D1DR in Parasagittal Explants with Multi-photon Laser Scanning Microscopy

3-1. OVERVIEW

Many aspects of this dissertation project were novel for our laboratory, making an initial characterization of: eGFP-D1DR sindbis virus, parasagittal explant and MPLSM necessary. For example, fluorescence following electroporation of BHK cells with eGFP-D1DR pSinRep5 and DH(26)S RNA indicated that eGFP was expressed, but no direct evidence that virions were made or that the D1DR was functional was provided. Therefore, the viral transfection system was characterized for its ability to produce functional D1DRs. The neuronal model used for imaging experiments was the parasagittal brain slice culture, or organotypic explant, which also required characterization to ascertain the presence of dopaminergic cells emanating from the VTA. To accomplish this, explants were stained by immunohistochemistry for the presence of TH. Finally, the MPLSM had to be characterized for the fluorophore eGFP and customized for explant imaging.

3-2. CHARACTERIZATION OF VIRAL EXPRESSION SYSTEM

3-2.1. Transfection of Neurons

To ascertain that virions were produced in BHK cells and released into the culture media, the media was collected and tested for its ability to infect other cells. Supplementary infection indicates that both of the sindbis expression system vectors were expressed and that virions were formed. Primary cultured neurons, slice cultures, and in vivo neurons were all used to demonstrate functional virion production. Primary cultures were infected

by direct addition of concentrated virus to the media (~ 30 uL/2 mL). Slice cultures were infected in a novel manner with concentrated virus injected under the surface of the slice culture using a glass capillary and delivered with a manual positive displacement microdispenser (VWR, West Chester, PA; capacity 10 uL). Glass capillaries for this dispenser were formed similar to patch electrodes, loaded with approximately 3-5 uL of the concentrated viral preparation, and used to infect explants at multiple points using 50-100 nL per injection. Mice were infected *in vivo* using the Small Animal Stereotaxic Instrument Model SAS75 (Cartesian Research, Inc.). Concentrated virus was delivered to the NAcc (AP +1.7, LAT +0.8, DV – 2.0) using a syringe pump (500-1000 nL over one minute).

The ability of the sindbis virus system to induce expression of eGFP-D1DR (as presumed by fluorescence emission) was verified by two-photon excitation in primary dissociated neuronal cultures, slice cultures, and slices following *in vivo* infection. We first observed expression of eGFP-D1DR in dissociated neurons from the ventral striatum (Figure 3-1A). The eGFP-D1DR expression was distributed extensively throughout the neuron, including the cell body and in the processes, including dendrites, as well as their well-known spiny protrusions (inset). Fluorescence of cultured dissociated cells was monitored via two-photon excitation approximately 1-3 days post-infection. Next, viral infection was assessed in parasagittal slice cultures that included the NAcc. Despite the difference in the method of infection in slice cultures (local injection) compared to dissociated cultured neurons (simple addition of virus to media), the time course of viral expression appeared to be similar. Expression 3 days post-infection in slice cultures is

shown in Figure 3-1B. Finally, viral infection was tested *in vivo* following local injection into mouse NAcc. *In vivo* infection also displayed a similar time frame for expression. Fluorescent cells along the injection tract were apparent three days post-infection (Figure 3-1C). Slices imaged prior to three days post- infection resulted in little or no detectable infection as measured by fluorescence. The ability of this virus to cause infection in many different neuronal models underscores the advantage of viral infection for successful gene expression in neurons.

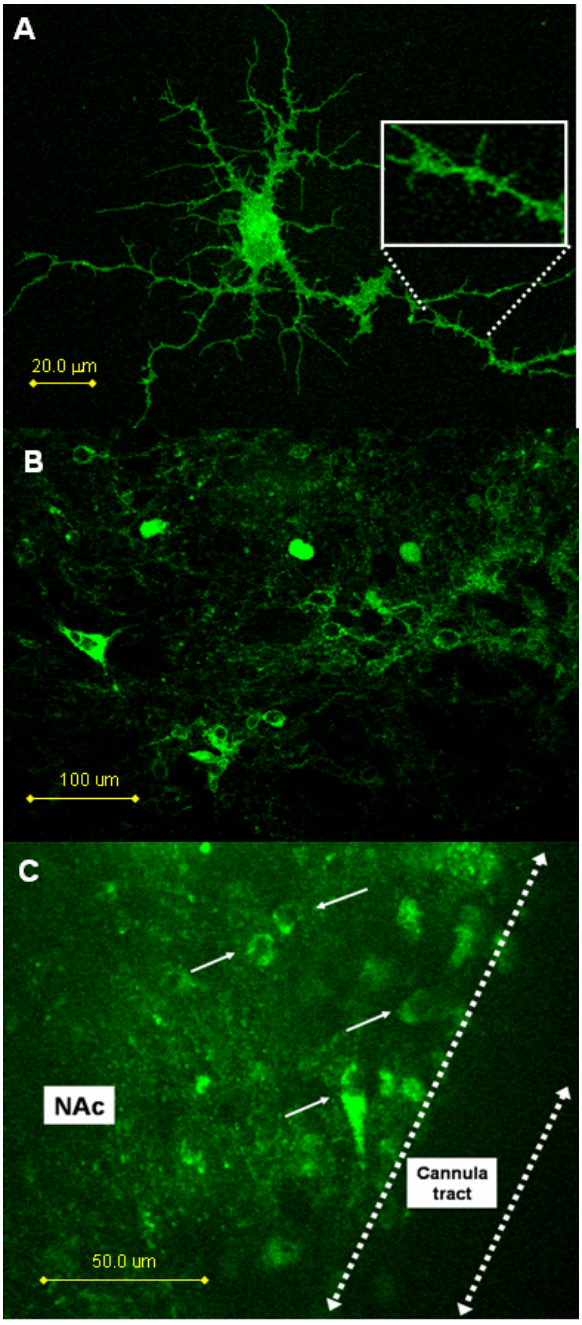

Figure 3-1. Viable neurons expressing eGFP-D1DR after infection with the sindbis virus. A) Ventral striatal dissociated cell infected with the eGFP-D1DR sindbis virus. This culture was 34 days *in vitro* and had been infected for 5 days. B) Fluorescence of cells in infected slice. This slice was infected using 4 injections of 100 nl virus and imaged 3 days later. C) *In vivo* infection. Virus (500 nL) was delivered into the NAcc (1.7 AP, 0.8 LAT, -2.0 DV) using a micropump. Slices were made and viewed 3 days after infusion.

3-2.2. Viral Titer

The sindbis expression system produces a suicide pseudovirion, so named because each virion can only infect once. The lack of genetic information encoding structural genes (since the helper vector is not repackaged) prevents viral replication, thereby making the conventional viral titer procedure of plaque formation inappropriate for viral characterization. Instead, infection by the sindbis expression system is determined more empirically by the number of infected cells using viral dilutions to determine the number of colony forming units per volume of concentrated viral stock.

BHK cells were infected with different dilutions of virus to calculate viral titer. First, BHK cells were grown to 80% confluency in 175 cm^2 flasks; these cells were then detached with 3 mL of trypsin. Trypsinization was halted with 10 mL of MEMcontaining 10% FBS. An aliquot (10 uL) of dissociated cell preparation was taken for cytometry (see Appendix II Protocol P2 for equation). The preparation was then diluted to 0.5-1.0 x 10^5 cells/mL. In a 6 chambered coverglass, 1 mL of diluted cells was dispensed in each chamber and then placed in a 37°C incubator for approximately 24 hours to allow cell attachment. The following day, six serial dilutions of virus were made at 1:10 each. Cells were infected as follows: one chamber received 90 uL of concentrated virus then subsequent chambers received 90 uL of each of the six progressive 1:10 serial dilutions, leaving an uninfected chamber for control. These cells were returned to the incubator at 37 °C for 24 hours. The titer was determined to be approximately 2 x 10^6 cfu/mL (colony forming units per mL). This was determined by counting the number of fluorescent cells

(2) present in the most dilute virus (10^6) that established infection. This titer was greater than other sindbis viral stocks that had not been concentrated and is a typical titer for viral stocks used in subsequent experiments.

3-2.3. eGFP-D1DR function

To determine if the D1DRs expressed by cells infected with the virus were functional, cAMP assays were performed (Assay Designs Inc. Cat # 900-066, Ann Arbor, MI). BHK cells were plated (~1.5 X 10^5 cells/well) in a 24 well dish. Approximately 18 hours later, wells were infected with 10 uL of concentrated sindbis virus expressing eGFP-D1DR to induce a high level of infection. Cultures were inspected by confocal imaging for infection 24 hours later, with approximately 90% of cells showing fluorescence. The cells were then treated with D1DR agonists and/or antagonists for 1 hour at 37°C. Cells were lysed with a combination of 0.1 M HCl and ultrasonication (Fischer Scientific Sonic Dismembrator Model 100). Samples were treated in triplicate and cAMP production was detected as per instructions of Direct cAMP kit. Absorbance was measured at 405 nm on a FL600 microplate reader (BioTek, Winooski, Vermont).

Cyclic AMP was measured in BHK cells that infected with a sindbis virus that induces the expression of eGFP-D1DR and in uninfected BHK cells. Cells were challenged with dopamine alone or in combination with the selective D1DR antagonist, SCH 23390 (Figure 3-2). Infected cells responded to dopamine challenge in a dose-related manner while control cells displayed no sensitivity to dopamine (Figure 3-2A). The ability of dopamine to stimulate cAMP production was antagonized by the D1DR antagonist SCH

23390 in a concentration-dependent manner (Figure 3-2B). Wildtype mammalian D1DRs have an affinity of 10-18 uM dopamine for the low affinity conformation of the receptor (for review see Neve and Neve, 1997). Although a comprehensive dose response curve of the virally-induced eGFP-D1DR was not completed, the EC_{50} for dopamine was within that range. For SCH 23390, the EC_{50} was approximately 1 nM. Maximum cAMP production in response to dopamine (1,000 uM) was 70 ± 0.7 pmol/mL in infected cells compared to only 3 ± 0.6 pmol/mL in uninfected cells. SCH 23390 (0 nM) plus dopamine (10 uM) resulted in maximal cAMP production of 50 pmol/mL ± 0.6 were within the range of cAMP standards.

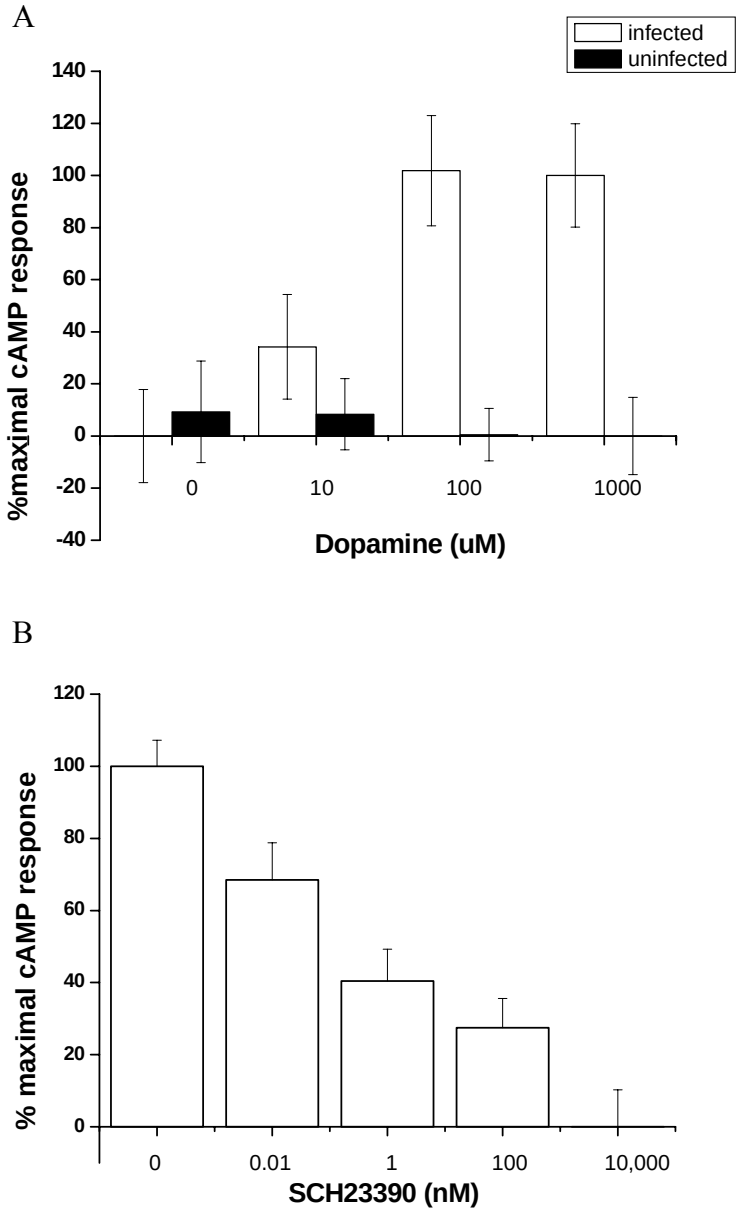

Figure 3-2. Cyclic AMP production demonstrates expression of functional D1DRs. A). Dopamine-stimulated cAMP response in virally-infected and uninfected BHK cells. B) Dopamine (10 uM) stimulated cAMP production in infected BHK cells treated with the dopamine antagonist SCH 23390.

3-3. PARASAGITTAL MESOLIMBIC EXPLANT CHARACTERIZATION

3-3.1. Explant Introduction

The first explants, or organotypic slice cultures, were prepared in 1956 by the roller tube method using non-neuronal tissue (Ehrmann and Gey, 1956). This method involved tissue fastened to a glass coverslip inside a capped tube that rotates for delivery of media without the tissue being constantly submerged. In 1981, a very similar technique was applied to hippocampal and other neuronal tissue (Gahwiler, 1981). Neuronal explants retain many of the connections present in the brain while the *in vitro* model of dissociated neuronal cell cultures has only random connections. In 1991, a less labor-intensive and less time-consuming method of explanting neuronal tissue was introduced that uses a semi-permeable membrane culture dish insert (Stoppini et al., 1991). With this method, acute slices of neuronal tissue can be easily produced and maintained in incubators. This viable tissue preparation still has intact neuronal connections. There are other advantages to organotypic slice cultures, including the ease of delivery of virally-transfected receptors. Moreover, Shi et al. (1999) showed differential expression of receptors on the cell surface between dissociated cultured hippocampal neurons and hippocampal explants. Therefore, trafficking studies that utilize explants may offer a more physiologically relevant system compared to trafficking studies using dissociated cultures.

Parasagittal explants that include the mesolimbic pathway provide a physiological system for studying neuroadaptive changes caused by drugs of abuse which are known to affect this area. These explants contain critical mesolimbic areas, including the VTA, NAcc, prefrontal cortex, and hippocampus that would facilitate study of the neurobiology of reward and abuse. Increased dopamine in the mesolimbic pathway appears to be important in the rewarding effects of drugs of abuse such as ethanol. Parasagittal explants, used in this dissertation project, thus offer a viable model for studying ethanol's action on D1DR localization and trafficking.

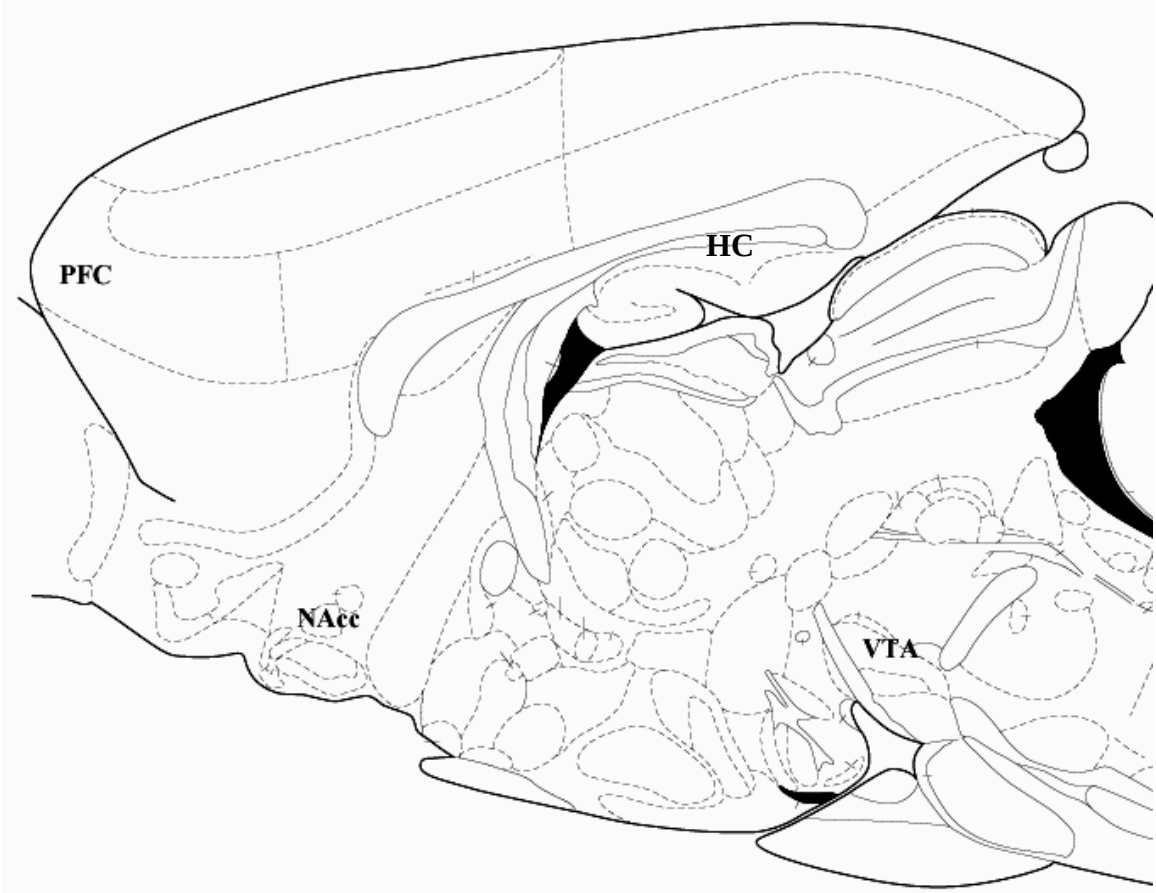

Figure 3-3. Approximate parasagittal plane used to make explants. This plate is altered from the Paxinos & Watson rat brain atlas (coordinate plate 80). The mesolimbic dopamine pathway initiating in the Ventral Tegmental Area (VTA) and terminating in the Nucleus Accumbens (NAcc) are included, as well as other areas implicated in addiction such as the Prefrontal Cortex (PFC) and the Hippocampus (HC).

3-3.2. Explant Methods

Parasagittal mesolimbic brain slice explants were prepared from Sprague Dawley rat pups (4-7 days old, University of Texas at Austin Animal Resource Center) under IACUC guidelines. The brain was removed quickly and placed in ice-cold cutting artificial cerebrospinal fluid (aCSF, in (mM): NaCl, (120); KCl, (3.3); NaH_2PO_4, (1.23); $NaHCO_3$, (25); $CaCl_2$, (2.0); $MgSO_4$, (0.9); dextrose, (10) and continuously gassed with 95% O_2/ 5% CO_2 (pH 7.2, 280-290 mOsm, 32 °C) for 2 minutes. The brain was then mounted on the stage of a vibrating slicer containing a Peltier temperature controller (World Precision Instruments, Sarasota, FL), and 500 um parasagittal slices were cut as in Figure 3-3. Slices containing the VTA and NAcc were incubated in cutting aCSF for approximately 40 minutes. Slices were then placed on 30 mm Millipore (Billerica, MA) CM membrane inserts housed in six well plates containing 1.2 mL per well of HEPES-buffered media (75% MEM, 25% heat activated horse serum, 3mM L-glutamine, 100 U/mL penicillin/streptomycin, and 5.5 mg/mL dextrose). Explants were incubated in 5% CO_2 at 37°C, and media was changed 24 hours after explanting and then subsequently every 48 hours. These explants were fully transformed into cultures and became translucent or "cleared" after 7- 10 days *in vitro*.

3-3.3. Tyrosine Hydroxylase Immunohistochemistry of Explants

Staining for TH was performed with a polyclonal rabbit anti-TH antibody (Chemicon International, Temecula, CA) and a secondary 3-3'-diaminobenzidine tetrahydrochloride (DAB) staining kit for rabbit antibodies (Santa Cruz Biotechnology, Inc, Santa Cruz,

CA). Explants were rinsed with PBS to remove all media. Fixation of the explant on the membrane insert was completed after a 1-4 hour incubation at room temperature with 4% paraformaldehyde and 0.12 M sucrose. The explants were then incubated in 0.1 M glycine in PBS overnight at 4 °C and were carefully removed from the insert membrane using a cell harvester and a precision sable brush. The slice was permeabilized with the detergent triton (0.2% in PBS) at 4 °C overnight. The following day, explants were incubated in 10% goat serum for 1 hour at room temperature on an oscillating shaker at 70 rpm. The explants were washed three times with 0.2% triton in PBS for 10 minutes at 70 rpm. Then the slice was incubated for 48 hours at 4 °C in primary antibody dilutions of 1:1000 in 0.2% triton containing 2.8% goat serum and washed three times in 0.2% triton in PBS as before. During these washes, the AB enzyme reagent was prepared 30 minutes before use. Reagent A (avidin, 50 uL) was added to reagent B (biotinylated horseradish peroxidase, 50 uL) in 2.5 mL of PBS. The tissue was incubated at room temperature for 1 hour in this AB reagent. Explants were again rinsed three times for 10 minutes in 0.2% triton in PBS. Distilled H_2O (1.6 mL) was then combined with 5 drops of 10x substrate buffer, 1 drop of 50x DAB chromogen, and 1 drop of 50x peroxidase substrate. Explants were incubated in this solution for approximately 40 seconds and then rinsed with PBS. Processed explants were mounted on gelatin-subbed slides and allowed to dry at 4°C before cover slips were attached.

Figure 3-4 shows examples of cells in the parasagittal explant that are positive for the enzyme TH. The presence of projecting TH positive dopaminergic cells in the appropriate brain regions suggests an intact mesolimbic pathway in the parasagittal

explant. All the explants from the immunocytochemistry experiments contained cell bodies that were positive for TH. Additionally, 85% of explants had staining in the ventral striatum which contains the NAcc. The remaining 15% were explants that were damaged during the staining process, and the ventral striatum could not be distinguished. Figure 3-4A shows a single cell with long projections toward the NAcc. Figure 3-4B is a low power magnification of the midbrain of an explant with many cells positive for TH in the area of the VTA. Although TH staining is seen in the ventral striatum and in the midbrain of these explants, it does not prove that dopaminergic cells and projections are intact for all explants.

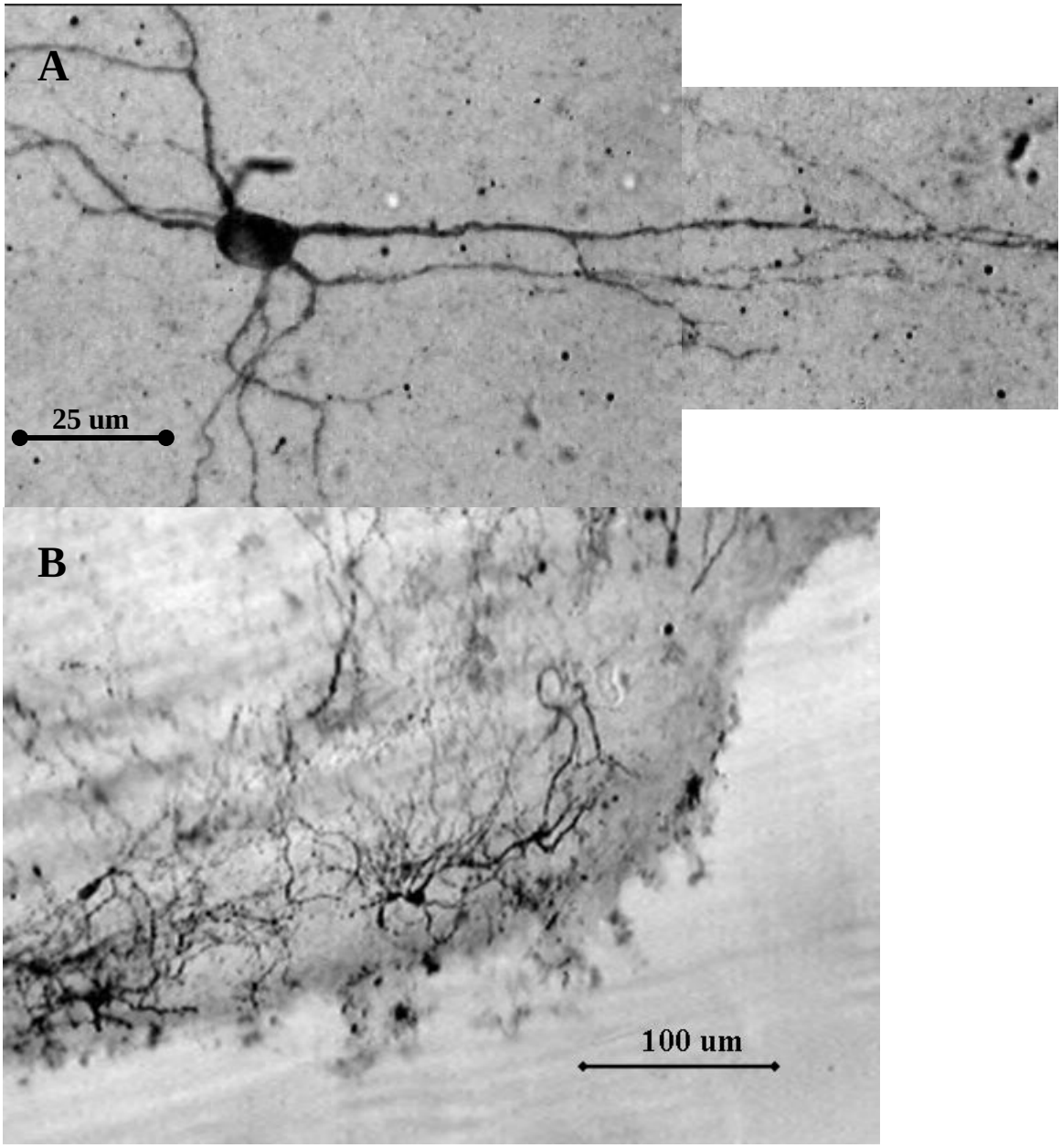

Figure 3-4. Tyrosine Hydroxylase (TH) immunohistochemically stained explants exemplifying the presence of dopaminergic cells in parasagittal explants. A) A single TH positive cell with its characteristic projecting processes. B) Low magnification of the midbrain of a TH stained explant shows many cells positive for TH in an area which includes the VTA.

3-4. MULTI-PHOTON LASER SCANNING MICROSCOPE PARAMETERS AND DETECTION OF EGFP FLUORESCENCE

The use of positive controls was invaluable for characterizing the MPLSM. Brain slices of transgenic mice with the S100 promoter coupled to GFP were fixed and placed on slides (kindly provided by Dr. Wes Thompson, University of Texas at Austin). They provided ideal positive controls, as a strong signal was always available and bleaching did not appear to be a factor. These slides were used to empirically determine the proper wavelength to excite eGFP to study laser power versus fluorescence emission phenomena, and for daily laser alignment of the detectors.

The bioluminescence marker GFP was first cloned from the jellyfish *Aequorea Victoria* in 1992 (Prasher et al., 1992). GFP is comprised of 238 amino acids. eGFP was generated following random mutations at the Ser-Tyr-Gly sequence at amino acids 65-67, and fluorescence-activated cell sorting established variants that were 35-times more fluorescently intense than wildtype GFP. Codon optimization also allowed for greater expression in mammalian cells, and codon optimization together with random mutation amplified fluorescence intensity by 100-fold compared to wildtype GFP (Cormack et al., 1996; Zhang et al., 1996a). A reduction in bleaching is also a molecular characteristic of eGFP; a beta-can molecular structure surrounds the fluorophore,, protecting it from reactive agents that cause bleaching (Yang et al., 1996). GFP and its variants are widely used, not only for protein localization, but as a marker for gene expression.

The laser/light path of the MPLSM was relatively simple. A Spectra-Physics (a division of the Newport Corp, Irvine, CA) Millenia 5W argon (532 nm) source was used as the constant wave laser pump. The pump laser powered the Spectra-Physics Tsunami titanium:sapphire laser which was tunable and has the ability to mode lock for multi-photon excitation. Excitation power independent of wavelength and mode lock was controlled via a ½ wave plate and a polarizer used as a laser attenuator placed between the titanium:sapphire source and scanhead. Laser wavelength and mode status were observed through an Ocean Optics (Dunedin, FL) spectrometer. Mirrors directed the laser to the modified Olympus (Melville, NY) Fluoview scanhead. The scanhead was originally designed for confocal microscopy; therefore, the conversion to two-photon mode required removal of the neutral density filter and confocal aperture pinhole assemblies. Standard galvo-mirrors were retained; however, an infrared pupil transfer lens was supplanted for the standard optic. Since the laser was mode locked, it could not be launched efficiently via a fiber optic and must therefore be direct-launched. The laser was directed onto the stage of an upright brain slice Olympus (Melville, NY) BX-50W1 microscope. eGFP emission was collected via the scanhead galvo-mirrors, filtered through a cuvette of $CuSO_4$, and detected using standard Fluoview photomultiplier tubes. The focal plane of the objective was motorized and controlled by Fluoview software (version 2.0.32) using a fine focus z-motor for optical sectioning. The microscope stage was also motorized in the xy-plane for specimen alignment. This overall configuration was similar to other Olympus confocal microscopes that have been altered for MPLSM (Mainen et al., 1999; Majewska et al., 2000).

The relationship between laser power and fluorescence emission is demonstrated in Figure 3-4. Detector settings and the wavelength were kept constant and only non-

saturated emission levels were used for this power-emission assessment. Figure 3-4 illustrates that as laser power increased, fluorescence emission also increased; however, multi-photon excitation is a non-linear fluorescence technique. The emission is quadratically related to the power of the laser. This is indicated by the log transformation of values and a resultant linear fit with a slope near two.

When working with living cells, it is important to keep damage to a minimum. For this reason, a laser power of no more than 100 mW was used in these experiments, which resulted in a consistent fluorescence emission but did not cause cell death during the course of experiments. Electrophysiological studies in our lab also indicated that dissociated cultured neurons reliably survived dozens of sequential scans with a laser power of 100 mW (data not shown). Photodamage is decreased in multi-photon excitation as compared to confocal excitation; however, due to the greater laser intensities needed for multi-photon excitation, some cellular damage may occur (Eggeling et al., 1998; Koester et al., 1999; Konig et al.,1999).

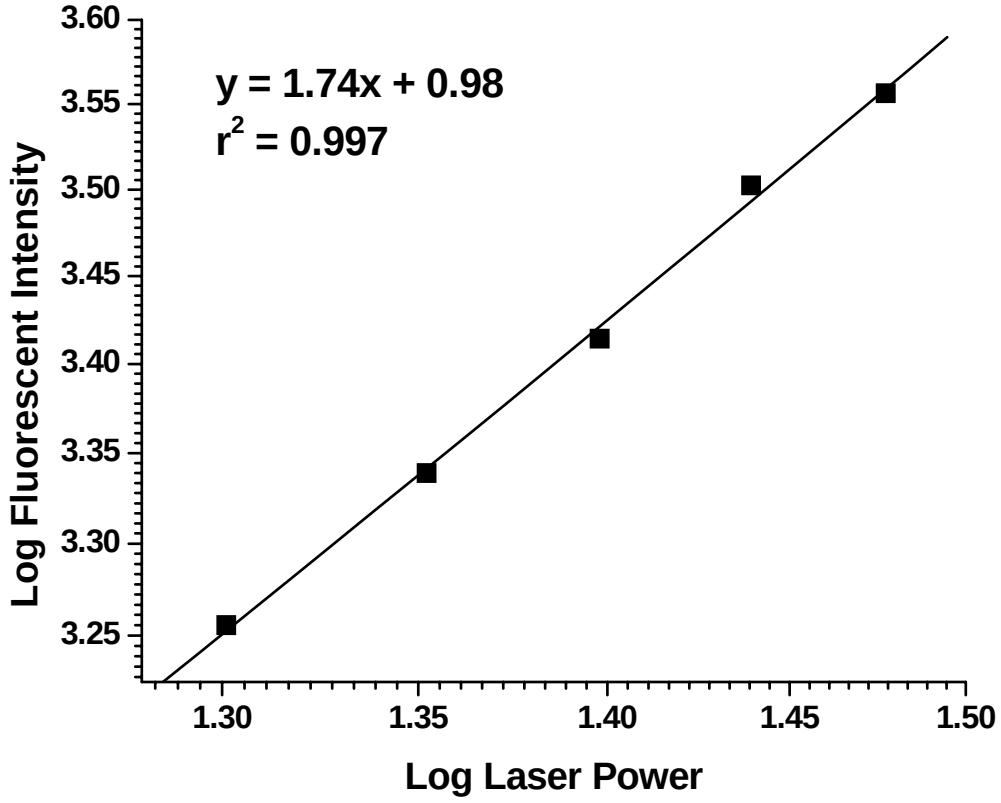

Figure 3-4. Log-log plot of laser power versus fluorescence emission. There is a strong linear relationship between log transformed laser power and log transformed fluorescence emission. With a resulting linear fit slope near two, the quadratic nature of multi-photon excitation and resultant fluorescence emission is observed.

The proper wavelength for optimal efficiency of eGFP excitation was also empirically determined. For this experiment, the power and detector settings were kept constant. As seen in Figure 3-5, a suitable wavelength for eGFP excitation was observed to be about 845 nm; shorter wavelengths displayed greater autofluorescence levels, whereas wavelengths longer than 845 nm did not elicit strong two-photon excitation of eGFP. The stability of the pulse was also taken into account; this MPLSM pulsed very reliably at 845 nm.

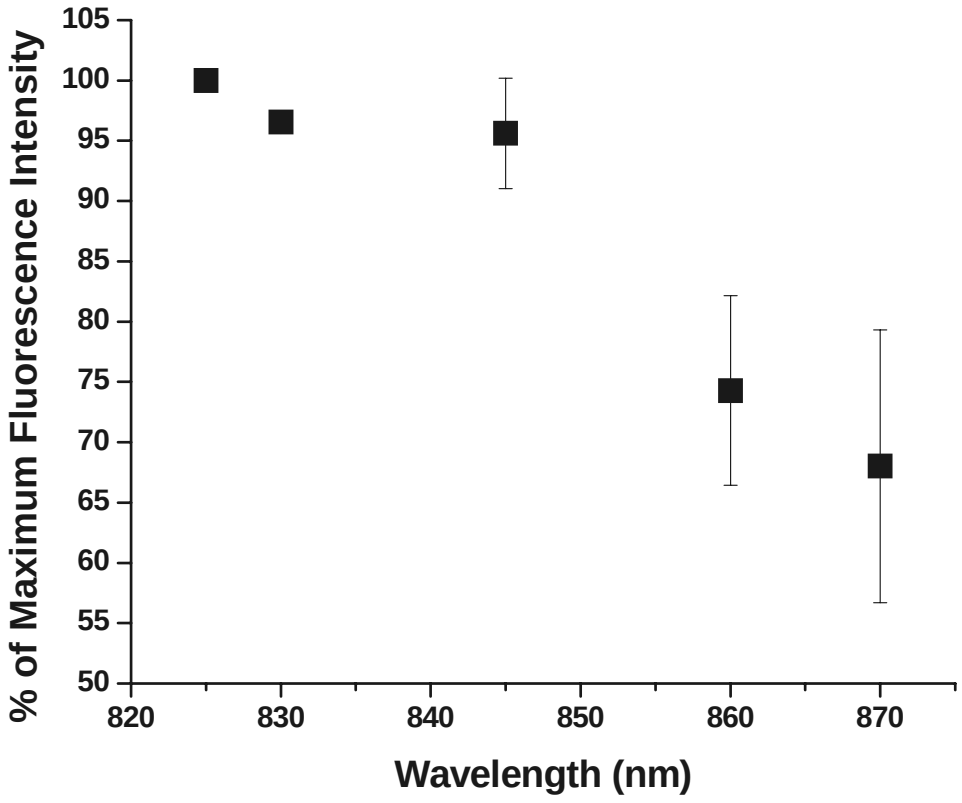

Figure 3-5. Wavelength of multi-photon laser versus the resulting fluorescence intensity as a percent of maximum.

The Olympus BX50WI microscope was equipped with a z-motor which functions in concert with Fluoview software and the multi-photon excitation laser to produce three-dimensional representations of cells by optical sectioning. This optical sectioning allowed "stacks" of images to be acquired that encompass an entire cell. These stacks were required to compare cells for receptor localization with MPLSM. Stacks are a set of two dimensional images, with the difference between two adjacent images being of a known distance controlled by the z-motor. Multi-photon excitation occurs at a very restricted focal volume since the coincidence requirement for two photons to excite one electron is spatially restricted to a very small plane. Additionally, there was thermal and physical drift of viable cells in intact explants that require a three-dimensional image to be reconstructed for cell comparisons. One image acquired of a cell would not reliably encompass the entire cell, and subsequent images of the same cell (although programmed at the same focal plane) may not be of the same focal plane due to thermal and or vibrational movement-induced aberrations. Therefore, to image an entire cell *in situ*, cells were "bracketed" by z-sectioning and resulting two-dimensional images were analyzed subsequently for changes in fluorescence localization.

The stacks were combined into a two-dimensional image (Figure 3-6) by aligning the brightest pixels from each image of the stack and combined into a three-dimensional representation (Figure 3-7), corresponding to the differences that occur between images in the stack by Metamorph imaging software (Universal Imaging Corporation, Downingtown, PA). Stacks rendered into two-dimensional images were quantified by the intensity of fluorescence along the entire cell. Details of these analyses are provided in

Chapter 4. As living cells were being treated, multiple stack-derived images of the same cell were compared for each treatment. Many characteristics were available for regions of interest (ROI) within each cellular image; however, the maximum fluorescence intensity was chosen because it is associated with clustering of the receptor since an increase in this value would indicate the coalescence of fluorescence puncta or clustering. An increase in maximum intensity of a ROI would be interpreted as receptor clustering as this would result in more fluorescence tags grouped together to form a cluster of D1DRs. Fluorescence in infected explants was stable or would decrease slightly as some fluorescence bleaching does occur for vehicle-treated explants. The maximum intensity of fluorescence does not change significantly in corresponding regions of the cell after 60 minutes except with a drug treatment that induces receptor trafficking.

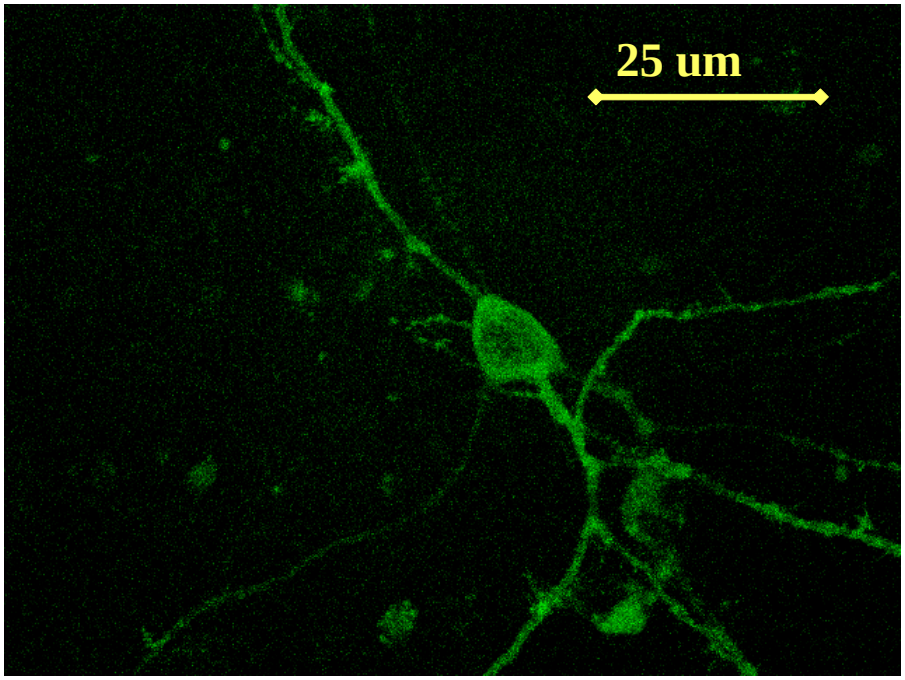

Figure 3-6. Two-dimensional representation of a z-axis stack. The brightest pixels in each image of the stack are combined to make one two-dimensional image.

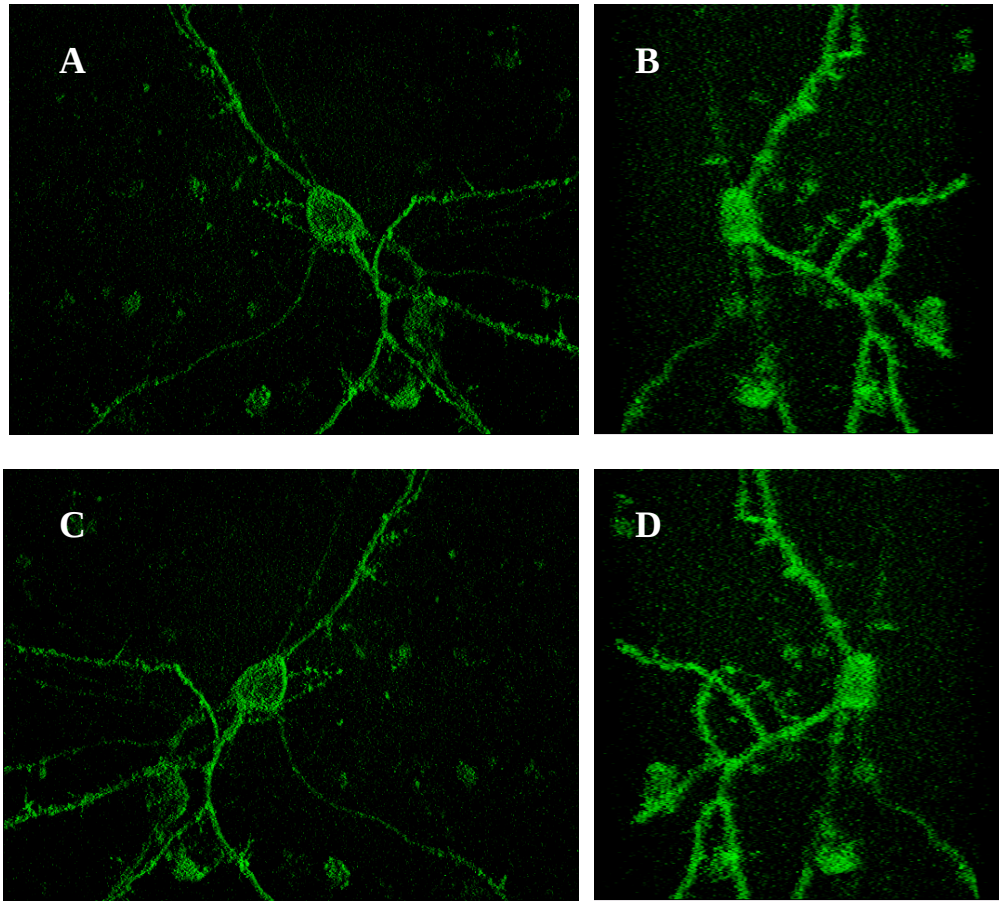

Figure 3-7. Different viewing angles from a three-dimensional image that was created from a z-axis stack. A) Results were the same as the two-dimensional image made in Figure 3-6. B) Right side view of cell. C) 180° view from A. D) Left side view of cell.

Orthogonal planes of the cell were also investigated since the stack is a three-dimensional representation of the cell. If the two-dimensional image made from the stack (as in Figure 3-6) was defined as the xy- plane, orthogonal planes of xz and yz were also made where z corresponds to the objective depth. The xz-plane corresponds to a plane protruding out of the xy-plane in a horizontal manner; while the yz-plane corresponds to a plane protruding out of the xy-plane in a vertical manner (see Figure 3-8). Orthogonal planes were examined in multiple cells where increases in fluorescence were observed in order to demonstrate a more conclusive localization of clustering and to show the position of the cluster of eGFP-D1DR relative to the cell surface.

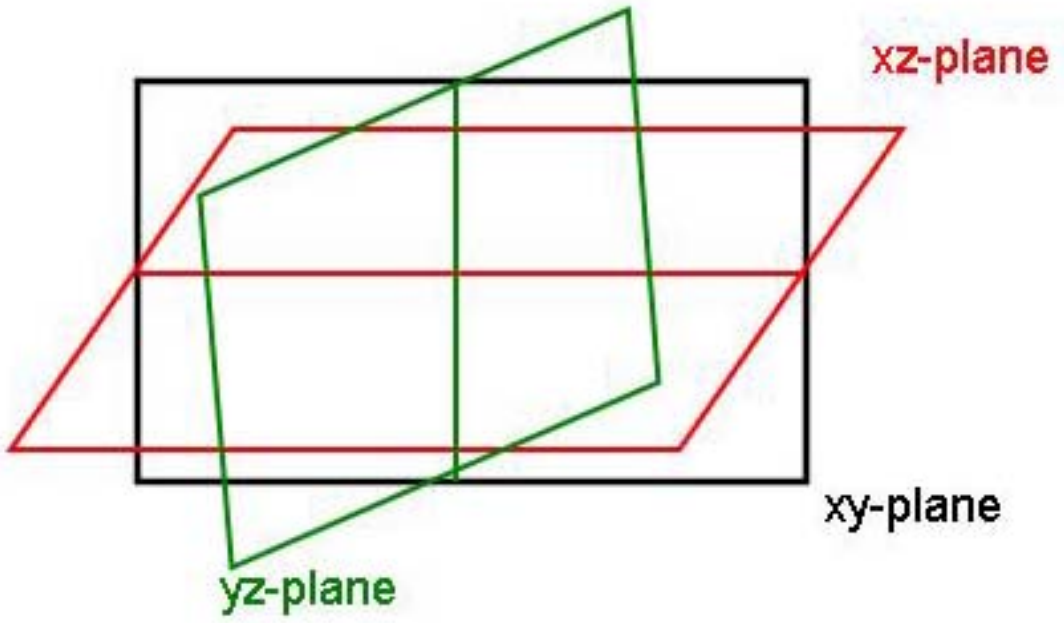

Figure 3-8. Illustration of the three orthogonal planes that can be examined using Metamorph. These additional views help to determine the localization of clusters to determine position relative to the cell surface.

Chapter 4: Dopamine and Ethanol Induced Trafficking of eGFP-D1DR in Parasagittal Explants

4-1. INTRODUCTION

The mesolimbic pathway has been implicated in the rewarding actions of drugs of abuse (Wise, 1996; Koob et al., 1998). This dopaminergic pathway originates in the VTA and projects to the NAcc and other areas (Ungerstedt, 1971; Oades and Halliday, 1987; Van Bockstaele and Pickel, 1995; Feldman et al., 1997). The principle neurons of the NAcc are medium spiny neurons (Meredith, 1999). The major output of the NAcc is to the ventral pallidum (Swanson and Cwan, 1975); however, medium spiny neurons also project back to the VTA, creating feed-back circuitry (Walaas and Fonnum, 1980; Heimer et al., 1991). Drugs of abuse increased extracellular dopamine in the NAcc through a variety of mechanisms. For instance, ethanol directly stimulated the dopaminergic cells of the VTA (Brodie et al., 1999) and increased the neuronal firing rate which induced the synaptic release of dopamine into the NAcc. Since ethanol and other drugs of abuse may be associated with enhanced extracellular dopamine levels in the NAcc, the post-synaptic neuroadaptations resulting from elevated dopamine may be significant to understanding drug abuse and addiction.

D1DRs mediate a substantial component of dopaminergic signaling in the NAcc (Boyson et al., 1986; Hersch et al., 1995; Caille et al., 1996). Like other receptors belonging to the GPCR family, these receptors undergo agonist-induced desensitization (Kallal and Benovic, 2000). D1DR desensitization may occur by multiple mechanisms, including 1)

uncoupling from the G-protein (Memo et al., 1982), 2) internalization of the receptor (Ng et al., 1995) and 3) down regulation of D1DR expression of the (Barton and Sibley, 1990). D1DR internalization upon agonist stimulation has not been observed previously in viable mammalian cells.

Not only can ethanol directly stimulate the dopaminergic cells of the VTA, it also alters cAMP-mediated cascades stimulated by dopamine and other receptors in a variety of cell types. Acute ethanol exposure increased cAMP production upon stimulation of receptors coupled to adenylyl cyclase (Hynie et al., 1980; Gordon et al., 1986). Since modulation of the cAMP cascade via cAMP analogs was associated with desensitization of the D1DR (Black et al., 1994), it is feasible that ethanol (acting on cAMP) could also induce D1DR desensitization. The hypothesis of this dissertation project is that ethanol will induce internalization of D1DRs; however, the distinction between pre- (dopamine release in the NAcc) and post-synaptic actions (cAMP modulation) of ethanol can not be concluded.

If dopamine and ethanol can individually induce D1DR clustering and internalization, then a pretreatment of ethanol, thereby priming cAMP cascades, may increase the internalization induced by dopamine alone. Dopamine and ethanol modulation of the localization and thereby function of the D1DR could contribute, at least in part, to the neuroadaptive changes associated with addiction in the mesolimbic system. In order to test this hypothesis, parasagittal brain slice explants were studied that include viable medium spiny neurons of the NAcc that retain many synaptic connections observed *in vivo*. Explants were infected with a sindbis pseudovirus modified to express eGFP-

D1DR. Thus, labeled D1DRs were localized in real-time using MPLSM. Our results indicate that high levels of dopamine receptor activation caused eGFP-D1DRs to cluster away from the cell surface, consistent with desensitization in the form of receptor internalization. However, a lower level of dopamine that did not induce receptor clustering alone, when pretreated with ethanol, appeared to act in concert with ethanol to cause clustering. Ethanol alone also produced receptor clustering. The clustering was inhibited by the D1DR antagonist SCH 23390.

4-2. METHODS

4-2.1. Explant Preparation

Parasagittal explants were prepared from Sprague Dawley rat pups as described previously (see section 3-3.2 Explant Methods).

4-2.2. Infection of Explant

The subcloning of eGFP-D1DR into the sindbis pseudovirus was described in chapter 2 and has also been published by our lab (Diaz et al., 2004). Explants were infected at 2-6 locations on each slice using 50-100 nL of virus per injection. Cells were imaged approximately 48 hours after infection.

4-2.3. Multi-photon Laser Scanning Microscopy

eGFP fluorescence was induced by two-photon excitation at 845 nm using a mode-locked Spectra-Physics (A division of Newport Corp, Irvine , CA) Tsunami titanium:sapphire laser pumped by a Millenia 5W argon source (as described previously in section 3-4.).

Acquisition of fluorescence data was controlled by a modified Olympus (Melville, NY) Fluoview scanhead mounted on an Olympus BX-50W1 microscope (40x WI objectives and 1-5 x digital zoom). Fluoview-controlled stacks were collected along the z-axis, with z-steps of 0.5-0.7 um for three-dimensional imaging of individual neurons in explants. Laser power was approximately 100 mW measured at the Tsunami and was confirmed before the acquisition of each stack in order to verify laser stability and constant excitation levels. The photomultiplier tube detector settings were kept constant for each cell at each time point. Therefore, differences in fluorescence were presumed to be indicative of biological changes and not of changes in excitation or detection. Offline quantification and image analysis were completed using Metamorph imaging software (Universal Imaging Corporation, Downingtown, PA).

4-2.4. Explant Treatments

Explant membrane inserts were securely attached to a removable custom-made chamber that was attached to the microscope stage. The chamber consisted of a base secured to the microscope stage with two small clamps that fastened the insert to the chamber base by thumbscrews. An opening was centered in the base of the chamber and a glass slide was glued for a transparent field of view. The perfusion buffer was Hank's Balanced Salt Solution (HBSS, Invitrogen, Carlsbad, CA) containing in (mM): $CaCl_2$ (1.3), $MgCl_2$-$6H_2O$ (0.5), $MgSO_4$-$7H_2O$ (0.4), KCl (5.3), KH_2PO_4 (0.4), NaCl (138), Na_2HPO_4-$7H_2O$ (0.3), Dextrose (5.5), with added HEPES (11), $NaHCO_3$ (25), and L-Ascorbic Acid (0.2). HBSS was gassed continuously with 95% O_2/ 5% CO_2) and perfused continuously across the chamber at 1.5 mL/min. HBSS was perfused through an in-line heater (32-35 °C)

located between the HBSS reservoir and the custom made chamber. The bath level was maintained by suction from a glass capillary (2mm) connected to a waste reservoir.

All explants were treated with HBSS for a baseline image collected at time zero minutes. A control group was exposed to HBSS for all time points: 0, 30 and 60 minutes. After baseline imaging, treatment groups were exposed to drug solutions in 30 minute intervals. Experiments were designed to test clustering and/or internalization induced by dopamine, ethanol pretreatment of dopamine, or ethanol treatment alone. Specific treatments are provided in Table 4-1-Table 4-3.

Table 4-1. Treatment groups for control and dopamine experiments

Group	Condition at t = 0 min	Condition at t = 30 min	Condition at t = 60 min
Control	HBSS	HBSS	HBSS
Dopamine (50 uM)	HBSS	HBSS	Dopamine (50 uM)
Dopamine (100 uM)	HBSS	HBSS	Dopamine (100 uM)
SCH 23390 (20 uM)	HBSS	SCH 23390 (20 uM)	SCH 23390 (20 uM) + Dopamine (100 uM)

Table 4-2. Treatment groups for ethanol pretreatment experiments

Group	Condition at t = 0 min	Condition at t = 30 min	Condition at t = 60 min
Dopamine (50 uM)	HBSS	HBSS	Dopamine (50 uM)
Ethanol (50 mM) / Dopamine (50 uM)	HBSS	Ethanol (50 mM)	Dopamine (50 uM)
Ethanol (100 mM) / Dopamine (50 uM)	HBSS	Ethanol (100 mM)	Dopamine (50 uM)
Pretreatment + SCH 23390 (20 uM)	HBSS	SCH 23390 (20 uM) + Ethanol (100 mM)	SCH 23390 (20 uM)+ Dopamine (50 uM)

Table 4-3. Treatment groups for ethanol experiments

Group	Condition at t = 0 min	Condition at t = 30 min	Condition at t = 60 min
Control	HBSS	HBSS	HBSS
Ethanol (50 mM)	HBSS	Ethanol (50 mM)	Ethanol (50 mM)
Ethanol (100 mM)	HBSS	Ethanol (100 mM)	Ethanol (100 mM)
Ethanol + SCH 23390 (20 uM)	HBSS	SCH 23390 (20 uM)+ Ethanol (100 mM)	SCH 23390 (20 uM)+ Ethanol (100 mM)

4-3. IMAGE ANALYSIS

Each stack of images was converted into a two-dimensional projection image using the Metamorph stack arithmetic command with the maximum factor chosen. This command acquires the maximum intensity for each pixel position throughout the entire stack, resulting in one image that represents the maximum intensity of the entire cell. This was done for each cell at time points 0, 30 and 60 minutes.

ROI were determined in a multi-step process. Typically, about 50-70 z-steps (0.5-0.7 um per step) were completed for a cross-section z-distance of about 25-50 um. The cells were not completely stable in position due to physical and thermal drift inherent in real-time imaging of a perfused preparation; this made direct image comparisons difficult since the required degree of overlay of cell processes was highly unlikely. Therefore, smaller more stable areas of each cell were aligned using Metamorph software at the baseline and final images. After alignment, an image subtraction was performed and this subtraction image then underwent thresholding. Thresholding enables the software to automatically detect ROIs which correspond to changes between the final and baseline images. These ROIs

were reassigned as circles with an approximate diameter of 15 pixels for uniformity. ROIs were then transferred from the subtraction image to the original stack-generated two-dimensional images for each sampled time point. Individual ROIs were realigned and analyzed using Metamorph to measure the maximum fluorescence intensity for each ROI at each time point. While many characteristics were available to quantitate ROIs, the maximum fluorescence intensity was chosen because it is associated with receptor clustering. Two primary measures were provided by this analysis: 1) the greatest increase in maximum fluorescence intensity of a ROI for each cell and 2) the number of ROIs that increased more than 20% from baseline. These two measures provided different aspects of receptor clustering within the cell. The number of ROIs that increased more than 20% from baseline provides an overall view of clustering by the cell while the peak increase in fluorescence intensity reflects the brightest cluster. Therefore, this detection protocol was comprehensive and unbiased as the software was utilized to autodetect ROIs representative of changes in receptor localization or clustering.

Changes in fluorescence localization were inspected further by constructing images of orthogonal planes. Using Metamorph software, multiple areas associated with increased maximum intensity in the xy-plane were inspected in both the xz- and yz-planes by reanalysis of the stacks at these positions. These orthogonal planes gave further information on the three dimensional position of fluorescence intensity associated with receptor clustering. It is presumed that the orthogonal planes indicate if the clustering appears on the cell surface or within the cell; such changes not only indicate alterations in receptor localization but function as well.

4-3.1. Statistical Analysis

Two-way ANOVAs (treatment, time) with repeated measures followed by Bonferroni correction were completed on raw greatest increase in maximum intensity data. Post-hoc analysis by Student's T-test with Bonferroni correction of 8 (4 treatments, 2 time points) comparisons of interest was performed. Two-way ANOVAs (treatment, time) with repeated measures and Bonferroni correction were also completed on data normalized to the baseline image. Non-parametric Kruskal-Wallis statistical analysis with Dunn's multiple comparison test were used on frequency of increases in maximum fluorescence intensity of 20% or more at the 60 minute time point compared to baseline.

4-4. RESULTS

Due to the visual nature of these studies, images have been provided for qualitative analysis, followed by tables of raw data and graphs that provide quantitative measures for the effects of dopamine alone, ethanol priming dopamine and ethanol alone.

4-4.1. Control and Dopamine Experiments

First, the stability of eGFP-D1DR fluorescence was assessed over extended scanning periods. As described above in the methods section, the ROI assignment protocol was used to identify ROIs where eGFP-D1DR puncta were observed. Control cells, as shown in Figure 4-1, displayed no significant increase in maximum fluorescence intensity. Cells that were exposed to 50 uM dopamine also showed no significant increase in maximum fluorescence intensity in any ROI (Figure 4-2). Fluorescence stability was evident since there were not any ROIs that increased in maximum fluorescence intensity of 20% or more (Figure 4-8). When cells were treated with higher concentrations of dopamine (100 uM), an increase in maximum fluorescence intensity was seen in discrete ROIs (Figure 4-

3). This clustering of fluorescence (and hence receptors) appeared to be centered inside of the cell process as illustrated using orthogonal planes. Interestingly, Figure 4-4 is a second example of dopamine (100 uM) treatment that exemplifies clustering of the receptor toward the cell surface as revealed by viewing the orthogonal planes. Clustering was partially blocked by the D1DR antagonist, SCH 23390 (20 uM) as seen in Figure 4-5.

We wanted to further verify that puncta identified by the automated ROI protocol were indeed discrete ROIs exhibiting consistent changes in eGFP-D1DR fluorescence. Thus, random ROIs were also measured by obtaining coordinates assigned using the random number generator in Microsoft Excel (2002 version 10.2614.2625 Microsoft, Redmond, WA). The dimensions of each image were 640 x 480 pixels; therefore, excel commands [RANDBETWEEN(0, 640), and RANDBETWEEN(0, 480)] were used to obtain random coordinates for ROIs. Random measurements illustrated that fluorescence intensity was stable despite treatment with SCH 23390 or 100 uM dopamine (Figure 4-6). Therefore, in this study clustering of receptors appears to occur only in discrete ROIs in cells that have been stimulated by a high level of dopamine (100 uM).

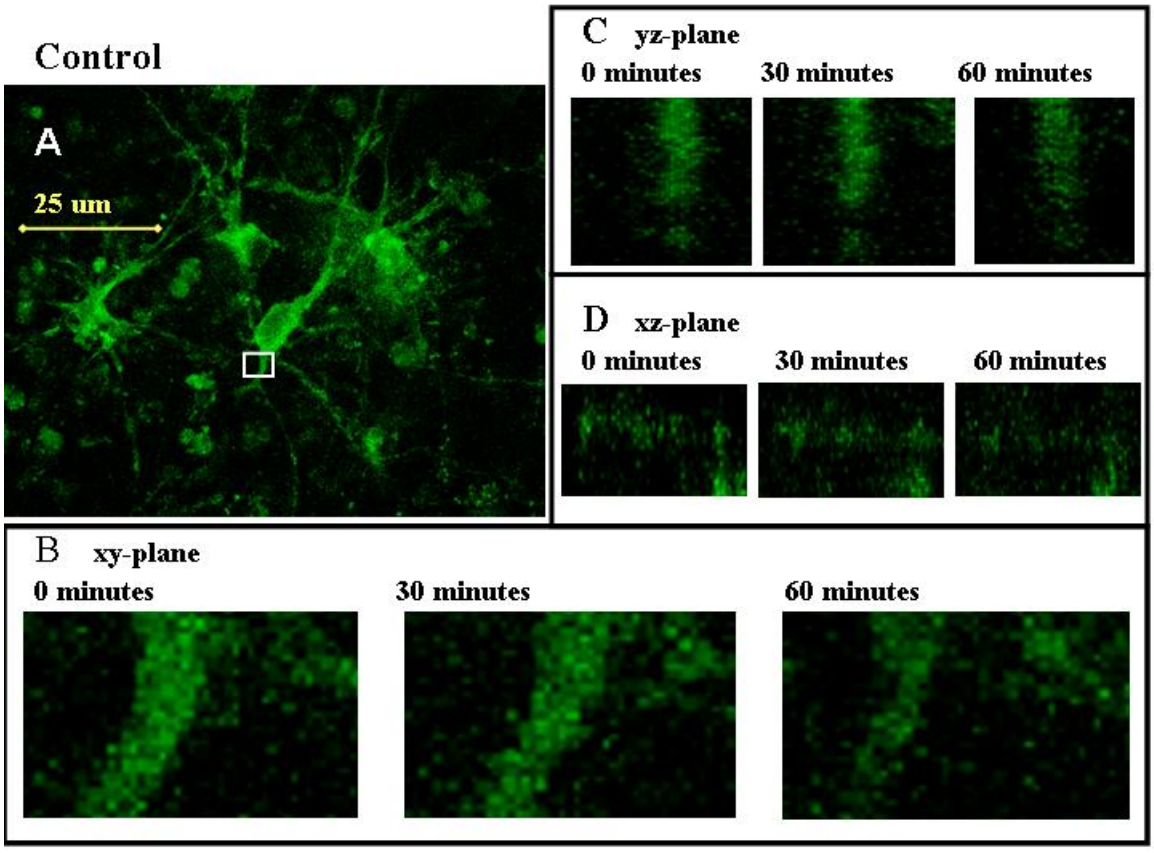

Figure 4-1. Example of a typical control neuron, treated with only HBSS buffer. A) A two-dimensional image of eGFP-D1DR fluorescence of a typical medium spiny neuron in the NAcc of a parasagittal explant (xy-plane). The white box indicates areas of magnification for additional planes. B) The xy-plane magnified in the area marked by the white box at 0, 30 and 60 minutes. C) The yz-plane magnified in the same area at 0, 30 and 60 minutes. D) The xz-plane magnified in the same area at 0, 30 and 60 minutes.

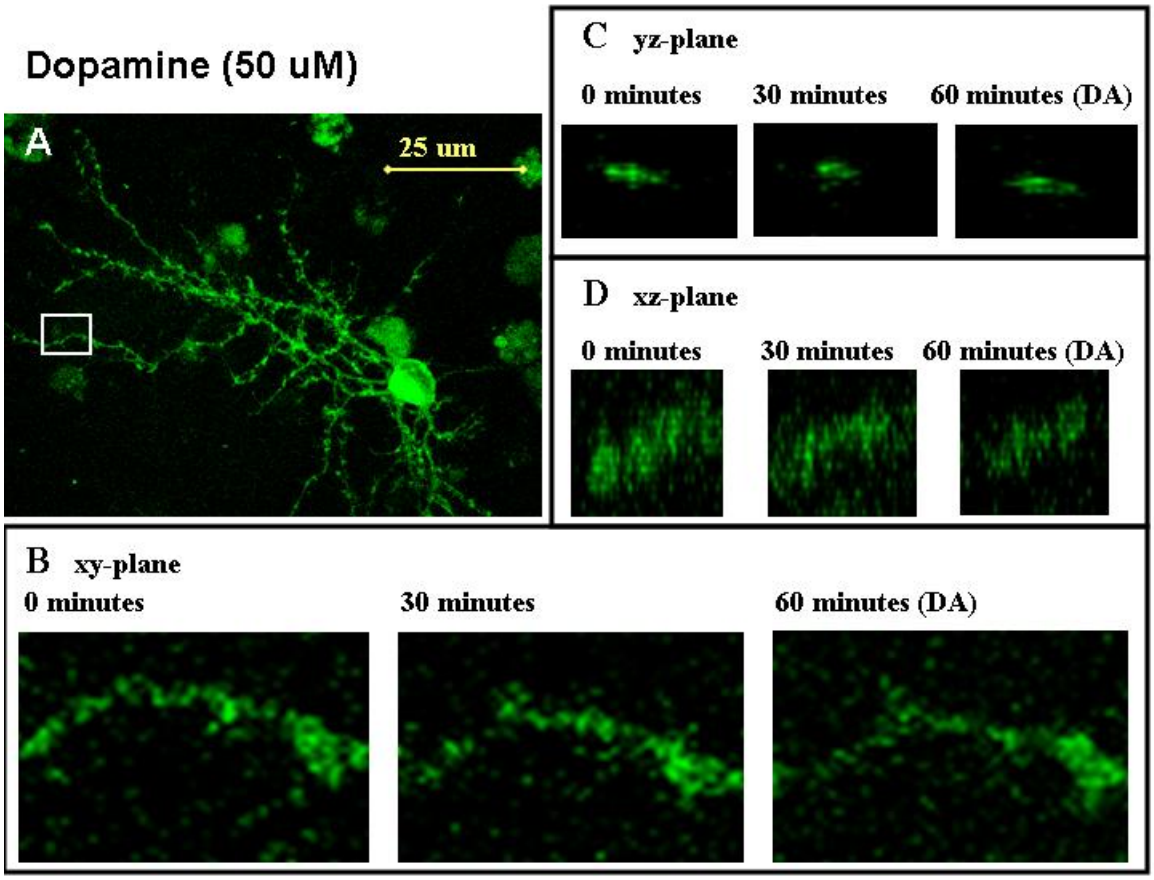

Figure 4-2. Example of a typical neuron exposed to dopamine (50 uM) for 30 minutes. A) A two-dimensional image of eGFP-D1DR fluorescence of a typical medium spiny neuron in the NAcc of a parasagittal explant (xy-plane). The white box indicates areas of magnification for additional planes. B) The xy-plane magnified in the area of the white box at 0, 30 and 60 minutes. C) The yz-plane magnified n the same area at 0, 30 and 60 minutes. D) The xz-plane magnified in the same area at 0, 30 and 60 minutes.

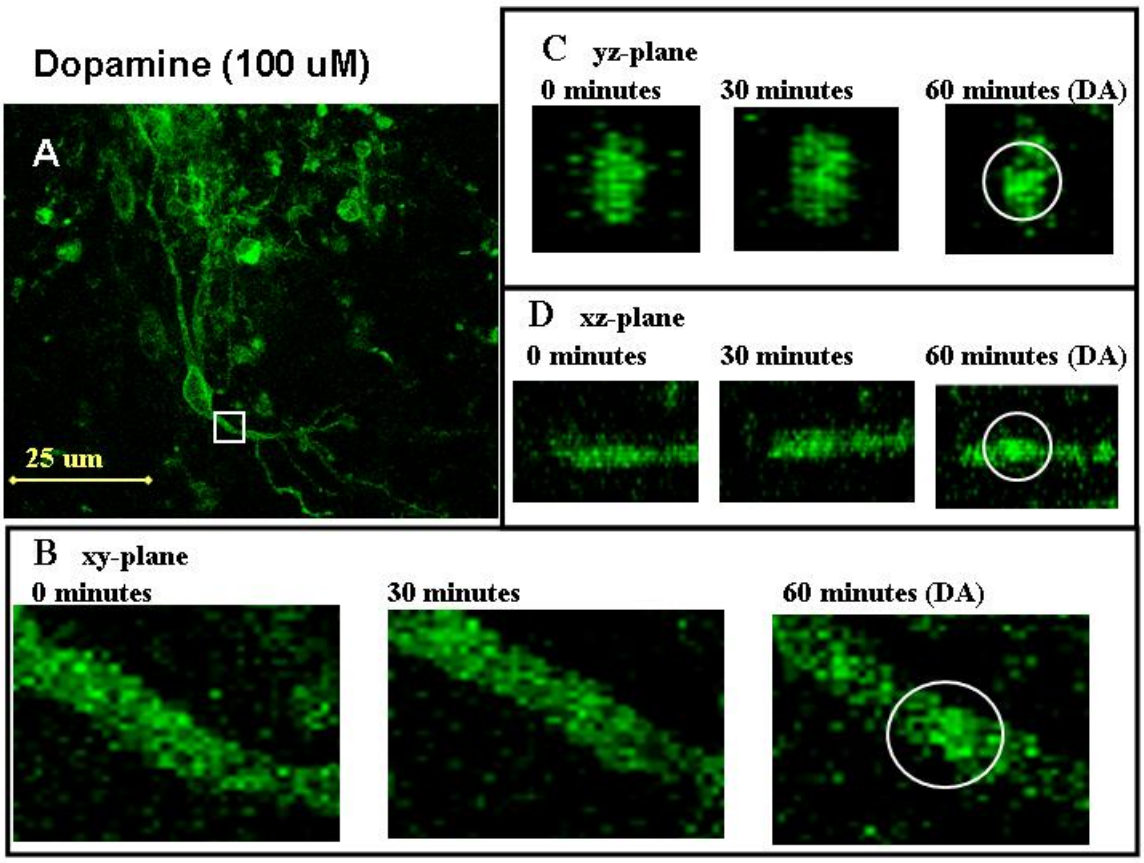

Figure 4-3. Example of a typical neuron exposed to dopamine (100 uM) for 30 minutes. A) A two-dimensional image of eGFP-D1DR fluorescence of a typical medium spiny neuron in the NAcc of a parasagittal explant (xy-plane). The white box indicates areas of magnification for additional planes. B) The xy-plane magnified in the area of the white box at 0, 30 and 60 minutes. C) The yz-plane magnified in the same area at 0, 30 and 60 minutes. D) The xz-plane magnified in the same area at 0, 30 and 60 minutes. The white circles show increase fluorescence intensity.

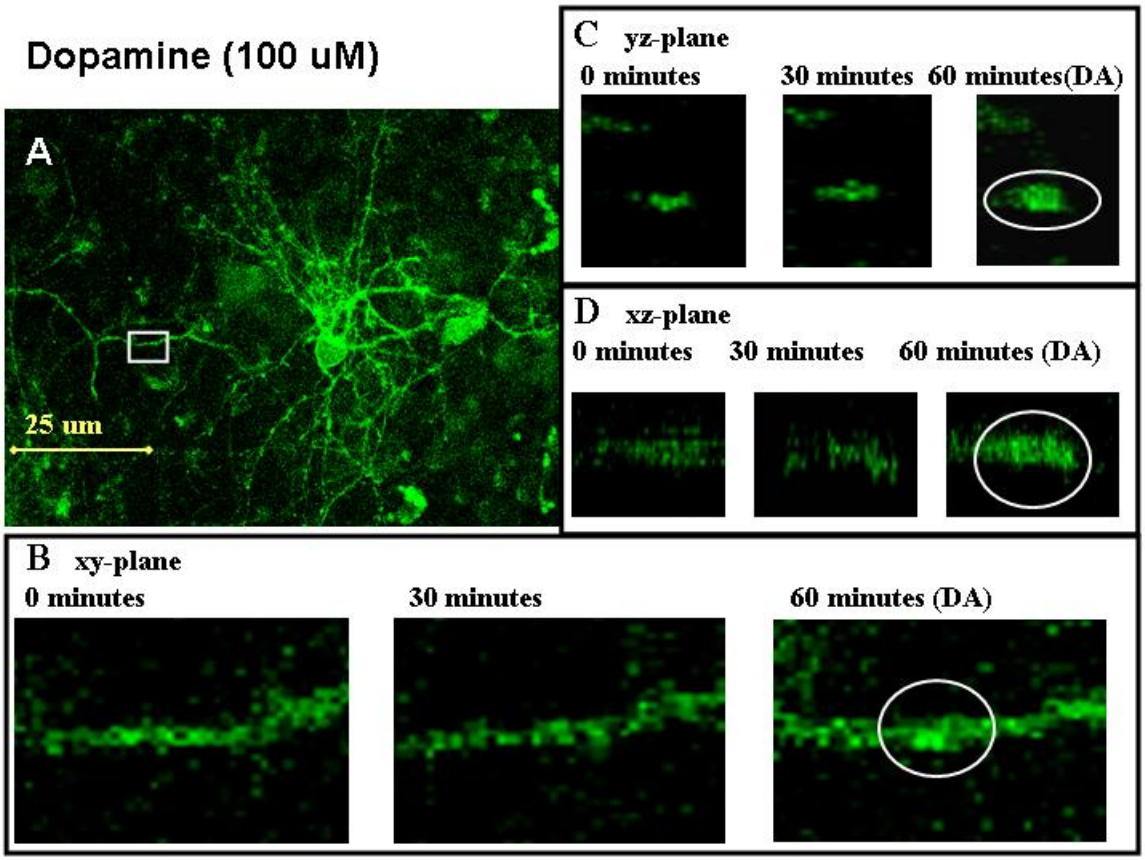

Figure 4-4. Example of a typical neuron exposed to dopamine (100 uM) for 30 minutes. A) A two-dimensional image of eGFP-D1DR fluorescence of a typical medium spiny neuron in the NAcc of a parasagittal explant (xy-plane). The white box indicates areas of magnification for additional planes. B) The xy-plane magnified in the area of the white box at 0, 30 and 60 minutes. C) The yz-plane magnified in the same area at 0, 30 and 60 minutes. D) The xz-plane magnified in the same area at 0, 30 and 60 minutes. The white circles show increase fluorescence intensity.

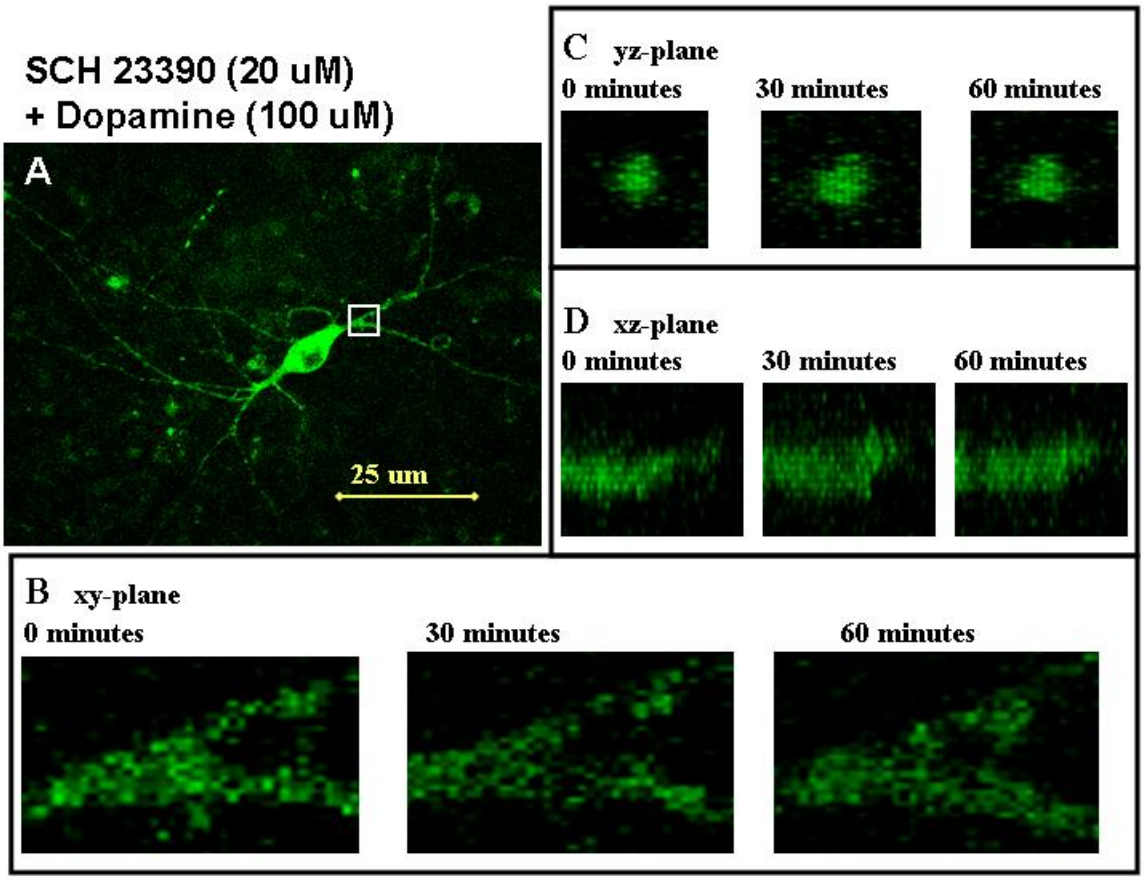

Figure 4-5. Example of a typical neuron exposed to SCH 23390 (20 uM) plus dopamine (100 uM) for 30 minutes. Treatment consisted of 20 uM SCH 23390 for 30 minutes followed by 20 uM SCH 23390 +100 uM dopamine for 30 minutes. A) A two-dimensional image of eGFP-D1DR fluorescence of a typical medium spiny neuron in the NAcc of a parasagittal explant (xy-plane). The white box indicates areas of magnification for additional planes. B) The xy-plane magnified in the area of the white box at 0, 30 and 60 minutes. C) The yz-plane magnified in the same area at 0, 30 and 60 minutes. D) The xz-plane magnified in the same area at 0, 30 and 60 minutes.

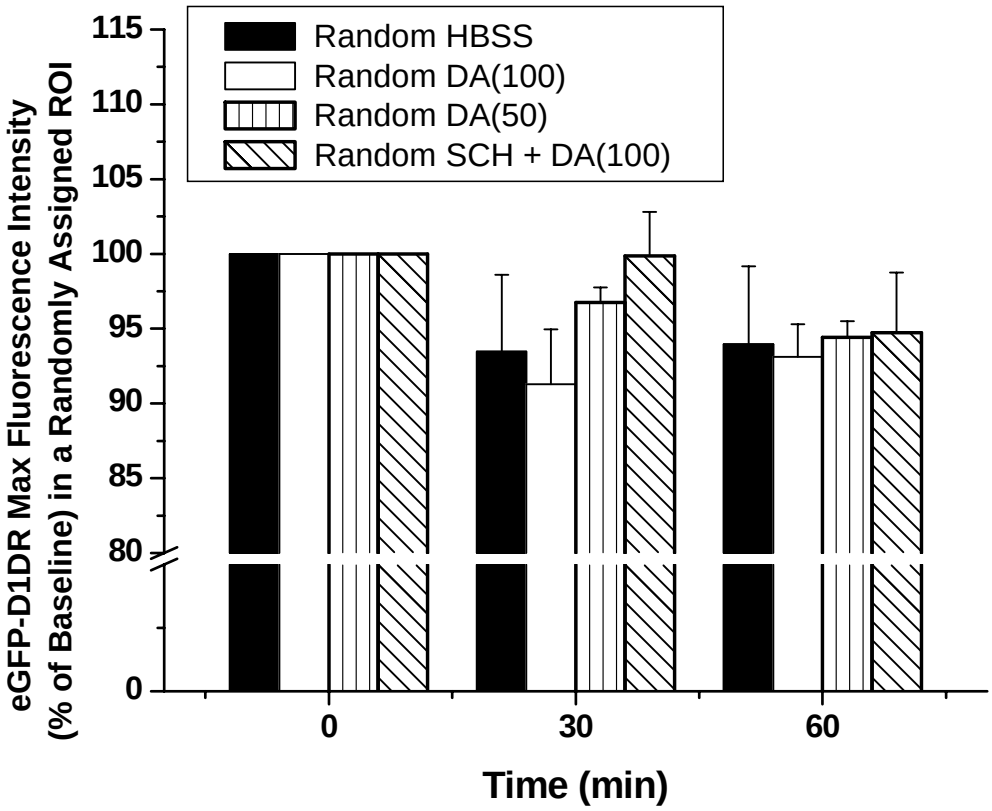

Figure 4-6. Randomly assigned regions of interest as a percent of baseline (0 time point) for dopamine experiments. Random coordinates were generated to determine that cells were generally stable. Cells displayed only a slight, non significant bleaching effect over time.

The raw data for the greatest increases in maximum fluorescence intensity (Table 4-4) were analyzed by two-way ANOVA (treatment, time); time was significantly different ($F(2, 32) = 9.86$ $P \leq 0.0005$) but treatment ($F(3, 32) = 1.56$, $P = 0.238$) and the interaction were not significantly different ($F(6, 32) = 2.26$, $P = 0.063$). Additionally, the baseline image and SCH 23390 (20 uM, 30 minutes) are not significantly different ($P = 0.658$), implying that SCH 23390 has no effect alone on D1DR clustering.

Table 4-4. Raw data for greatest increase in maximum fluorescence intensity at the 60 minute time point compared to baseline (0 minute time point) for dopamine experiments. Maximum fluorescence intensities are given in arbitrary units on a 12 bit scale (0 to 4095).

Treatment	Avg Max Intensity (0 min)	SEM	Avg Max Intensity (30 min)	SEM	Avg Max Intensity (60 min)	SEM
HBSS / HBSS / HBSS	2409	139	2262	267	2500	141
HBSS / HBSS / DA (50 uM)	2970	279	2853	191	3045	263
HBSS / HBSS / DA (100 uM)	2082	118	2258	154	2936	61
HBSS / SCH 23390 (20 uM) / SCH 23390 + DA (100 uM)	2238	353	2320	335	2565	396

Figure 4-7 illustrates the greatest increase in maximum fluorescence intensity as a percent of baseline (0 minute time point) for the 30 and 60 minute time points. A two-way ANOVA (treatment, time) analysis on the values (expressed as percent of baseline) revealed significant treatment ($F(3, 6) = 3.50$, $P \leq 0.05$) and time ($F(1, 16) = 11.92$, $P \leq 0.005$) effects but no significant interaction ($F(3, 16) = 2.37$, $P = 0.109$). A post-hoc evaluation by Student's T-test with 8 comparisons of interest (4 treatments, 2 time points) showed a significant difference for the 60 minute time point between control and dopamine (100 uM) treatment ($P \leq 0.05$) as well as a significant difference between dopamine (100 uM) and SCH 23390 (20 uM) plus dopamine (100 uM) ($P \leq 0.05$).

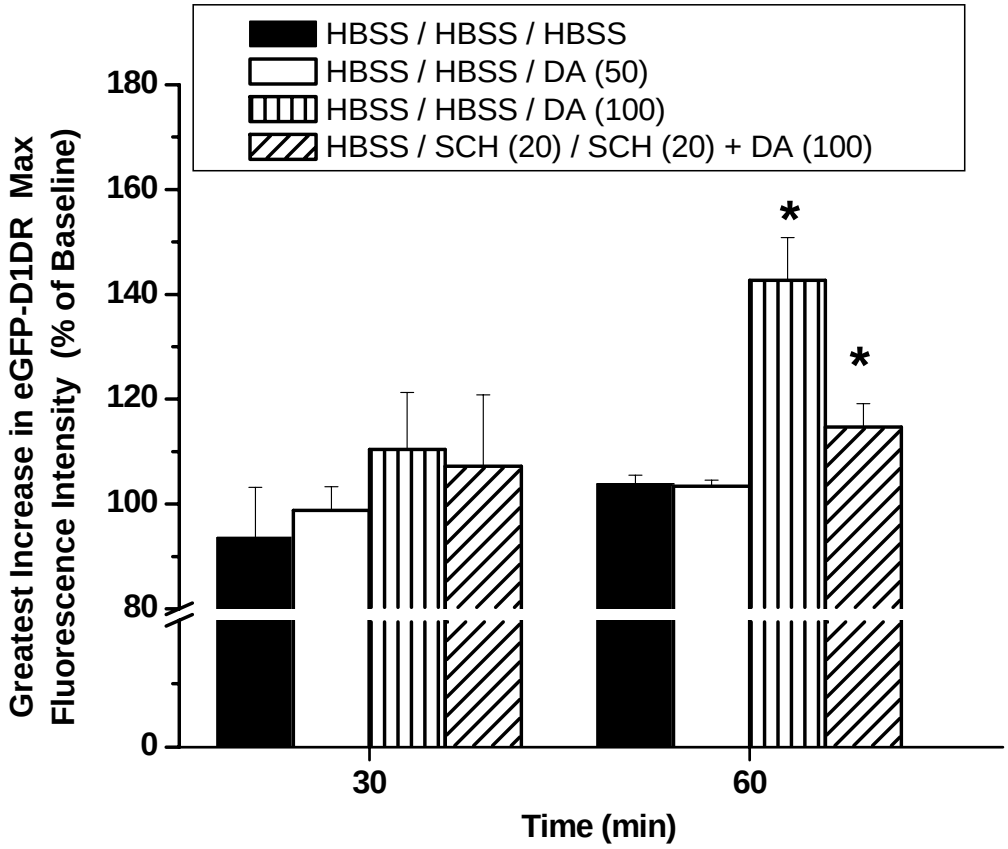

Figure 4-7. Control and dopamine experiment greatest increases in maximum fluorescence intensity at the 60 minute time point compared to baseline (0 minute time point). Control and dopamine- (100 uM) treated cells were significantly different at the 60 minute time point. SCH 23390 (20 uM) treatment significantly inhibited the effect of dopamine (100 uM). Error bars are ± SEM. Asterisks indicate results of statistical tests (see text for details).

No increases in maximum fluorescence intensity above 20% were observed at the 60 minute time point in control cells or cells exposed to 50 uM dopamine, thereby indicating that clustering of D1DRs was not detectable under these conditions. However, a higher concentration of dopamine (100 uM) produced D1DR clustering as seen by an increase in maximum intensity above 20% at the 60 minute time point compared to the baseline image (Figure 4-8). Kruskal-Wallis nonparametric statistics with Dunn's multiple comparison test showed a significant difference between dopamine (100 uM) treatment and control or dopamine (50 uM) treatment ($P \leq 0.01$) as well as between dopamine (100 uM) and SCH 23390 (20 uM) plus dopamine (100 uM) ($P \leq 0.05$).

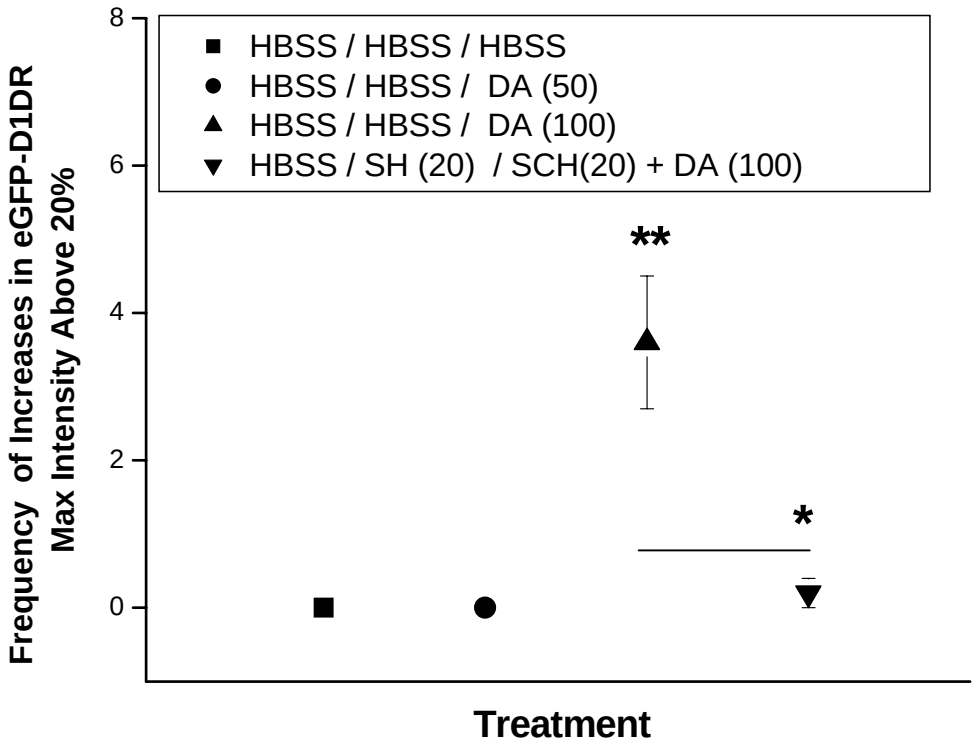

Figure 4-8. Control and dopamine experiment frequency of increases in maximum fluorescence intensity above 20% at the 60 minute time point compared to baseline (0 minute time point). There were significant differences between 100 uM dopamine and control or 50 uM dopamine; there was also a significant inhibition of 100 uM dopamine by 20 uM SCH 23390. Error bars are ± SEM. Asterisks indicate results of statistical tests (see text for details).

4-4.2. Ethanol Pretreatment Experiments

Cells exposed to dopamine (50 uM) displayed no detectable increases in eGFP-D1DR maximum fluorescence intensity as shown in Figure 4-9. However, if cells were pretreated with ethanol (50 or 100 mM) and then exposed to dopamine (50uM), clustering was observed. Figure 4-10 shows an example of 50 mM ethanol preceding 50 uM dopamine treatment, and clustering is indicated by white outlines in Figure 4-10B, C and D. Clustering was also observed with 100 mM ethanol pretreatment of 50 uM dopamine as seen in Figure 4-11. This effect was inhibited by the D1DR antagonist SCH 23390 (20 uM) (see Figure 4-12).

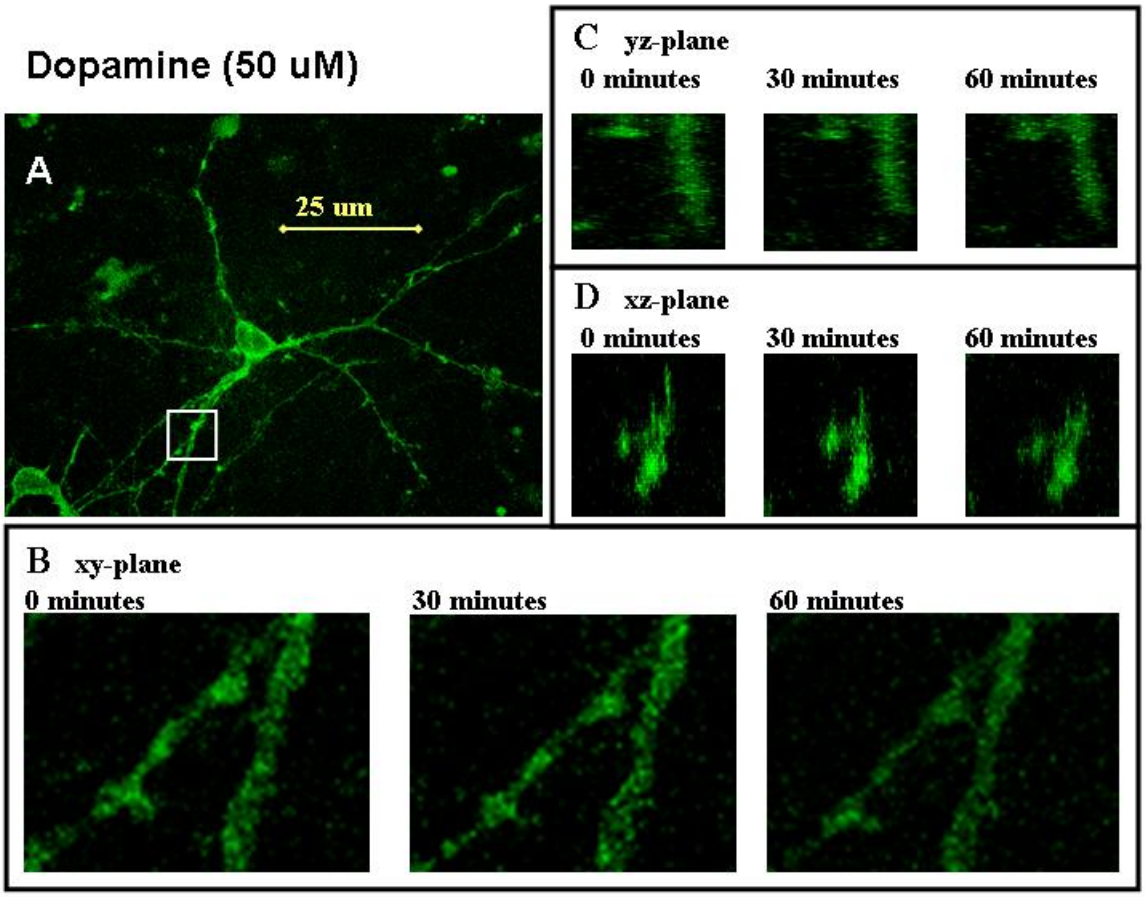

Figure 4-9. Example of a typical neuron treated with dopamine (50 uM) for 30 minutes. A) A two-dimensional image of eGFP-D1DR fluorescence of a typical medium spiny neuron in the NAcc of a parasagittal explant (xy-plane). The white box indicates areas of magnification for additional planes. B) The xy-plane magnified in the area of the white box at 0, 30 and 60 minute time points. C) The yz-plane magnified in the same area at 0, 30 and 60 minutes. D) The xz-plane magnified in the same area at 0, 30 and 60 minutes.

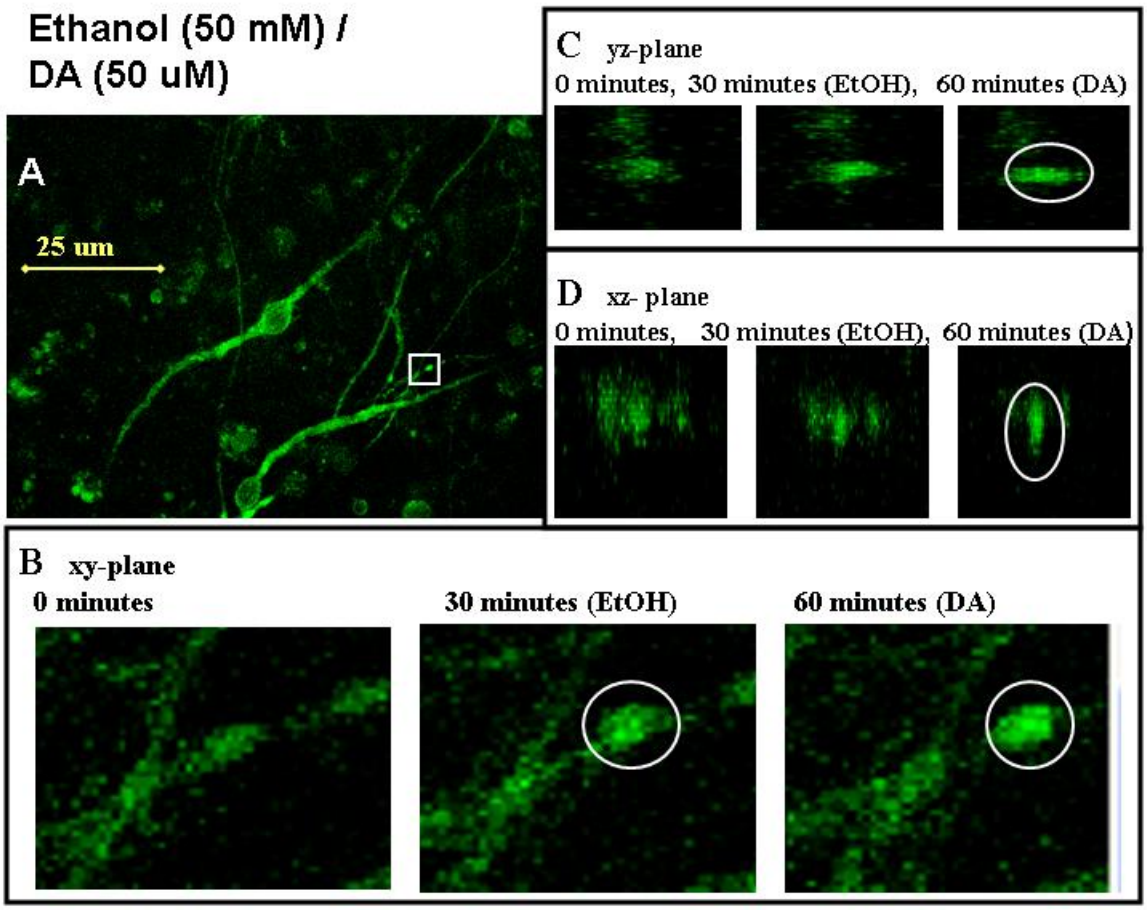

Figure 4-10. Example of a typical neuron exposed to ethanol (50 mM) for 30 minutes followed by dopamine (50 uM) for 30 minutes. A) A two-dimensional image of eGFP-D1DR fluorescence of a typical medium spiny neuron in the NAcc of a parasagittal explant (xy-plane). The white box indicates areas of magnification for additional planes. B) The xy-plane magnified in the area of the white box at 0, 30 and 60 minutes. C) The yz-plane magnified in the same area at 0, 30 and 60 minutes. D) The xz-plane magnified in the same area at 0, 30 and 60 minutes. The white circles show increased fluorescence intensity.

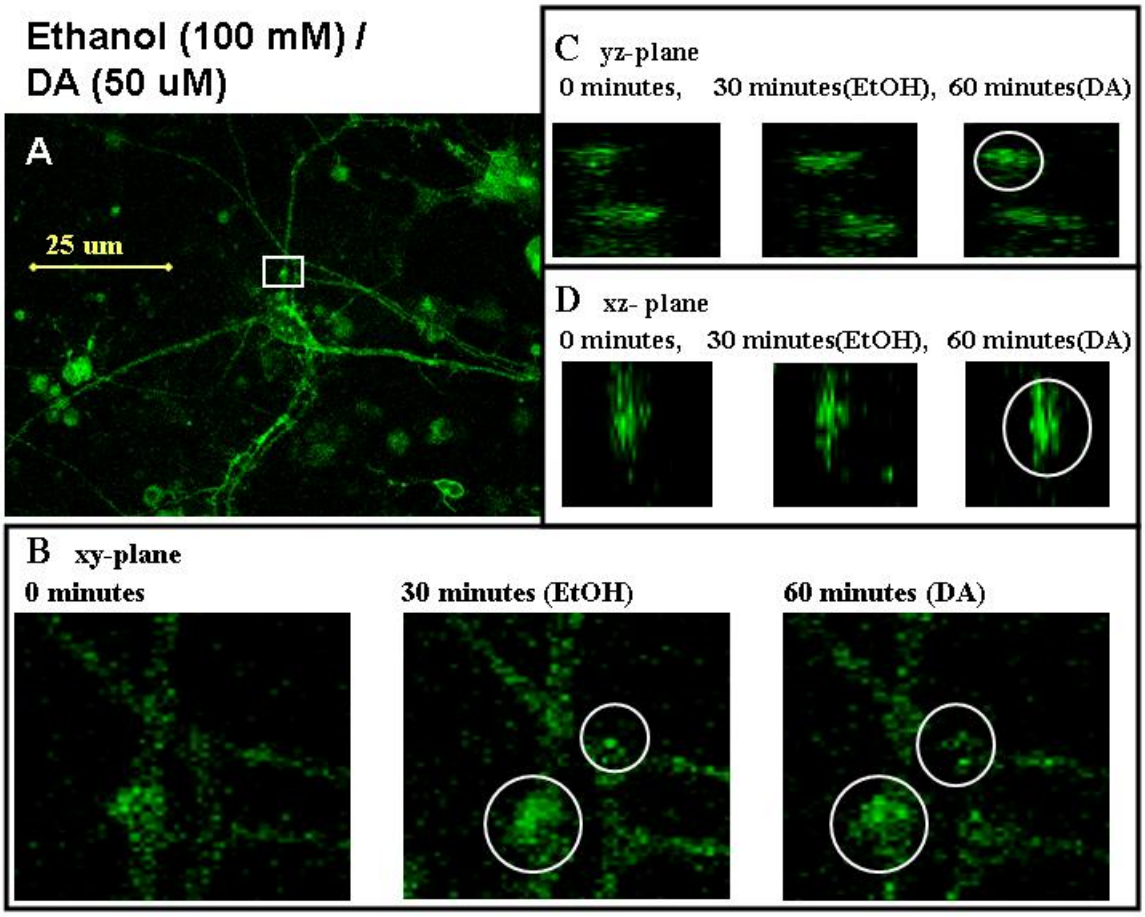

Figure 4-11. Example of a typical neuron exposed to ethanol (100 mM) for 30 minutes followed by dopamine (50 uM) for 30 minutes. A) A two-dimensional image of eGFP-D1DR fluorescence of a typical medium spiny neuron in the NAcc of a parasagittal explant (xy-plane). The white box indicates areas of magnification for additional planes. B) The xy-plane magnified in the area of the white box at 0, 30 and 60 minutes. C) The yz-plane magnified in the same area at 0, 30 and 60 minutes. D) The xz-plane magnified in the same area at 0, 30 and 60 minutes. The white circles show increased fluorescence intensity.

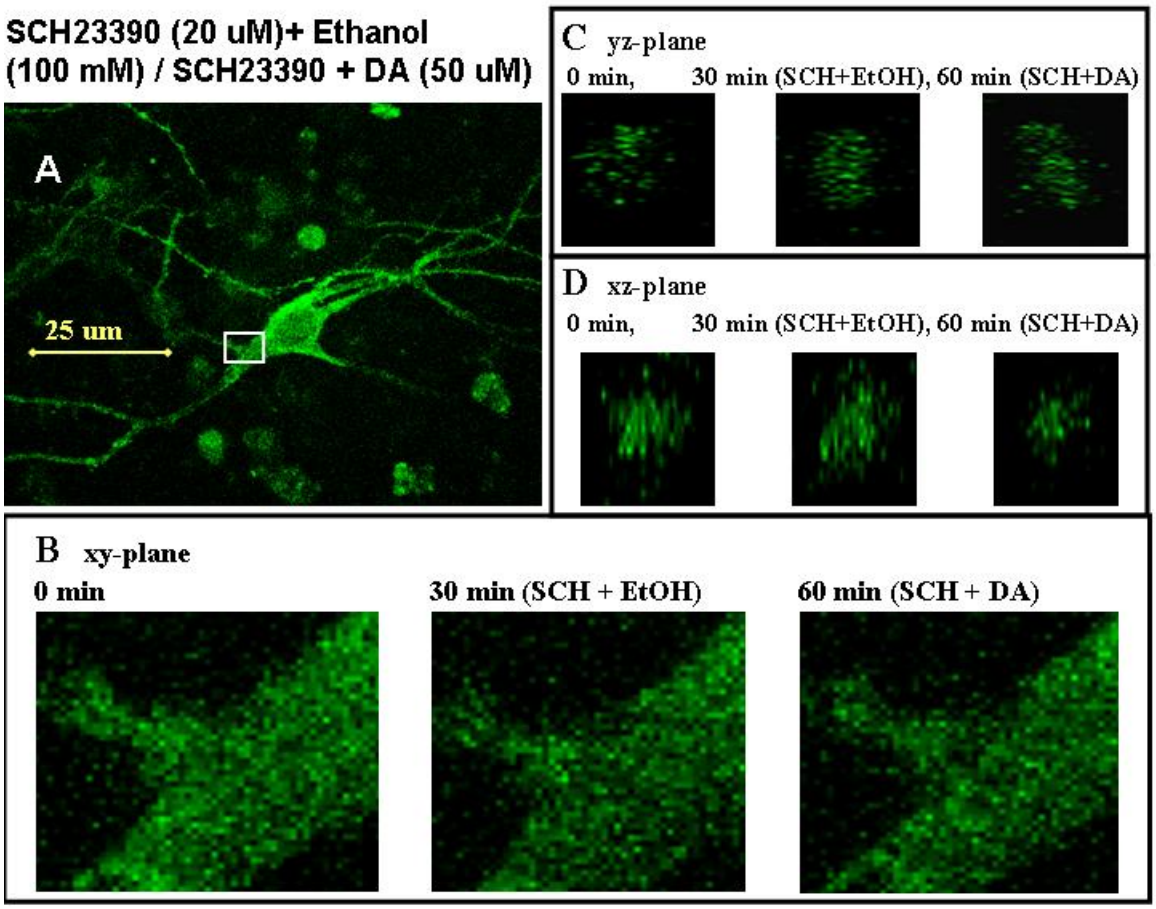

Figure 4-12. Example of a typical neuron exposed to SCH 23390 (20 uM) plus ethanol (100 mM) for 30 minutes followed by SCH 23390 plus dopamine (50 uM) for 30 minutes. A) A two-dimensional image of eGFP-D1DR fluorescence of a typical medium spiny neuron in the NAcc of a parasagittal explant (xy-plane). The white box indicates areas of magnification for additional planes. B) The xy-plane magnified in the area of the white box at 0, 30 and 60 minutes. C) The yz-plane magnified in the same area at 0, 30 and 60 minutes. D) The xz-plane magnified in the same area at 0, 30 and 60 minutes.

These images were quantified using Metamorph software as described previously; both raw data (Table 4-5) and data expressed as percent of baseline for the greatest increases in maximum intensity at the 60 minute time point have been provided. A two-way ANOVA (treatment, time) performed on the raw values showed a significant effect of treatment ($F(3, 32) = 4.20$, $P \leq 0.05$), time ($F(2, 32) = 33.47$, $P \leq 0.0001$), and the interaction ($F(6, 32) = 6.28$, $P \leq 0.0005$) of ethanol pretreatment of dopamine (50 uM).

Table 4-5. Raw data for greatest increase in maximum fluorescence intensity at the 60 minute time point as compared to baseline for ethanol pretreatment experiments. Maximum fluorescence intensities are given in arbitrary units on a 12 bit scale (0 to 4095).

Treatment	Avg Max Intensity (0 min)	SEM	Avg Max Intensity (30 min)	SEM	Avg Max Intensity (60 min)	SEM
HBSS / HBSS / DA (50 uM)	2970	278	2853	191	3045	263.
HBSS / EtOH (50 mM) / DA (50 uM)	2294	76	3015	128	3438	95
HBSS / EtOH (100 mM) / DA (50 uM)	1316	106	2303	319	2748	242
HBSS / SCH 23390 (20 uM) + EtOH (100 mM) / SCH 23390 (20 uM) + DA (50 uM)	2304	210	2491	257	2715	287

Figure 4-13 depicts the effect of ethanol pretreatment on the greatest increase in maximum fluorescence intensity of a ROI in each cell at 30 and 60 minutes. A two-way ANOVA (treatment, time) performed on the values expressed as percent of baseline showed a significant treatment ($F(3, 16) = 18.29$, $P \leq 0.0001$) but no time ($F(1, 16) = 3.52$, $P = 0.079$) or interaction ($F(3, 16) = 0.43$, $P = 0.7377$) effect. A post-hoc evaluation by Student's T-test with a Bonferroni correction for 8 (4 treatments, 2 time points) comparisons of interest revealed a significant difference at the 60 minute time point between dopamine (50 uM) and dopamine (50 uM) pretreated with ethanol (50 mM, $P \leq 0.00005$ and 100 mM, $P \leq 0.00005$). A significant difference was also observed between SCH 23390, applied during the ethanol (100 mM) pretreatment and during the

subsequent dopamine (50 uM) application, compared to ethanol (100 mM) pre-exposure of dopamine (50 uM) in the absence of SCH 23390 ($P \leq 0.0005$).

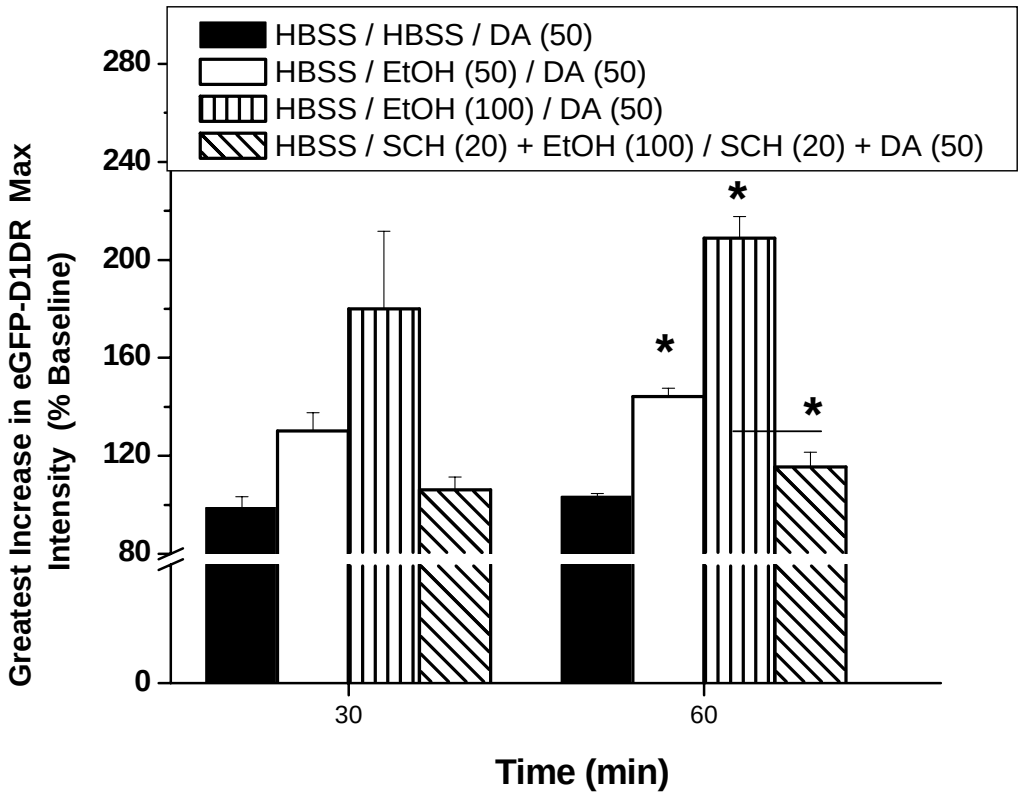

Figure 4-13. Ethanol pretreatment experiment greatest increases in maximum fluorescence intensity at the 60 minute time point compared to baseline (0 minute time point). There was a significant difference between dopamine- (50 uM) exposed cells and those that were pretreated with ethanol (50 or 100 mM) at the 60 minute time point. SCH 23390 (20 uM) significantly inhibited the effect of ethanol (100 mM) pretreatment of dopamine (50 uM). Error bars are ± SEM. Asterisks indicate results of statistical tests (see text for details).

Figure 4-14 represents frequency of increases (above 20%) in maximum fluorescence intensity at 60 minutes compared to baseline for each treatment. No such increases were observed in cells treated with dopamine (50 uM), indicating that D1DRs did not undergo detectable clustering under this condition. However, when this concentration of dopamine was pretreated with ethanol (50 mM or 100 mM), clustering did occur as indicated by increases in maximum intensity above 20%. Kruskal-Wallis non-parametric statistical comparisons with Dunn's multiple comparison tests revealed significant differences between cells treated with dopamine (50 uM) alone and cells pretreated with ethanol (50 or 100 mM) followed by dopamine (50 uM) ($P \leq 0.05$, $P \leq 0.01$ respectively). The frequency was also significantly different between ethanol (100 mM) pretreatment of dopamine (50 uM) exposure and ethanol pretreatment in the presence of SCH 23390 ($P \leq 0.05$).

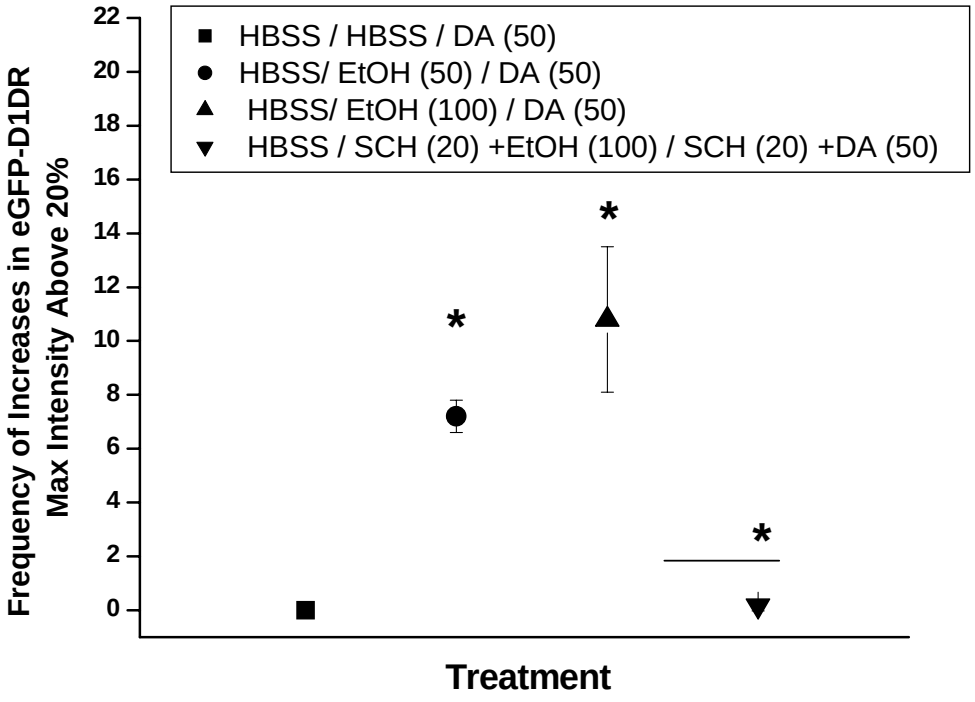

Figure 4-14. Ethanol pretreatment experiment frequency of increase in maximum fluorescence intensity above 20% at the 60 minute time point as percent of baseline (0 minute time point). There were significant differences between dopamine (50 uM) and ethanol (50 or 100 mM) pretreatment of dopamine and a significant inhibition when SCH 23390 (20 uM) was present with ethanol (100). Error bars are ± SEM. Asterisks indicate results of statistical tests (see text for details).

4-4.3. Ethanol Experiments

Ethanol treatment alone (in the absence of dopamine) was also investigated. Figure 4-15 is another example of a control cell, and again there is no significant increase in fluorescence intensity apparent across time. Figure 4-16 shows a cell that was exposed to ethanol (50mM) for 1 hour after the baseline image. Specific ROIs indicative of fluorescence puncta were enhanced. Figure 4-17 is an example of a cell exposed to ethanol (100mM) for one hour after the baseline image was acquired; again, increases in ROIs indicating enhancement of fluorescence intensity, were noted at 30 and 60 minutes. Very distinct translocation of cell surface fluorescence was reproducibly indicated by orthogonal images, showing initial absence of intracellular fluorescence in baseline images that were increased after ethanol exposure (Figures 4-16 C and D and 17 C and D). Figure 4-18 shows a cell that was exposed to SCH 23390 (20 uM) plus ethanol (100mM) for 1 hour; no significant increases in fluorescence intensity were observed at 30 or 60 minutes in the presence of this D1DR antagonist.

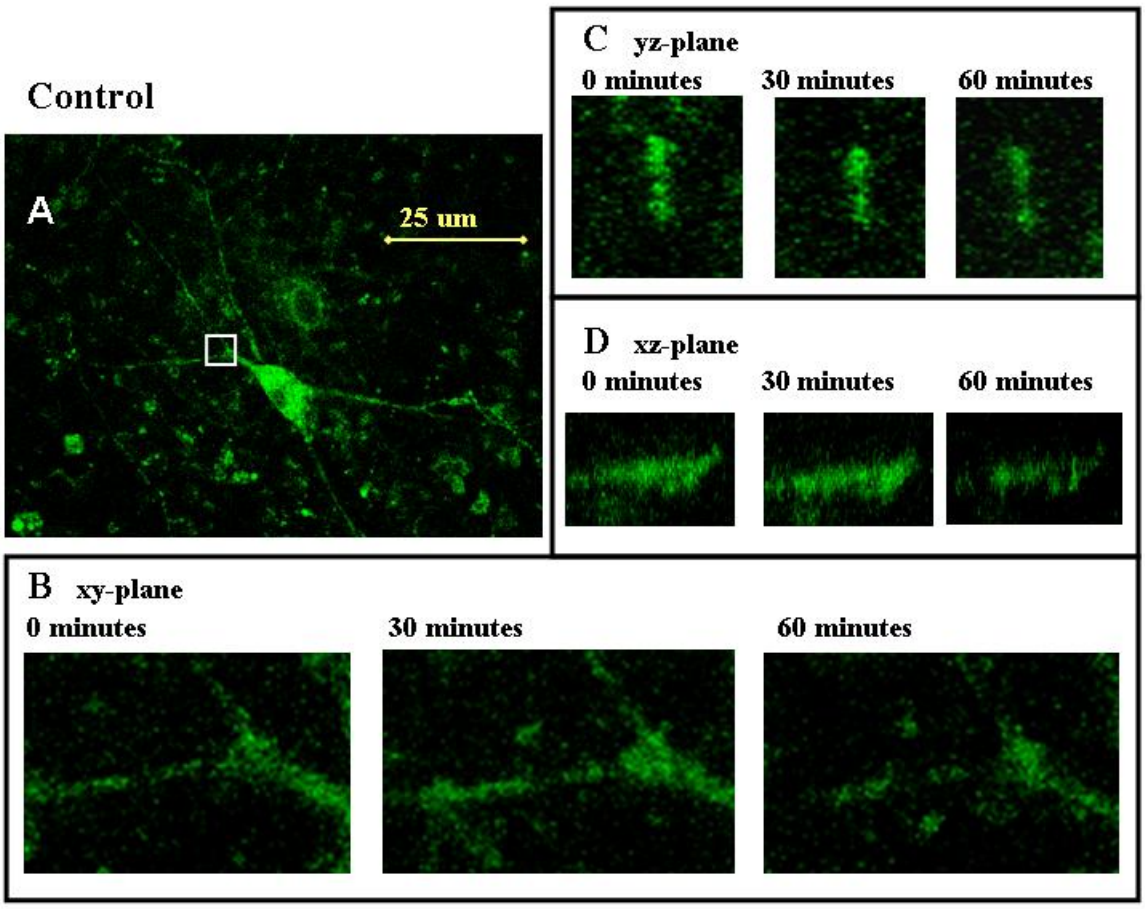

Figure 4-15. Example of a typical control neuron treated only with HBSS. A) A two-dimensional image of eGFP-D1DR fluorescence of a typical medium spiny neuron in the NAcc of a parasagittal explant (xy-plane). The white box indicates areas of magnification for additional planes. B) The xy-plane magnified in the area of the white box at 0, 30 and 60 minutes. C) The yz-plane magnified in the same area at 0, 30 and 60 minutes. D) The xz-plane magnified in the same area at 0, 30 and 60 minutes.

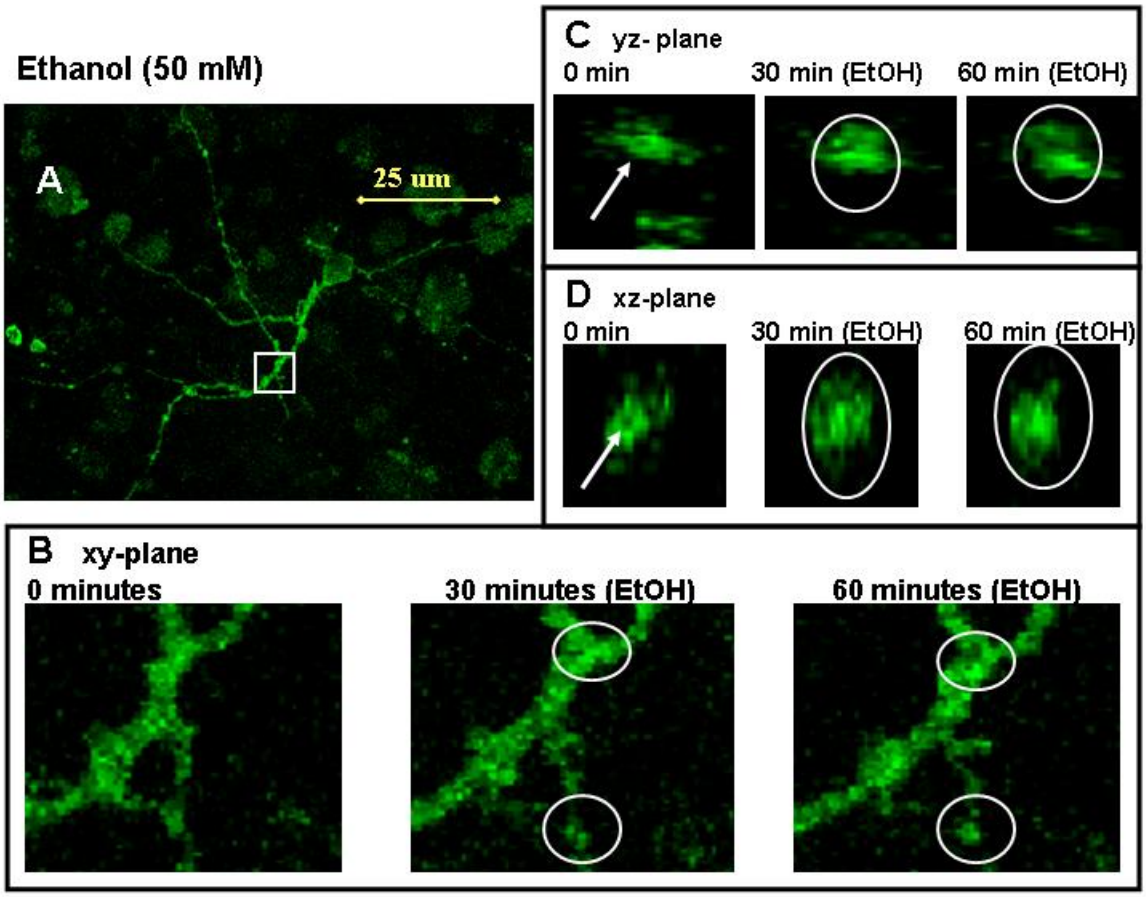

Figure 4-16. Example of a typical neuron exposed to ethanol (50 mM) for 60 minutes. A) A two-dimensional image of eGFP-D1DR fluorescence of a typical medium spiny neuron in the NAcc of a parasagittal explant (xy-plane). The white box indicates areas of magnification for additional planes. B) The xy-plane magnified in the area of the white box at 0, 30 and 60 minutes. C) The yz-plane magnified in the same area at 0, 30 and 60 minutes. D) The xz-plane magnified in the same area at 0, 30 and 60 minutes. The white circles show increases in fluorescence intensity. White arrows indicate the lack of fluorescence intracellularly which then increases following ethanol exposure.

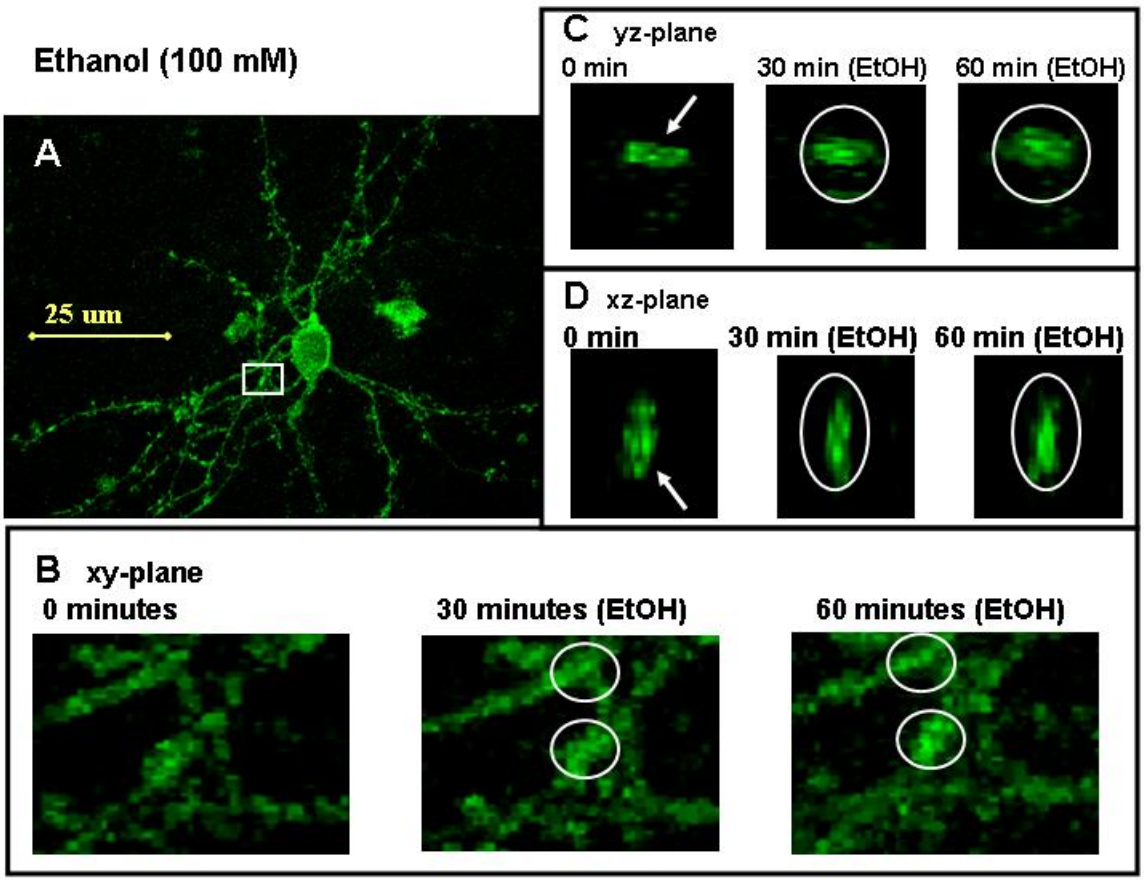

Figure 4-17. Example of a typical neuron exposed to ethanol (100 mM) for 60 minutes. A) A two-dimensional image of eGFP-D1DR fluorescence of a typical medium spiny neuron in the NAcc of a parasagittal explant (xy-plane). The white box indicates areas of magnification for additional planes. B) The xy-plane magnified in the area of the white box at 0, 30 and 60 minutes. C) The yz-plane magnified in the same area at 0, 30 and 60 minutes. D) The xz-plane magnified in the same area at 0, 30 and 60 minutes. The white circles show increases in fluorescence intensity. White arrows indicate the lack of fluorescence intracellularly which then increases following ethanol exposure.

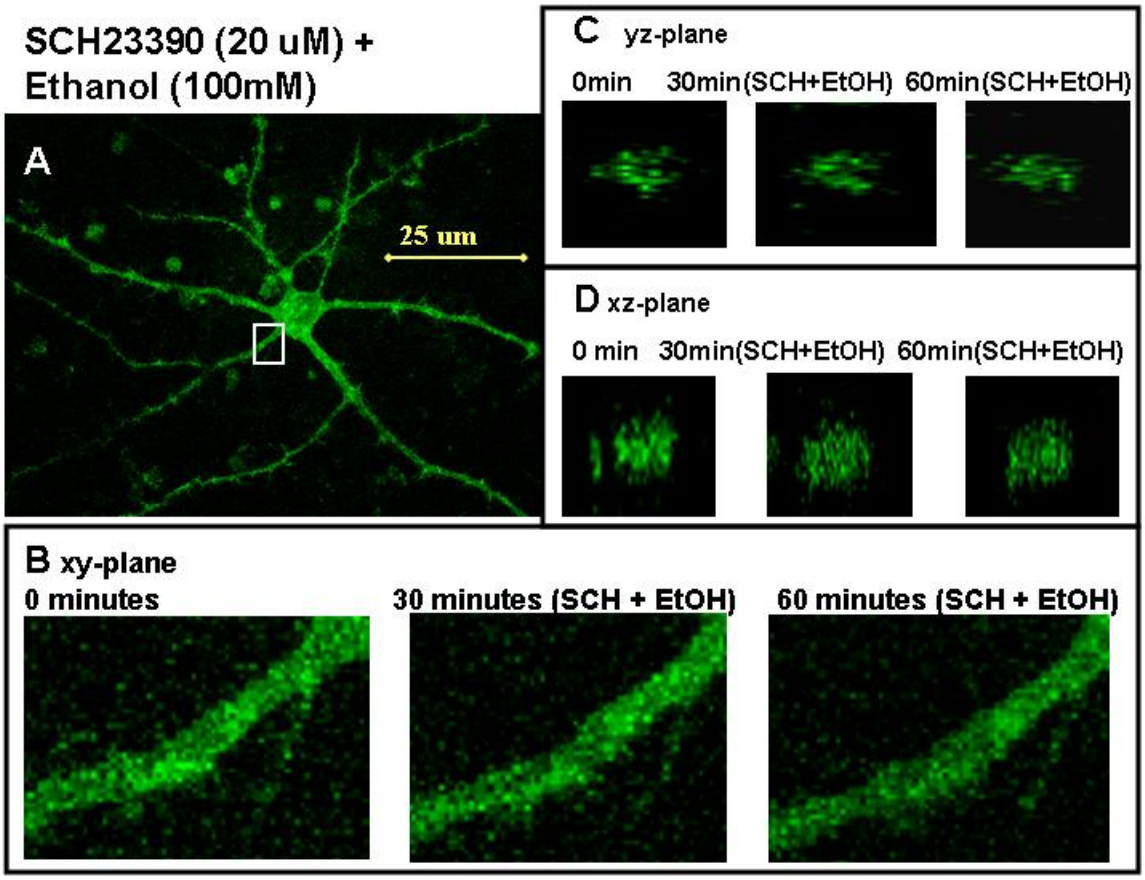

Figure 4-18. Example of a typical neuron exposed to SCH 23390 (20 uM) plus ethanol (100 mM) for 60 minutes. A) A two-dimensional image of eGFP-D1DR fluorescence of a typical medium spiny neuron in the NAcc in a parasagittal explant (xy-plane). The white box indicates areas of magnification for additional planes. B) The xy-plane magnified in the area of the white box at 0, 30 and 60 minutes. C) The yz-plane magnified in the same area at 0, 30 and 60 minutes. D) The xz-plane magnified in the same area at 0, 30 and 60 minutes.

These images were quantified using Metamorph software as described previously; both raw data and data expressed as percent increases in maximum fluorescence intensity at the 60 minute time point (when compared to baseline) are provided. A two-way ANOVA (treatment, time) performed on the raw values of maximum intensity (Table 4-6) showed a significant time ($F(2, 32) = 24.86$, $P \leq 0.0001$) and interaction ($F(6, 32) = 3.84$, $P \leq 0.01$) but no treatment ($F(3, 32) = 0.63$, $P = 0.6057$) effect by ethanol alone.

Table 4-6. Raw data for greatest increase in maximum fluorescence intensity at the 60 minute time point as compared to baseline (0 minute time point) for ethanol experiments. Maximum fluorescence intensities are given in arbitrary units on a 12 bit scale (0 to 4095).

Treatment	Avg Max Intensity (0 min)	SEM	Avg Max Intensity (30 min)	SEM	Avg Max Intensity (60 min)	SEM
HBSS / HBSS / HBSS	2409	138	2262	266	2500	140
HBSS / EtOH (50 mM) / EtOH	1484	153	2041	204	2418	236
HBSS / EtOH (100 mM) / EtOH	1678	245	2076	322	2646	312
HBSS / SCH 23390 (20 uM) + EtOH (100 mM) / SCH 23390 + EtOH	2022	185	2377	286	2410	310

The normalization of these data is represented in Figure 4-19. This depicts the greatest increase as a percent of baseline in a ROI for each cell in each treatment at 30 and 60 minutes. A two-way ANOVA (treatment, time) performed on the percent values showed a significant treatment ($F(3, 16) = 12.09$, $P \leq 0.0005$), time ($F(1, 16) = 11.69$, $P \leq 0.005$), but not interaction ($F(3, 16) = 2.25$, $P = 0.1216$) effect. A post-hoc evaluation by Student's T-test with 8 comparisons of interest (4 treatments, 2 time points) revealed a significant difference at the 60 minute time point between control cells and those exposed to 50 mM ethanol ($P \leq 0.00001$) or 100 mM ethanol ($P \leq 0.001$). A significant difference was also observed between SCH 23390 plus ethanol (100 mM) compared to ethanol (100 mM) alone ($P \leq 0.05$).

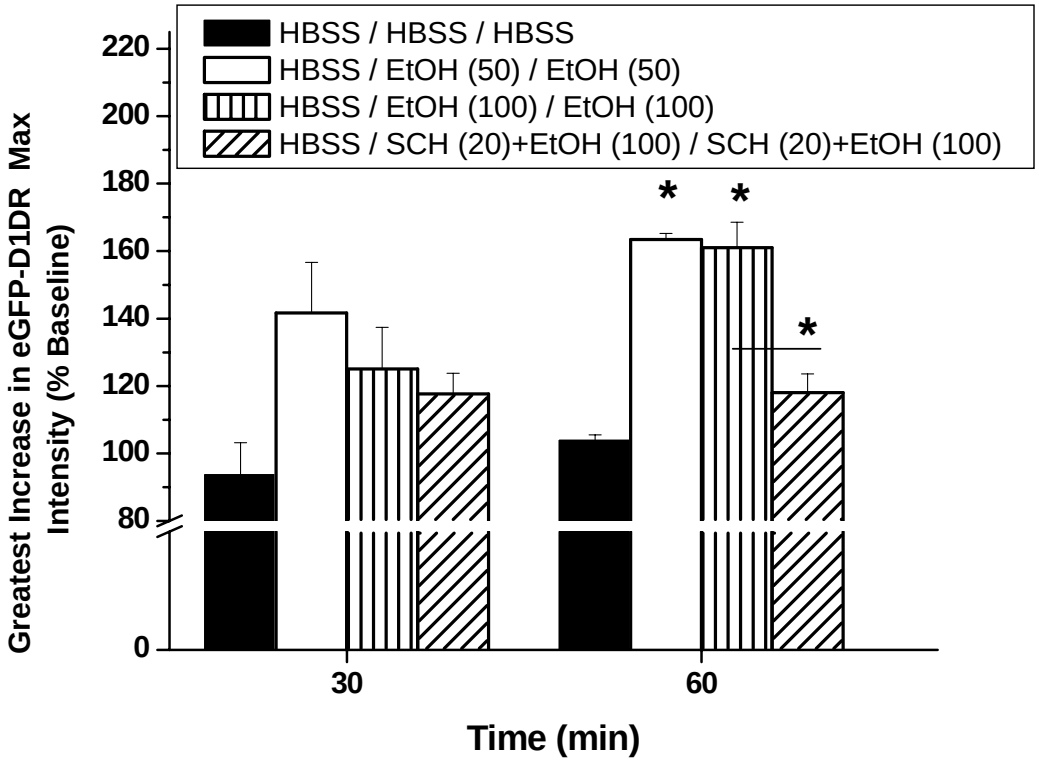

Figure 4-19. Ethanol experiment greatest increases of maximum fluorescence intensity at the 60 minute time point compared to baseline (0 minute time point). The greatest increase in maximum fluorescence intensity for a ROI was determined. Control cells and cells exposed to ethanol (50 mM as well as 100 mM) were significantly different at the 60 minute time point; SCH 23390 (20 uM) treatment significantly inhibited the effect of ethanol (100 mM). Error bars are ± SEM. Asterisks indicate results of statistical tests (see text for details).

Figure 4-20 represents frequency of increases above 20% in the maximum fluorescence intensity at 60 minutes compared to baseline. No such increases were observed in control cells, indicating the lack of D1DR clustering. However, when ethanol (50 mM or 100 mM) was added to the perfusion buffer, distinct clustering and internalization occurred as indicated by strong increases in maximum intensity. Kruskal-Wallis non-parametric statistical analysis with Dunn's multiple comparison tests showed a significant difference between the frequency of increases above 20% in control cells and cells that were exposed to ethanol (50 mM or 100 mM) for one hour ($P \leq 0.01$, $P \leq 0.05$ respectively). A significant difference was also observed between ethanol (50 mM) and SCH 23390 plus ethanol (100 mM) ($P \leq 0.05$).

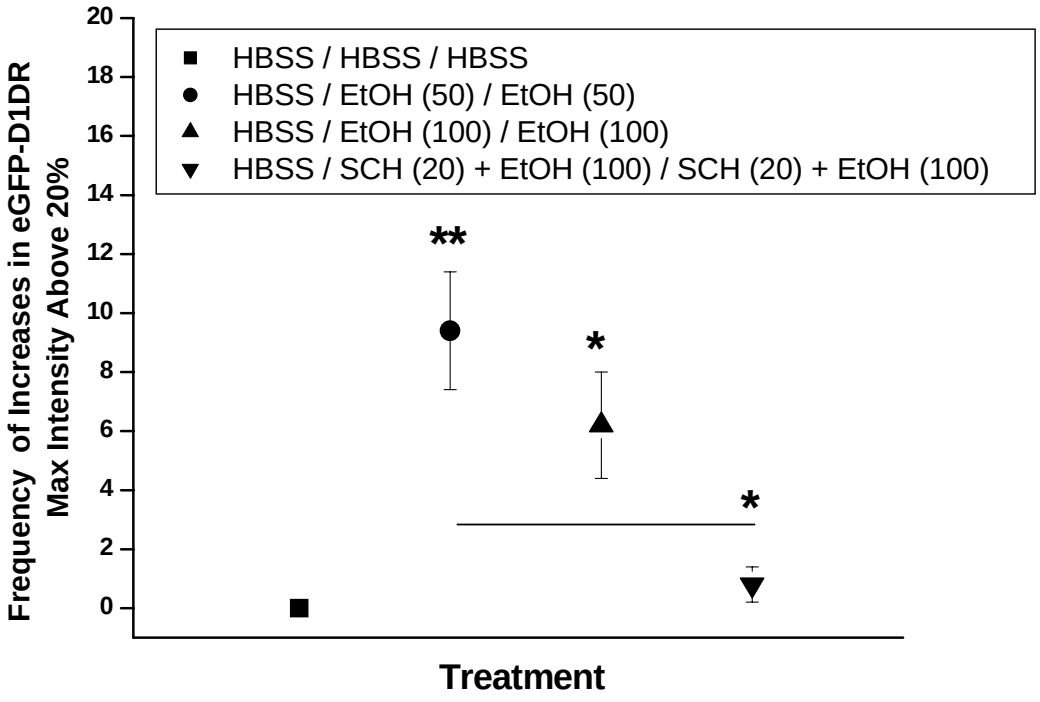

Figure 4-20. Ethanol experiment frequency of increases in maximum fluorescence intensity above 20% at the 60 minute time point as percent of baseline (0 minute time point). There was a significant difference between control and ethanol- (50 or 100mM) exposed cells and a significant difference between ethanol- (50mM) treatment and SCH 23390 (20 uM) plus ethanol (100 mM). Error bars are ± SEM. Asterisks indicate results of statistical tests (see text for details).

4-5. DISCUSSION

Receptor clustering of expressed D1DRs was observed in parasagittal explants imaged by two-photon laser scanning microscopy. The principle outcomes of this study included the following: (1) An automated procedure was developed to locate coalescence of fluorescent puncta that was both comprehensive and unbiased. (2) Orthogonal views of fluorescent puncta indicative of receptor clustering revealed that a majority of cell clustering was due to internalization of the receptor compared to only a few examples of cell-surface clustering. (3) Dopamine (100 uM) and ethanol (50 or 100 mM) causedD1DRs to cluster and internalize. (4) A lower concentration of dopamine (50 uM) produced no detectable internalization of the receptor; however, when the same concentration of dopamine was pretreated with ethanol (50 or 100 mM), internalization was observed. (5) Internalization of the receptor was inhibited by the D1DR antagonist SCH 23390 (20 uM). These are the first studies to show dopamine- or ethanol-induced D1DR internalization in real-time in viable mammalian neurons.

Native D1DRs are widely expressed throughout the central nervous system. For example, D1DRs are expressed in the NAcc, frontal cortex, caudate-putamen, olfactory tubercle, entopeduncular nucleus (the rodent homolog of a portion of the globus pallidus), hippocampus, and the substantia nigra (Boyson et al., 1986; Altar and Marien, 1987; Ariano et al., 1991; Lidow et al., 1991; Mansour et al., 1992; Vincent et al., 1993). This extensive expression may be one reason why dopamine dysfunction has been associated with many disorders including Parkinson’s disease, Huntington’s disease, schizophrenia, hypertension, Tourette’s syndrome and addiction to drugs of abuse.

The subcellular localization of D1DRs is region specific; synaptic and extra-synaptic as well as post- and pre-synaptic localization have all been observed. In the striatum, D1DRs were highly expressed in the dendrites (especially the dendritic spines) and the cell body while axonal expression was observed less often (Levey et al., 1993; Hersch et al., 1995; Yung et al., 1995; Caille et al., 1996). Dendritic expression was occasionally postsynaptically opposed to afferent terminals. Double labeling of D1DRs and tyrosine hydroxylase (TH), the dopamine synthesis enzyme (Bagchi and McGeer, 1964), often showed D1DRs postsynaptic to TH, thereby demonstrating that striatal D1DRs may be extra-synaptic (Smiley et al., 1994; Caille et al., 1996).

The eGFP tag on D1DRs allowed localization of the D1DR in neurons by MPLSM. This was accomplished by inserting the labeled D1DR into a sindbis virus expression system that produced functional D1DRs; this represented the first viral system for expressing eGFP-tagged D1DRs in mammalian cells (Diaz et al., 2004). The explants were infected with the sindbis psuedovirus in the NAcc which is composed of > 90% medium spiny neurons (Meredith, 1999) that endogenously express D1DRs (Altar and Marien, 1987; Ariano et al., 1991; Lidow et al., 1991; Mansour et al., 1992; Vincent et al., 1993; Wong et al., 1999) and is the primary target field of the dopaminergic cells from the VTA. However, it is possible that infected explants did not express eGFP-D1DR exclusively in the NAcc or did not have intact dopaminergic pathways. Physiological dopamine release is reported to begin at or before postnatal day 6 in the mouse ventromedial striatum, and striatal D1DRs are capable of transducing extracellular effects by postnatal day 4 in the mouse striatum (Kim et al., 2002a). This suggests that the development of dopamine transmission was complete or near completion at the time explants were prepared for our studies.

Explants may also offer other advantages. Not only are there synaptic connections that may reflect *in vivo* pathways, but the viral expression of receptors in explants produced more physiological responses compared to dissociated neurons (Shi et al., 1999). In dissociated cells, viral-mediated expression of homomeric eGFP-tagged GluR1 receptors caused abnormal receptor transport to the synapse in the absence of conditioning stimulation; however, in explants conditioning stimuli were required for eGFP-tagged GluR1 receptor subunit insertion into the synapse. A difference in synaptic assembly between these two cellular models would be a critical factor, especially when studying receptor trafficking.

Moreover, explants provide a more stable expression system with almost no evidence of viral-induced toxicity during the time-frame of these experiments. When using viral transfection to over-express proteins, compensatory changes and toxicity concerns must be considered. Although over expressing the D1DR may have long-term adverse effects, these cells were only infected for a short time; the infection period was approximately two days with expression occurring for less than two days. Many experiments were initially attempted in dissociated neuronal cultures that were more sensitive to infection, resulting in viral toxicity and cell death. However, very few cells in explants (approximately two in 200 scanned cells) showed toxicity. Explant cultures have been reported to tolerate sindbis pseudovirus infection quite well, depending on infection duration (Kim et al., 2004a). The sindbis pseudovirus, a suicide virus, theoretically infects only once since the structural proteins are not re-packaged in new virions; however, in practice approximately 15% of cells may be positive for structural proteins detected by antibodies raised against sindbis structural proteins (Kim et al., 2004a).

As seen in Figures 4-3 and 4-4, a high concentration of dopamine (100 uM) increased fluorescence intensity in discrete cell areas or puncta. Clustering may occur in particular areas that contain the necessary proteins for D1DR activation and trafficking. The differential location of receptor clustering is an interesting though not fully understood observation. For example, as shown in Figure 4-3 clustering occurred more centrally in the process while in Figure 4-4 clustering was more localized to the cell surface. Cell surface clustering has been reported following agonist stimulation for D1DRs on axons in fixed dissociated neurons whereas receptors on the cell body and dendrites clustered intracellularly (Martin-Negrier et al., 2000). Over-expression of D1DRs throughout the cell would be expected when using viral infection, so it is likely that axons also expressed D1DRs in our studies. Dissociated cell cultures displayed fluorescence throughout the cell (in all processes); therefore, explant expression was assumed to be similar. Cell surface clustering was observed in few cases possibly restricted to axons. In the NAcc axonal receptors would be extra-synaptic; extra-synaptic axonal D1DRs appear physiologically, although the purpose of these receptors is not well understood (Smiley et al., 1994; Caille et al., 1996). Dopamine transmission can be high volume, making these extra-synaptic receptors physiologically important under this condition. Native dendritic receptors would be activated by endogenous dopamine in the synapse, causing these receptors to internalize, in contrast with axonal receptors that would be exposed to less endogenous dopamine and may localize on the cell surface.

The raw data for increases in the greatest maximum fluorescence intensity were dependent on many factors, thereby requiring data normalization compared to a baseline image. For example, the expression level of the eGFP-D1DR for each preparation was

variable, even though the same viral stock solution was used for most experiments. Another source of variability comes from the explants. On average, about six slices were prepared from one rat; therefore, the portion of NAcc present per explant differed. Laser alignment and other laser and detector characteristics could also vary from experiment to experiment. Because of the above factors, it was advantageous to image in real-time in viable cells from explants since this ensured that a baseline image could be made for direct within cell comparisons. However, the return of receptors to the cell surface could not be studied in our experiments. Previous reports have noted a seven hour requirement for D1DRs to return to the cell surface after internalization (Martin-Negrier et al., 2000). It is not feasible for explants to survive such a long time period on the microscope stage.

The D1DR antagonist SCH 23390 inhibited receptor clustering in this study as well as in other studies reported in the literature. In several reports, D1DR desensitization was inhibited by SCH 23390 (Ofori et al., 1993; Lin et al., 1996; Dumartin et al., 1998; Lewis et al., 1998; Martin-Negrier et al., 2000; Gardner et al., 2001). In fact, repeated SCH 23390 treatments caused an up-regulation of D1DR binding in several areas,including the rat striatum (Creese and Chen, 1985; Hess et al., 1986; Lappalainen et al., 1990; Schwartz et al., 2003). Since D1DR antagonists such as SCH 23390 bind without activating the receptor, this suggests that direct stimulation of the receptor is needed for desensitization.

Amphetamine, a drug of abuse, that indirectly enhances catecholamine release from nerve terminals, also induces D1DR desensitization. A high dose of amphetamine (5.0 mg/kg) produced a smaller increase in cAMP production compared to a lower dose (1 mg/kg) (Barnett and Kuczenski, 1986; Roberts-Lewis et al., 1986). Chronic

administration of a moderate dose (3 mg/kg) of amphetamine also decreased cAMP production but had no effect on D1DR binding (Barnett et al., 1987), and a single maximal dose of 7.5 mg/kg amphetamine had similar results (Roseboom and Gnegy, 1989). Internalization of D1DRs was observed upon amphetamine intraperitoneal injection, and this effect was inhibited when co-administered with the D1DR antagonist SCH 23390 (Dumartin et al., 1998). Therefore, other drugs of abuse that elevate extracellular dopamine levels also induce D1DR internalization. This underscores the importance of the D1DR in drug abuse and addiction.

Other receptors have been reported to traffic to and from the plasma membrane of neurons. One example is the G-protein coupled mu-opioid receptor. Acute morphine administration caused internalization of mu-receptors, specifically in neuronal processes of the NAcc (Haberstock-Debic et al., 2003). This may be involved in opiate abuse and addiction. Also, GluR1 subunits of the AMPA receptor, a ligand-gated ion channel receptor, were redistributed to the cell surface upon conditioning stimulation (Shi et al., 1999). AMPA receptor trafficking is believed to be part of the cellular mechanism of learning and memory and has also been implicated in the addiction process (Berke and Hyman, 2000). Additionally, D1DR stimulation increases surface expression of GluR1 on neurons in the NAcc, further suggesting a role for D1DR in addiction (Chao et al., 2002).

The mechanism for ethanol-induced D1DR internalization is not fully understood; local effects of ethanol on cAMP cascades versus more systemic increases in dopamine release in the NAcc by activation of dopaminergic cells in the VTA were not differentiated.

Increased dopamine in the NAcc of explants by ethanol may not be sufficient to induce internalization, given that rather high levels of dopamine (100 uM) were required to induce clustering of the D1DR. Ethanol has been shown to have local effects on cAMP cascades (Hynie et al., 1980; Lucchi et al., 1983; Gordon et al., 1986; Tabakoff et al., 2001; Maldve et al., 2002), and therefore ethanol action on such intracellular processes may be responsible for ethanol induction of D1DR trafficking. For example, alteration in the palmitoylation of the $G_{\alpha s}$ subunit of the G-protein upon ethanol exposure has been reported (Hallak and Rubin, 2004). This could modify expression, activity, or regulationof the $G_{\alpha s}$ subunit which in turn could affect adenylyl cyclase activity. Other ethanol effects may also play a role in the ethanol modulation of cAMP cascades, including the combination of a local increase in dopamine levels and alterations in the cAMP cascade.

In conclusion, viral-mediated expression of eGFP-tagged D1DRs in parasagittal explants was used to study localization of D1DRs in viable mammalian neurons with MPLSM. An automated ROI protocol was developed to identify fluorescence punctate in ROIs which were sensitive to dopamine and/or ethanol application. Dopamine (100 uM) and ethanol (50 and 100 mM) exposure caused clustering of D1DRs away from the cell surface as seen by the three-dimensional images of cells transfected with eGFP-D1DR. This was the first study to demonstrate agonist-induced D1DR internalization in viable mammalian neurons. It was also the first study to provide evidence that ethanol induces D1DR internalization.

Chapter 5: Summary, Conclusions, and Future Directions

5-1. SUMMARY AND CONCLUSIONS

The sindbis pseudovirus was utilized to induce expression of eGFP-D1DRs in neurons of the NAcc in parasagittal brain slice culture (Diaz et al., 2004). Briefly, DNA for eGFP-D1DR was inserted into the pSinRep5 vector, and RNA was transcribed *in vitro* from this vector and a helper vector encoding structural proteins. Electroporation was used to transfect BHK cells, and these cells then served as hosts to form pseudovirions that budded into the culture medium. Media was then collected and concentrated over a discontinuous sucrose gradient by ultra-centrifugation. The concentrated viral stock successfully infected dissociated neuronal cultures, brain slice explants, and mice *in vivo*. The ability of this virus to transfect different neuronal preparations demonstrates the utility of gene-transfer by viral infection.

Evidence of functional receptors was shown by the ability of dopamine to stimulate cAMP in a concentration-dependent manner (Figure 3-2A). Moreover, the D1DR antagonist SCH 23390 inhibited dopamine-stimulated cAMP production in a concentration-dependent manner (Figure 3-2B). Thus, the virally-transfected D1DRs appeared to function similar to endogenous receptors since the expressed receptors bound agonist and activated synthesis of a second messenger via coupling to the G-protein, G_s and were also sensitive to the antagonist. Although an extensive concentration-response curve was not conducted, an estimated EC_{50} for the transfected eGFP-D1DR was approximately 11 uM dopamine which was similar to that reported for endogenous

D1DRs (for review see Neve and Neve, 1997). Cells expressing receptors showed a maximum cAMP production of 70 ± 0.7 pmol/mL, well within the range of the standard curve supplied by the cAMP detection kit (0.78-200 pmol/mL). In contrast, uninfected BHK cells displayed a maximum cAMP production of only 3 ± 0.6 pmol/mL, demonstrating that the cAMP response was dependent on the presence of functional D1DRs. The affinity estimate of the transfected D1DR (11 uM) was very similar to the low-affinity state of wildtype D1DRs that have a K_D of 10-18 uM dopamine (for review see Neve and Neve, 1997). The EC_{50} for SCH 23390 in expressed D1DRs was approximately 1 nM which was similar to the wildtype D1DR affinity of 0.1-0.6 nM (for review see Neve and Neve, 1997). Therefore, there is ample evidence that the D1DRs expressed in explants were functionally similar to wildtype D1DRs.

The parasagittal explants used in our studies were infected with the eGFP-D1DR sindbis pseudovirus in the NAcc, but the explants also contained the VTA, prefrontal cortex, and hippocampus. Since many brain regions associated with addiction to drugs of abuse were present in the explant, it may provide a physiological model for *in vitro* studies of drug-induced neuroadaptive changes. TH staining further verified the presence of dopaminergic cells.

MPLSM was used to localize eGFP-D1DRs in parasagittal explants. This imaging technique required characterization of the excitation and detection of eGFP in explants. Wavelength and power levels were determined for proper eGFP excitation through empirical tests, resulting in a laser wavelength of 845 nm and laser power of approximately 100 mW. Detection and power levels were kept constant for each experiment. Thus, only cellular differences in imaging were variable.

These experiments allowed monitoring of D1DR localization during the course of different pharmacological treatments. Images underwent a ROI protocol to search for increases in maximum fluorescence intensity, providing the greatest increase in maximum fluorescence intensity and the total number of increases above 20% that occurred upon pharmacological manipulation. The techniques used in this project allowed rapid measures of D1DR trafficking (30 minutes). Virally-transfected eGFP-D1DRs internalized in response to dopamine or ethanol treatment. Internalization was also induced in response to ethanol pretreatment of dopamine, and the effect was greater than that observed after either treatment alone. This marked the first study to show acute ethanol action on the internalization of D1DRs. The identification of dopamine- and ethanol-induced D1DR internalization may aid in the understanding of addiction since D1DR internalization may be a neuroadaptation to chronic drug exposure. Specifically, D1DR internalization may be a cellular mechanism involved in the development of acute tolerance to ethanol.

Receptors that internalize are no longer available for activation. In the case of exposure to ethanol or other drug of abuse, any enhanced extracellular dopamine levels would not activate D1DRs that had internalized. This might lead to increasing amounts of ethanol (or other abused drug) that would be required in order to achieve the original effect desired by an individual and is a characteristic of tolerance. As this effect happens quickly, the cellular mechanism of receptor internalization may be, at least in part, responsible for acute tolerance.

Internalization of some opioid receptors has been associated with recycling of the receptor to a fully active state so that desensitization was not observed (Whistler et al., 1999; Alvarez et al., 2001). In this model, internalization was hypothesized to reactivate receptors that had been desensitized. For example, dephosphorylation of receptors may occur in endocytosed vesicles followed by reinsertion into the cellular membrane. However, D1DRs do not require internalization in order for receptor dephosphorylation to occur (Gardner et al., 2001). The state of the internalized receptor may thus be different for D1DRs and opiod receptors. Functional data of the D1DRs were not collected for our localization studies, although it is reasonable to assume that internalized D1DRs would not be accessible to ligands, and thus not be activated by them, which in turn would cause receptor desensitization.

The use of a high dopamine concentration for some experiments may not necessarily represent a non-physiological level. For example, this high concentration of dopamine (100 uM) was necessary for maximal cAMP production in virally-infected BHK cells. This dopamine concentration was also required for receptor trafficking (in the absence of ethanol) in explants. However, the actual synaptic concentration of dopamine that reached these expressed receptors was unknown. Dopamine transporters would be expected to remove some of the dopamine from the synaptic space. Therefore, the dopamine concentration that produced D1DR trafficking may have been within a physiological range.

5-2. FUTURE DIRECTIONS

Since D1DRs cluster inside the cell upon ethanol treatment, it would be expected that ethanol may also induce other forms of D1DR desensitization. For example, cAMP

production by ethanol may decrease as a result of uncoupling of the D1DR from the G-protein. cAMP assays in the absence and presence of ethanol could be performed to test for desensitization involving cAMP.

Another form of D1DR desensitization is down regulation of gene expression. This type of desensitization would only be applicable to endogenously expressed D1DRs and could not be studied with this viral system which causes over expression of the protein through viral mediated RNA production of the gene to be studied. Moreover, down regulation would also not occur within the time frame of these experiments. The effect of chronic ethanol on receptor trafficking should be also studied as a comparison to the acute actions of ethanol in explants.

Further studies could focus on the mechanism(s) of ethanol-induced D1DR desensitization by internalization. Candidates for these mechanistic studies could include mediators in the cAMP cascade. Pharmacological modulation of the enzymes of this cascade may inhibit the trafficking of D1DRs by ethanol. Another question to consider is if activation of dopaminergic cells in the VTA is entirely responsible for ethanol-induced D1DR trafficking, or if local cellular effects also play a part in ethanol's action? One method to determine this would be the use of dissociated neurons from the ventral striatum (which contain the NAcc but are no longer innervated by the VTA) to study trafficking of D1DRs by ethanol. This preparation would allow the study of direct ethanol effects on neurons. Preliminary studies have been completed in this area, and the use of a new sindbis mutant (nsP2S726) expression system, displaying substantial reduced toxicity, has been developed (Jeromin et al., 2003; Kim et al., 2004). This mutant viral

expression system would allow studies in dissociated neurons without such toxicity problems.

Other experiments could further corroborate the clustering seen in the current study. For example, electron microscopy could more definitively locate D1DRs after dopamine or ethanol treatment. Binding studies would provide another method to verify internalization. Moreover, other drugs of abuse could be tested in infected explants to determine if D1DR trafficking is a common effect for abused drugs.

Many G-protein coupled receptors undergo receptor oligomerization. D1DRs have been associated with the NR1 subunit of NMDA receptors (Fiorentini et al., 2003) and the adenosine A1 receptor (Gines et al., 2000). Hetero-oligomerization of other dopamine receptor subtypes have also been proposed (Tsai and Hong, 2003). Homodimers or higher level homo-oligomers have not been observed conclusively but may exist physiologically. Moreover, co-immunoprecipitation techniques require solubilization which may form oligomers caused by solubilization artifacts (Bouvier, 2001). The presence of oligomers is determined by detection of BRET (bioluminescence resonant energy transfer) or FRET (fluorescence resonant energy transfer) in living cells. The effects of dopamine and/or ethanol treatment on hetero-oligomers of D1DRs would be an additional avenue for future studies.

Finally, the pseudovirus causes over expression of D1DRs *in vivo*, and there are numerous areas in the brain where a local amplification in D1DRs may change a variety of behaviors. For example, our collaborators have observed that over expression of D1DRs in the bed nucleus of the amygdala caused a reduction in ethanol self-

administration in C57BL/6J (B6) mice (RSA, 2004 Vancouver). Therefore, the virus is extraordinarily useful for molecular, biochemical, histological, and behavioral analysis of complex disease states such as addiction.

Appendix I

RECIPES (R)

R1-AGAROSE PLATES:

(100 mL to make 4 plates)

luria broth base: 2.5 g

agarose : 2.0 g

100 mL dH_20

Autoclave: liquid setting 15 minutes.

When cool (but not gelled) add antibiotics.

kanamycin 30ug/mL [stock solution 30 mg/mL, then use 1 uL/1 mL]

ampicillin 50 ug/mL [stock solution 50 mg/mL, then use 1 uL/1 mL]

Pour ~ 25 mL into plates inside of sterile hood and let solidify, store at 4 °C.

R2-LURIA BASE (LB) BROTH FOR GROWING BACTERIA

(100 mL per maxi-prep isolation, 3 uL per mini prep isolation)

luria broth base: 2.5 g

100 mL dH_20

Autoclave: liquid setting15 minutes

When cool add antibiotics (this does not gel)

kanamycin 30ug/mL

ampicillin 50 ug/mL

R3-AGAROSE GELS

DNA, 1% Gel

agarose: 0.3 g

d H20: 30 mL

Microwave 30 seconds to allow agarose to dissolve, when cooled (but not gelled) add:

50X TAE: 600 uL

ethidium bromide (30 mg/mL): 3 uL

Pour into gel mold with appropriate comb (inserted on the black side) for samples. Running Buffer, 1X TAE, is poured over the gel once it has solidified. Then samples are loaded in the openings the comb creates on the black side of the gel. A voltage is applied across the gel for separation of the DNA from the black side toward the red side.

RNA, 0.7% agarose gels

Soak gel box and attachments in ~3N HCl for 15-30 minutes

Rinse out box with RNase free TBE

Make 0.7% RNA gel

agarose 0.21 g

RNase free TBE 30 mL

microwave 1 minute, then allow to cool

ethidium bromide 3 uL

Use RNase free TAE as the running buffer. All other steps are the same as DNA gels.

R4-DEPC H_2O

Diethylpyrocarbonate (DEPC) is a very toxic substance that destroys enzymatic activity by modifying –NH, -SH, and –OH groups in RNases and other proteins. DEPC H_2O is used to make all RNase free solutions.

Make 1 L of DEPC H_2O:

In a 1 L autoclavable glass bottle add 1 mL of DEPC to 999 mL dH_2O and over low heat and mix overnight. The next morning this mixture is autoclaved on a liquid setting for 15 minutes. The autoclaving will inactivate the DEPC but it should still be treated carefully and handled to avoid contamination with RNases.

R5-50 MM TRIS-CL, 100 MM NACL, 0.5 MM EDTA = TNE BUFFER

1 mM Tris-Cl, pH= 7.4	5 mL
2 M NaCl	3.33 mL
0.25 M EDTA	200 uL
qs with DEPC H_2O to 100mL	

R6-55% SUCROSE IN TNE BUFFER

55 g sucrose/100 mL TNE Buffer, autoclave 15 minutes

R7-20% SUCROSE IN TNE BUFFER

20 g sucrose/ 100 mL TNE Buffer, autoclave 15 minutes

Appendix II

PROTOCOLS (P)

P1-IN VITRO TRANSCRIPTION OF SINDBIS VIRUS DNA

DNA, enzymes, kits and buffers in –20 °C freezer
RNA in –80 °C freezer
Most other solutions are in either 4° fridge, or at room temperature in cabinets

1) Cut DNA to make circular DNA linear. Different constructs will require different enzymes to linearalize the DNA.

pSinRep5GLUR1	pSinRep5D1	DH(26)S
DNA 1-10 ug	DNA 5-10 ug	DNA 5-10 ug
BSA 1 uL	BSA 1 uL	BSA 1 uL
Buffer D 10 uL	Buffer 2 10X 10uL	Buffer 2 10 X 10 uL
Not1 5 uL	Xho1 5 uL	Xho1 5 uL
Balance with		
DEPC WATER	**DEPC WATER**	**DEPC WATER**
total volume 100 uL	100 uL	100 uL

Tap tubes, spin, incubate at 37°C for 3 hours.

2) Make 0.7% agarose gel:

0.21 g agarose
30 mL water
600 uL 50X TAE
3 uL ethidium bromide

} Microwave > 1 min

3) Add 3 uL of loading gel to 3 uL of each sample and run on gel with ~ 5 uL 1 kb ladder. Add TAE to the box, connect cables to matching colors and run at 85 V

4) Protease K treatment (removes extra enzymes)
Add 1 uL to each tube and incubate at 37 °C for 30 minutes.

5) Phenol Chloroform Isolation (done in hood to avoid fumes)
   a. Add 1x the volume of phenol:$CHCl_3$:IAA shake, and centrifuge at 14,000 rpm for 1 minute, take top layer, discard bottom layer
   b. Add 1x the volume of phenol:$CHCl_3$:IAA shake, and centrifuge at 14,000 rpm for 1 minute, take top layer, discard bottom layer
   c. Add 1x the volume of chloroform shake, and centrifuge at 14,000

rpm for 1 minute, take top layer, discard bottom layer

d. Add 1/10x 3 M sodium acetate

e. Add 2x 100% ethanol

f. Mix and incubate in –80 °C freezer for 1-12 hours

g. Centrifuge balanced tubes for 15 minutes at 14,000 rpm
Pipette off liquid to dry out pellet

h. Add 4 uL DEPC H_2O to resuspend pellet, let sit ~ 10 minutes at room temperature.

6) mMessage mMachine SP6 Kit (Ambion, Austin, TX catalog # 1340)
for each reaction:

4 uL DEPC linearized DNA
10 uL 2x NTP/Cap
2 uL 10x Reaction Buffer
2 uL Enzyme mix
1 uL GTP
Incubate for 1 hour at 37 °C
Then add 1uL enzyme mix and incubate for a 2 nd hour at 37 °C.

7) Add 130 uL DEPC H_2O

8) Phenol:chloroform isolation again
   a. Add 1x the volume of phenol:$CHCl_3$:IAA shake, and centrifuge at 14,000 rpm for 1 minute, take top layer, discard bottom layer
   b. Add 1x the volume of chloroform shake, and centrifuge at 14,000 rpm for 1 minute, take top layer, discard bottom layer
   c. Add 1/10x 3 M sodium acetate
   d. Add 2x 100% ethanol
   e. Mix and place in –80 °C freezer for 1-12 hours

9) Centrifuge balanced tubes for 15 minutes at 14,000 rpm at 4 °C.

10) Prepare RNA gel
Soak gel box and attachments in ~3N HCl for 15-30 minutes
Rinse out box with RNase free TBE
Make 0.7% RNA gel

agarose	0.21 g
RNase free TBE	30 mL
ethidium bromide	3 uL

11) Pipette off fluid

12) Add 200 uL 80% ethanol, centrifuge 5 minutes at 14,000 rpm

13) Pipette off all fluid let air dry

14) Add 20 uL DEPC H_2O, let sit at room temperature
1uL RNA + 3 uL loading dye run on gel (using RNase free TBE in bath)
1uL RNA for Nano-drop analysis

P2-ELECTROPORATION OF BHK CELLS WITH SINDBIS VECTORS

RNA kept at -80 °C freezer
Biorad Gene Pulsar in Dr. Bergessons Lab in MBB

1) Wash cells in 10 mL RNase free PBS without cations at room temperature.
2) Add 3 mL trypsin per flask, one flask at a time. Under trypsinizing results in not enough cells detatching, over trypsinizing results in clumping and inefficient electroporation.
3) Stop trypsinization reaction by adding 5 mL media.
4) Pour this mixture of cells, trypsin, and media into a 15 mL sterile tube.
5) Centrifuge these cells for 5 minutes at 500 rpm at room temperature.
6) Resuspend the cells in 5 mL ice cold RNase free PBS without cations. Centrifuge for 5 minutes at 500 rpm at room temperature.
7) Repeat wash by resuspending the cells in 5 mL ice cold RNase free PBS without cations. Centrifuge for 5 minutes at 500 rpm at room temperature.
8) Take an aliquot of the cells and determine the total number of cells.

(Hemactymotor average) x (10^4) x (volume of cells) = total number of cells

9) Third RNase free PBS wash as in #6 or 7
10) Resuspend the cells at a density of 1.5 x10^7 cells/mL ice cold RNase free PBS without cations.
11) In ice cold eppendorf tubes mix 500 uL of cells + 10-15 ug DH(26)S RNA + 10-15 ug RNA of pSinRep5 containing your gene of interest.
12) Transfer this mixture to cuvettes and shock them 2x:
    BioradGene Pulsar with Pulse Controller
    0.2 mm electrode gap cuvettes from biorad
    1.5 kV, 25 uFD, resistance = infinity
    time constant should result in 0.7 msec
13) After shock let cuvettes sit at room temperature for 10 minutes. Using sterile glass pipette remove all solution especially foamy cells and add 9.5 mL MEM + 10% FBS. Then pipette 2 mL into 35 mm dishes.
14) Verify glowing BHK cells in 24-60 hours.
15) Collect all or a portion of media (that has virons in it) as long as you see glowing cells.

Bibliography

Ahola T, Kaariainen L (1995) Reaction in alphavirus mRNA capping: formation of a covalent complex of nonstructural protein nsP1 with 7-methyl-GMP. Proc Natl Acad Sci U S A 92:507-511.

Albanese A, Bentivoglio M (1982) The organization of dopaminergic and non-dopaminergic mesencephalo-cortical neurons in the rat. Brain Res 238:421-425.

Altar CA, Marien MR (1987) Picomolar affinity of 125I-SCH 23982 for D1 receptors in brain demonstrated with digital subtraction autoradiography. J Neurosci 7:213-222.

Alvarez V, Arttamangkul S, Williams JT (2001) A RAVE about opioid withdrawal. Neuron 32:761-763.

American Psychiatric Association (1987) Diagnostic and Statistical Manual of Mental Disorders. 3rd ed Washington CD, American Psychiatry Press.

Anderson W, Jaworski C (1979) Isoproterenol-induced desensitization of adenylate cyclase responsiveness in a cell-free system. J Biol Chem 254:4596-4601.

Ariano MA, Kang HC, Haugland RP, Sibley DR (1991) Multiple fluorescent ligands for dopamine receptors. II. Visualization in neural tissues. Brain Res 547:208-222.

Ariano MA, Sortwell CE, Ray M, Altemus KL, Sibley DR, Levine MS (1997) Agonist-induced morphologic decrease in cellular D1A dopamine receptor staining. Synapse 27:313-321.

Bagchi SP, McGeer PL (1964) Some Properties of Tyrosine Hydroxylase From the Caudate Nucleus. Life Sciences 305:1195-1200.

Balmforth AJ, Warburton P, Ball SG (1990) Homologous desensitization of the D1 dopamine receptor. J Neurochem 55:2111-2116.

Barnett JV, Kuczenski R (1986) Desensitization of rat striatal dopamine-stimulated adenylate cyclase after acute amphetamine administration. J Pharmacol Exp Ther 237:820-825.

Barnett JV, Segal DS, Kuczenski R (1987) Repeated amphetamine pretreatment alters the responsiveness of striatal dopamine-stimulated adenylate cyclase to amphetamine-induced desensitization. J Pharmacol Exp Ther 242:40-47.

Barton AC, Sibley DR (1990) Agonist-induced desensitization of D1-dopamine receptors linked to adenylyl cyclase activity in cultured NS20Y neuroblastoma cells. Mol Pharmacol 38:531-541.

Bates MD, Olsen CL, Becker BN, Albers FJ, Middleton JP, Mulheron JG, Jin SL, Conti M, Raymond JR (1993) Elevation of cAMP is required for down-regulation, but not agonist-induced desensitization, of endogenous dopamine D1 receptors in opossum kidney cells. Studies in cells that stably express a rat cAMP phosphodiesterase (rPDE3) cDNA. J Biol Chem 268:14757-14763.

Berke JD, Hyman SE (2000) Addiction, dopamine, and the molecular mechanisms of memory. Neuron 25:515-532.

Bermak JC, Li M, Bullock C, Weingarten P, Zhou QY (2002) Interaction of gamma-COP with a transport motif in the D1 receptor C-terminus. Eur J Cell Biol 81:77-85.

Black LE, Smyk-Randall EM, Sibley DR (1994) Cyclic AMP-mediated desensitization of D1 dopamine receptor-coupled adenylyl cyclase in NS20Y neuroblastoma cells. Mol Cell Neurosci 5:567-575.

Bockaert J, Pin JP (1999) Molecular tinkering of G protein-coupled receptors: an evolutionary success. EMBO J 18:1723-1729.

Boehm SL, 2nd, Piercy MM, Bergstrom HC, Phillips TJ (2002) Ventral tegmental area region governs GABA(B) receptor modulation of ethanol-stimulated activity in mice. Neurosci 115:185-200.

Bouvier M (2001) Oligomerization of G-protein-coupled transmitter receptors. Nat Rev Neurosci 2:274-286.

Boyson SJ, McGonigle P, Molinoff PB (1986) Quantitative autoradiographic localization of the D1 and D2 subtypes of dopamine receptors in rat brain. J Neurosci 6:3177-3188.

Bredenbeek PJ, Frolov I, Rice CM, Schlesinger S (1993) Sindbis virus expression vectors: packaging of RNA replicons by using defective helper RNAs. J Virol 67:6439–6446.

Brodie MS, Pesold C, Appel S (1999) Ethanol directly excites dopaminergic ventral tegmental area reward neurons. Alcohol Clin Exp Res 23:1848-1852.

Bunzow JR, Van Tol HH, Grandy DK, Albert P, Salon J, Christie M, Machida CA, Neve K, Civelli O (1988) Cloning and expression of a rat D2 dopamine receptor cDNA. Nature 336:783-787.

Caille I, Dumartin B, Bloch B (1996) Ultrastructural localization of D1 dopamine receptor immunoreactivity in rat striatonigral neurons and its relation with dopaminergic innervation. Brain Res 730:17-31.

Carpenter-Hyland EP, Woodward JJ, Chandler LJ (2004) Chronic ethanol induces synaptic but not extrasynaptic targeting of NMDA receptors. J Neurosci 24:7859-7868.

Carr DB, O'Donnell P, Card JP, Sesack SR (1999) Dopamine terminals in the rat prefrontal cortex synapse on pyramidal cells that project to the nucleus accumbens. J Neurosci 19:11049-11060.

Casaccia-Bonnefil P, Benedikz E, Shen H, Stelzer A, Edelstein D, Geschwind M, Brownlee M, Federoff HJ, Bergold PJ (1993) Localized gene transfer into organotypic hippocampal slice cultures and acute hippocampal slices. J Neurosci Methods 50:341-351.

Celentano JJ, Gibbs TT, Farb DH (1988) Ethanol potentiates GABA- and glycine-induced chloride currents in chick spinal cord neurons. Brain Res 455:377-380.

Chandler LJ, Harris RA, Crews FT (1998) Ethanol tolerance and synaptic plasticity. Trends Pharmacol Sci 19:491-495.

Chao SZ, Ariano MA, Peterson DA, Wolf ME (2002) D1 dopamine receptor stimulation increases GluR1 surface expression in nucleus accumbens neurons. J Neurochem 83:704-712.

Chen J, Wersinger C, Sidhu A (2003) Chronic stimulation of D1 dopamine receptors in human SK-N-MC neuroblastoma cells induces nitric-oxide synthase activation and cytotoxicity. J Biol Chem 278:28089-28100.

Chneiweiss H, Glowinski J, Premont J (1990) Dopamine-induced homologous and heterologous desensitizations of adenylate cyclase-coupled receptors on striatal neurons. Eur J Pharmacol 189:287-292.

Clemmesen L, Jorgensen OS, Hemmingsen R, Barry DI, Bolwig TG (1987) Brain marker protein changes after short- and long-term ethanol intoxication and withdrawal in the rat. J Psychiatr Res 21:171-183.

Cools AR, Van Rossum JM (1976) Excitation-mediating and inhibition-mediating dopamine-receptors: a new concept towards a better understanding of electrophysiological, biochemical, pharmacological, functional and clinical data. Psychopharmacologia 45:243-254.

Cormack BP, Valdivia RH, Falkow S (1996) FACS-optimized mutants of the green fluorescent protein (GFP). Gene 173:33-38.

Creese I, Chen A (1985) Selective D-1 dopamine receptor increase following chronic treatment with SCH 23390. Eur J Pharmacol 109:127-128.

Dal Toso R, Sommer B, Ewert M, Herb A, Pritchett DB, Bach A, Shivers BD, Seeburg PH (1989) The dopamine D2 receptor: two molecular forms generated by alternative splicing. EMBO J 8:4025-4034.

D'Apuzzo M, Mandolesi G, Reis G, Schuman EM (2001) Abundant GFP expression and LTP in hippocampal acute slices by in vivo injection of sindbis virus. J Neurophysiol 86:1037-1042.

Davies M (2003) The role of GABAA receptors in mediating the effects of alcohol in the central nervous system. J Psychiatry Neurosci 28:263-274.

De I, Fata-Hartley C, Sawicki SG, Sawicki DL (2003) Functional analysis of nsP3 phosphoprotein mutants of Sindbis virus. J Virol 77:13106-13116.

De Montis MG, Gambarana C, Gessa GL, Meloni D, Tagliamonte A, Stefanini E (1993) Reduced [3H]SCH 23390 binding and DA-sensitive adenylyl cyclase in the limbic system of ethanol-preferring rats. Alcohol Alcohol 28:397-400.

Dearry A, Gingrich JA, Falardeau P, Fremeau RT, Jr. , Bates MD, Caron M (1990) Molecular cloning and expression of the gene for a human D1 dopamine receptor. Nature 347:72-76.

Denk W, Svoboda K (1997) Photon upmanship: why multiphoton imaging is more than a gimmick. Neuron 18:351-357.

Denk W, Strickler JH, Webb WW (1990) Two-photon laser scanning fluorescence microscopy. Science 248:73-76.

Denk W, Delaney, KR., Gelperin, A., Kleinfeld, D., Strowbridge, BW., Tank, DW., Yuste, R. (1994) Anatomical and functional imaging of neurons using 2-photon laser scanning microscopy. J Neurosci Methods 54:151-162.

Diaz LM, Maiya R, Sullivan MA, Han Y, Walton HA, Boehm SL, 2nd , Bergeson SE, Mayfield RD, Morrisett RA (2004) Sindbis viral-mediated expression of eGFP-dopamine D1 receptors in situ with real-time two-photon microscopic detection. J Neurosci Methods 139:25-31.

Dildy JE, Leslie SW (1989) Ethanol inhibits NMDA-induced increases in free intracellular Ca2+ in dissociated brain cells. Brain Res 488:383-387.

Ding MX, Schlesinger MJ (1989) Evidence that Sindbis virus NSP2 is an autoprotease which processes the virus nonstructural polyprotein. Virology 171:280-284.

Djouma E, Lawrence AJ (2002) The effect of chronic ethanol consumption and withdrawal on mu-opioid and dopamine D(1) and D(2) receptor density in Fawn-Hooded rat brain. J Pharmacol Exp Ther 302:551-559.

Dubuisson J, Rice CM (1993) Sindbis virus attachment: isolation and characterization of mutants with impaired binding to vertebrate cells. J Virol 67:3363-3374.

Dumartin B, Caille I, Gonon F, Bloch B (1998) Internalization of D1 dopamine receptor in striatal neurons in vivo as evidence of activation by dopamine agonists. J Neurosci 18:1650-1661.

Dyr W, McBride WJ, Lumeng L, Li TK, Murphy JM (1993) Effects of D1 and D2 dopamine receptor agents on ethanol consumption in the high-alcohol-drinking (HAD) line of rats. Alcohol 10:207-212.

Eggeling C, Widengren J, Rigler R, C. S (1998) Photobleaching of fluorescent dyes under conditions used for single-molecule detection: evidence of two-step photolysis. Annal Chem 70:2651-2659.

Ehrengruber MU (2002) Alphaviral gene transfer in neurobiology. Brain Research Bulletin 59:13-22.

Ehrengruber MU, Lundstrom K, Schweitzer C, Heuss C, Schlesinger S, Gahwiler BH (1999) Recombinant Semliki Forest virus and Sindbis virus efficiently infect neurons in hippocampal slice cultures. Proc Natl Acad Sci U S A 96:7041-7046.

Ehrmann RL, Gey GO (1956) The Growth of Cells on a Transparent Gel of Reconstituted Rat-Tail Collagen. J Natl Cancer Inst 16:1375-1585.

El-Ghundi M, George SR, Drago J, Fletcher PJ, Fan T, Nguyen T, Liu C, Sibley DR, Westphal H, O'Dowd BF (1998) Disruption of dopamine D1 receptor gene expression attenuates alcohol-seeking behavior. Eur J Pharmacol 353:149-158.

Feldman RS, Meyer JS, Quenzer LF (1997) Priciples of Neuropsychpharmacology. Sunderland:Sinauer Associates.

Fiorentini C, Gardoni F, Spano P, Di Luca M, Missale C (2003) Regulation of dopamine D1 receptor trafficking and desensitization by oligomerization with glutamate NMDA receptors. J Biol Chem 278:20196-20202.

Gahwiler BH (1981) Organotypic monolayer cultures of nervous tissue. Journal of Neuroscience Methods 4:329-342.

Gardner B, Liu ZF, Jiang D, Sibley DR (2001) The role of phosphorylation/dephosphorylation in agonist-induced desensitization of D1 dopamine receptor function: evidence for a novel pathway for receptor dephosphorylation. Mol Pharmacol 59:310-321.

Gatto GJ, McBride WJ, Murphy JM, Lumeng L, Li TK (1994) Ethanol self-infusion into the ventral tegmental area by alcohol-preferring rats. Alcohol 11:57-64.

George SR, Lee SP, Varghese G, Zeman PR, Seeman P, Ng GY, O'Dowd BF (1998) A transmembrane domain-derived peptide inhibits D1 dopamine receptor function without affecting receptor oligomerization. J Biol Chem 273:30244-30248.

Gili-Martin E, Fernandez-Briera A, Calvo P (1997) Effects of chronic ethanol treatment and ethanol withdrawal on [3H]SCH23390 binding to rat striatal membranes. Neuropharmacology 36:101-106.

Gil-Martin E, Fernandez-Briera A, Fernandez-Lopez A, Calvo P (1994) Effect of chronic treatment with ethanol and withdrawal of ethanol on binding of [3H]SCH23390 to D1 dopamine receptor in rat visual cortex and hippocampus. An autoradiographic study. Neuropharmacology 33:1203-1209.

Gines S, Hillion J, Torvinen M, Le Crom S, Casado V, Canela E, Rondin S, Lew JY, Watson S, Zoli M, Agnati LF, Verniera P, Lluis C, Ferre S, Fuxe K, Franco R (2000) Dopamine D1 and adenosine A1 receptors form functionally interacting heteromeric complexes. Proc Natl Acad Sci U S A 97:8606-8611.

Gnegy ME, Uzunov P, Costa E (1976) Regulation of dopamine stimulation of striatal adenylate cyclase by an endogenous Ca++ -binding protein. Proc Natl Acad Sci U S A 73:3887-3890.

Gonzales RA, Job MO, Doyon WM (2004) The role of mesolimbic dopamine in the development and maintenance of ethanol reinforcement. Pharmacol Ther 103:121-146.

Gordon AS, Collier K, Diamond I (1986) Ethanol regulation of adenosine receptor-stimulated cAMP levels in a clonal neural cell line: an in vitro model of cellular tolerance to ethanol. Proc Natl Acad Sci U S A 83:2105-2108.

Grandy DK, Zhou QY, Allen L, Litt R, Magenis RE, Civelli O, Litt M (1990) A human D1 dopamine receptor gene is located on chromosome 5 at q35.1 and identifies an EcoRI RFLP. Am J Hum Genet 47:828-834.

Grandy DK, Litt M, Allen L, Bunzow JR, Marchionni M, Makam H, Reed L, Magenis RE, Civelli O (1989a) The human dopamine D2 receptor gene is located on chromosome 11 at q22-q23 and identifies a TaqI RFLP. Am J Hum Genet 45:778-785.

Grandy DK, Marchionni MA, Makam H, Stofko RE, Alfano M, Frothingham L, Fischer J, Burke-Howie KJ, Bunzow JR, Server AC (1989b) Cloning of the cDNA and gene for a human D2 dopamine receptor. Proc Natl Acad Sci U S A 86:9762-9766.

Groenewegen HJ, Wright CI, Beijer AV, Voorn P (1999) Convergence and segregation of ventral striatal inputs and outputs. Ann NY Acad Sci 877:49-63.

Gupta SK, Mishra RK (1993) Desensitization of D1 dopamine receptors down-regulates the Gs alpha subunit of G protein in SK-N-MC neuroblastoma cells. J Mol Neurosci 4:117-123.

Gwag BJ, Kim EY, Ryu BR, Won SJ, Ko HW, Oh YJ, Cho YG, Ha SJ, Sung YC (1998) A neuron-specific gene transfer by a recombinant defective Sindbis virus. Brain Res Mol Brain Res 63:53-61.

Haberstock-Debic H, Wein M, Barrot M, Colago EE, Rahman Z, Neve RL, Pickel VM, Nestler E, von Zastrow M, Svingos AL (2003) Morphine acutely regulates opioid receptor trafficking selectively in dendrites of nucleus accumbens neurons. J Neurosci 23:4324-4332.

Hallak H, Rubin R (2004) Ethanol inhibits palmitoylation of G protein G alpha(s). J Neurochem 89:919-927.

Hamdi A, Prasad C (1993) Bidirectional changes in striatal D1-dopamine receptor density during chronic ethanol intake. Life Sciences 52:251-257.

Heimer L, Zahm DS, Churchill L, Kalivas PW, Wohltmann C (1991) Specificity in the projection patterns of accumbal core and shell in the rat. Neurosci 41:89-125.

Hendricson AW, Thomas MP, Lippmann MJ, Morrisett RA (2003) Suppression of L-type voltage-gated calcium channel-dependent synaptic plasticity by ethanol: analysis of miniature synaptic currents and dendritic calcium transients. J Pharmacol Exp Ther 307:550-558.

Hersch SM, Ciliax BJ, Gutekunst CA, Rees HD, Heilman CJ, Yung KK, Bolam JP, Ince E, Yi H, Levey AI (1995) Electron microscopic analysis of D1 and D2 dopamine receptor proteins in the dorsal striatum and their synaptic relationships with motor corticostriatal afferents. J Neurosci 15:5222-5237.

Hess EJ, Albers LJ, Le H, Creese I (1986) Effects of chronic SCH23390 treatment on the biochemical and behavioral properties of D1 and D2 dopamine receptors: potentiated behavioral responses to a D2 dopamine agonist after selective D1 dopamine receptor upregulation. J Pharmacol Exp Ther 238:846-854.

Hietala J, Salonen I, Lappalainen J, Syvalahti E (1990) Ethanol administration does not alter dopamine D1 and D2 receptor characteristics in rat brain. Neurosci Lett 108:289-294.

Hitz CBE, J. J.; Hecht, J. (2001) Introduction to Laser Technology. New York John Wiley & Sons, Inc (US), 3rd edition.

Hodge CW, Samson HH, Chappelle AM (1997) Alcohol self-administration: further examination of the role of dopamine receptors in the nucleus accumbens. Alcohol Clin Exp Res 21:1083-1091.

Hoffman PL, Rabe CS, Moses F, Tabakoff B (1989) N-methyl-D-aspartate receptors and ethanol : inhibition of calcium flux and cyclic GMP production. J Neurochem 52:1937-1940.

Hruska RE (1988) Effect of ethanol administration of striatal D1 and D2 dopamine receptors. J Neurochem 50:1929-1933.

Huang X, Lawler CP, Lewis MM, Nichols DE, Mailman RB (2001) D1 Dopamine Receptors. International Review of Neurobiology 48:65-139.

Hynie S, Lanefelt F, Fredholm BB (1980) Effects of ethanol on human lymphocyte levels of cyclic AMP. In vitro: Potentiation of the response to isoproterenol, prostaglandin E2 or adenosine stimulation. Acta Pharmacol Toxicol 47:58-65.

Ikemoto S, Kohl RR, McBride WJ (1997) GABA(A) receptor blockade in the anterior ventral tegmental area increases extracellular levels of dopamine in the nucleus accumbens of rats. J Neurochem 69:137-143.

Imperato A, Di Chiara G (1986) Preferential stimulation of dopamine release in the nucleus accumbens of freely moving rats by ethanol. J Pharmacol Exp Ther 239:219-228.

Jackson A, Iwasiow RM, Chaar ZY, Nantel MF, Tiberi M (2002) Homologous regulation of the heptahelical D1A receptor responsiveness: specific cytoplasmic tail regions mediate dopamine-induced phosphorylation, desensitization and endocytosis. J Neurochem 82:683-697.

Jeromin A, Yuan LL, Frick A, Pfaffinger P, Johnston D (2003) A modified Sindbis vector for prolonged gene expression in neurons. J Neurophysiol 90:2741-2745.

Jiang D, Sibley DR (1999) Regulation of D(1) dopamine receptors with mutations of protein kinase phosphorylation sites: attenuation of the rate of agonist-induced desensitization. Mol Pharmacol 56:675-683.

Kaiser W, Garrett CGB (1961) Two-photon excitation in CaF2:Eu2+. Phys Rev Lett 7:229-231.

Kallal L, Benovic JL (2000) Using green fluorescent proteins to study G-protein-coupled receptor localization and trafficking. Trends Pharmacol Sci 21:175-180.

Kebabian JW, Calne DB (1979) Multiple Receptors for Dopamine. Nature 277:93-96.

Kim DS, Froelick GJ, Palmiter RD (2002a) Dopamine-dependent desensitization of dopaminergic signaling in the developing mouse striatum. J Neurosci 22:9841-9849.

Kim J, Dittgen T, Nimmerjahn A, Waters J, Pawlak V, Helmchen F, Schlesinger S, Seeburg PH, Osten P (2004a) Sindbis vector SINrep(nsP2S726): a tool for rapid heterologous expression with attenuated cytotoxicity in neurons. J Neurosci Methods 133:81-90.

Kim O, Gardner, BR., Williams, DB., Marinec, PS., Cabrera, DM., Peters, JD., Mak, CC., Kim, KM., Sibley, DR. (2004b) The role of phosphorylation in D1 dopamine receptor desensitization: evidence for a novel mechanism of arrestin association. J Biol Chem 279:7999-8010.

Kim OJ, Ariano MA, Lazzarini RA, Levine MS, Sibley DR (2002b) Neurofilament-M interacts with the D1 dopamine receptor to regulate cell surface expression and desensitization. J Neurosci 22:5920-5930.

Koester HJ, Baur D, Uhl R, Hell SW (1999) Ca2+ fluorescence imaging with pico- and femtosecond two-photon excitation: signal and photodamage. Biophys J 77:2226-2236.

Konig K, Becker TW, Fischer P, Riemann I, Halbhuber K-J (1999) Pulse-length dependenceof cellular response to intense near-infraredlaser pulses in multiphoton microscopes. Opt Lett 24:113-115.

Koob GF, Le Moal M (2001) Drug addiction, dysregulation of reward, and allostasis. Neuropsychopharmacology 24:97-129.

Koob GF, Sanna PP, Bloom FE (1998) Neuroscience of addiction. Neuron 21:467-476.

Kumar S, Kralic JE, O'Buckley TK, Grobin AC, Morrow AL (2003) Chronic ethanol consumption enhances internalization of alpha1 subunit-containing GABAA receptors in cerebral cortex. J Neurochem 86:700-708.

Kwong E, Gu Q (2000) Activity-dependent and use-dependent regulation of dopamine-receptor clustering. NeuroReport 11:2703-2706.

Lamey M, Thompson M, Varghese G, Chi H, Sawzdargo M, George SR, O'Dowd BF (2002) Distinct residues in the carboxyl tail mediate agonist-induced desensitization and internalization of the human dopamine D1 receptor. J Biol Chem 277:9415-9421.

Lappalainen J, Hietala J, Koulu M, Seppala T, Sjoholm B, Syvalahti E (1990) Chronic treatment with SCH 23390 and haloperidol: effects on dopaminergic and serotonergic mechanisms in rat brain. J Pharmacol Exp Ther 252:845-852.

Le Gal La Salle G, Robert JJ, Berrard S, Ridoux V, Stratford-Perricaudet LD, Perricaudet M, Mallet J (1993) An adenovirus vector for gene transfer into neurons and glia in the brain. Science 259:988-990.

Lemm JA, Rumenapf T, Strauss EG, Strauss JH, Rice CM (1994) Polypeptide requirements for assembly of functional Sindbis virus replication complexes: a model for the temporal regulation of minus- and plus-strand RNA synthesis. EMBO J 13:2925-2934.

Lescar J, Roussel A, Wien MW, Navaza J, Fuller SD, Wengler G, Wengler G, Rey FA (2001) The Fusion glycoprotein shell of Semliki Forest virus: an icosahedral assembly primed for fusogenic activation at endosomal pH. Cell 105:137-148.

Levey AI, Hersch SM, Rye DB, Sunahara RK, Niznik HB, Kitt CA, Price DL, Maggio R, Brann MR, Ciliax BJ (1993) Localization of D1 and D2 dopamine receptors in brain with subtype-specific antibodies. Proc Natl Acad Sci U S A 90:8861-8865.

Lewis MM, Watts VJ, Lawler CP, Nichols DE, Mailman RB (1998) Homologous desensitization of the D1A dopamine receptor: efficacy in causing desensitization dissociates from both receptor occupancy and functional potency. J Pharmacol Exp Ther 286:345-363.

Lezcano N, Bergson C (2002) D1/D5 dopamine receptors stimulate intracellular calcium release in primary cultures of neocortical and hippocampal neurons. J Neurophysiol 87:2167-2175.

Li ML, Stollar V (2004) Identification of the amino acid sequence in Sindbis virus nsP4 that binds to the promoter for the synthesis of the subgenomic RNA. Proc Natl Acad Sci U S A 101:9429-9434.

Lidow MS, Goldman-Rakic PS, Gallager DW, Rakic P (1991) Distribution of dopaminergic receptors in the primate cerebral cortex: quantitative autoradiographic analysis using [3H]raclopride, [3H]spiperone and [3H]SCH23390. Neurosci 40:657-671.

Liljestrom P, Garoff H (1991) A new generation of animal cell expression vectors based on the Semliki Forest virus replicon. Biotechnology (N Y) 9:1356-1361.

Lin CW, Bianchi BR, Miller TR, Stashko MA, Wang SS, Curzon P, Bednarz L, Asin KE, Britton DR (1996) Persistent activation of the dopamine D1 receptor contributes to prolonged receptor desensitization: studies with A-77636. J Pharmacol Exp Ther 276:1022-1029.

Lovinger DM, White G, Weight FF (1989) Ethanol inhibits NMDA-activated ion current in hippocampal neurons. Science 243:1721-1724.

Lucchi L, Covelli V, Anthopoulou H, Spano PF, Trabucchi M (1983) Effect of chronic ethanol treatment on adenylate cyclase activity in rat striatum. Neurosci Lett 40:187-192.

Maiman TH (1960) Stimulated optical radiation in ruby. Nature 187:493-494.

Mainen ZF, Maletic-Savatic M, Shi SH, Hayashi Y, Malinow R, Svoboda K (1999) Two-photon imaging in living brain slices. Methods 18:231-239.

Majewska A, Yiu G, Yuste R (2000) A custom-made two-photon microscope and deconvolution system. Pflugers Arch 441:398-408.

Maldve RE, Zhang TA, Ferrani-Kile K, Schreiber SS, Lippmann MJ, Snyder GL, Fienberg AA, Leslie SW, Gonzales RA, Morrisett RA (2002) DARPP-32 and regulation of the ethanol sensitivity of NMDA receptors in the nucleus accumbens. Nat Neurosci 5:641-648.

Mansour A, Meador-Woodruff JH, Zhou Q, Civelli O, Akil H, Watson SJ (1992) A comparison of D1 receptor binding and mRNA in rat brain using receptor autoradiographic and in situ hybridization techniques. Neurosci 46:959-971.

Marsh M, Helenius A (1989) Virus entry into animal cells. Adv Virus Research 36:107-151.

Martin-Negrier M, Charron G, Bloch B (2000) Agonist stimulation provokes dendritic and axonal dopamine D(1) receptor redistribution in primary cultures of striatal neurons. Neuroscience 99:257-266.

Mason JN, Kozell LB, Neve KA (2002) Regulation of dopamine D(1) receptor trafficking by protein kinase A-dependent phosphorylation. Mol Pharmacol 61:806-816.

Masters BR, So PT (2004) Antecedents of two-photon excitation laser scanning microscopy. Microsc Res Tech 63:3-11.

Memo M, Lovenberg W, Hanbauer I (1982) Agonist-induced subsensitivity of adenylate cyclase coupled with a dopamine receptor in slices from rat corpus striatum. Proc Natl Acad Sci U S A 79:4456-4460.

Memo M, Hanbauer, I. (1984) Phosphorylation of membrane proteins in response to persistent stimulation of adenylate cyclase-linked dopamine receptors in slices of striatum. Neuropharmacology 23:449-455.

Meredith GE (1999) The synaptic framework for chemical signaling in nucleus accumbens. Ann NY Acad Sci 877:140-156.

Mi S, Durbin R, Huang HV, Rice CM, Stollar V (1989) Association of the Sindbis virus RNA methyltransferase activity with the nonstructural protein nsP1. Virology 170:385-391.

Mihic SJ (1999) Acute effects of ethanol on GABA(A) and glycine receptor function. Neurochem Int 35:115-123.

Monsma FJ, Jr., Mahan LC, McVittie LD, Gerfen CR, Sibley DR (1990) Molecular cloning and expression of a D1 dopamine receptor linked to adenylyl cyclase activation. Proc Natl Acad Sci U S A 87:6723-6727.

Moore MS, DeZazzo J, Luk AY, Tully T, Singh CM, Heberlein U (1998) Ethanol intoxication in Drosophila: Genetic and pharmacological evidence for regulation by the cAMP signaling pathway. Cell 93:997-1007.

Muriel MP, Orieux G, Hirsch EC (2002) Levodopa but not ropinirole induces an internalization of D1 dopamine receptors in parkinsonian rats. Mov Disord 17:1174-1179.

Nakamura O (1999) Fundamental of two-photon microscopy. Microsc Res Tech 47:165-171.

Neumaier JF, Vincow ES, Arvanitogiannis A, Wise RA, Carlezon WA, Jr. (2002) Elevated expression of 5-HT1B receptors in nucleus accumbens efferents sensitizes animals to cocaine. J Neurosci 22:10856-10863.

Neve KA, Neve RL (1997) The Dopamine Receptors. Humana Press.

Ng GY, George SR (1994) Dopamine receptor agonist reduces ethanol self-administration in the ethanol-preferring C57BL/6J inbred mouse. Eur J Pharmacol 269:365-374.

Ng GY, Trogadis J, Stevens J, Bouvier M, O'Dowd BF, George SR (1995) Agonist-induced desensitization of dopamine D1 receptor-stimulated adenylyl cyclase activity is temporally and biochemically separated from D1 receptor internalization. Proc Natl Acad Sci U S A 92:10157-10161.

Ng GY, Mouillac B, George SR, Caron M, Dennis M, Bouvier M, O'Dowd BF (1994) Desensitization, phosphorylation and palmitoylation of the human dopamine D1 receptor. Eur J Pharmacol Mar 15;267:7-19.

Oades RD, Halliday GM (1987) Ventral tegmental (A10) system: neurobiology. 1. Anatomy and connectivity. Brain Res 434:117-165.

O'Donnell P, Greene J, Pabello N, Lewis B, Grace AA (1999) Modulation of cell firing in the nucleus accumbens. Ann NY Acad Sci 877:157-175.

Ofori S, Bugnon O, Schorderet M (1993) Agonist-induced desensitization of dopamine D-1 receptors in bovine retina and rat striatum. J Pharmacol Exp Ther 266:350-357.

Pellegrino SM, Druse MJ (1992) The effects of chronic ethanol consumption on the mesolimbic and nigrostriatal dopamine systems. Alcohol Clin Exp Res 16:275-280.

Peranen J, Rikkonen M, Liljestrom P, Kaariainen L (1990) Nuclear localization of Semliki Forest virus-specific nonstructural protein nsP2. J Virol 64:1888-1896.

Pettit DL, Koothan T, Liao D, Malinow R (1995) Vaccinia virus transfection of hippocampal slice neurons. Neuron 14:685-688.

Piomelli D, Pilon C, Giros B, Sokoloff P, Martres MP, Schwartz JC (1991) Dopamine activation of the arachidonic acid cascade as a basis for D1/D2 receptor synergism. Nature 353:164-167.

Prasher DC, Eckenrode VK, Ward WW, Prendergast FG, Cormier MJ (1992) Primary structure of the Aequorea victoria green-fluorescent protein. Gene 111:229-233.

Quadros IM, Nobrega JN, Hipolide DC, de Lucca EM, Souza-Formigoni ML (2002) Differential propensity to ethanol sensitization is not associated with altered binding to D1 receptors or dopamine transporters in mouse brain. Addict Biol 7:291-299.

Rassnick S, Pulvirenti L, Koob GF (1993) SDZ-205,152, a novel dopamine receptor agonist, reduces oral ethanol self-administration in rats. Alcohol 10:127-132.

Rikkonen M (1996) Functional significance of the nuclear-targeting and NTP-binding motifs of Semliki Forest virus nonstructural protein nsP2. Virology 218:352-361.

Roberts-Lewis JM, Roseboom PH, Iwaniec LM, Gnegy ME (1986) Differential down-regulation of D1-stimulated adenylate cyclase activity in rat forebrain after in vivo amphetamine treatments. J Neurosci 6:2245-2251.

Robinson TE, Kolb B (1997) Persistent structural modifications in nucleus accumbens and prefrontal cortex neurons produced by previous experience with amphetamine. J Neurosci 17:8291-8297.

Rodd ZA, Melendez RI, Bell RL, Kuc KA, Zhang Y, Murphy JM, McBride WJ (2004) Intracranial self-administration of ethanol within the ventral tegmental area of male Wistar rats: evidence for involvement of dopamine neurons. J Neurosci 24:1050-1057.

Rodd-Henricks ZA, McKinzie DL, Crile RS, Murphy JM, McBride WJ (2000) Regional heterogeneity for the intracranial self-administration of ethanol within the ventral tegmental area of female Wistar rats. Psychopharmacology (Berl) 149:217-224.

Roseboom PH, Gnegy ME (1989) Acute in vivo amphetamine produces a homologous desensitization of dopamine receptor-coupled adenylate cyclase activities and decreases agonist binding to the D1 site. Mol Pharmacol 35:139-147.

RSA (2004 Vancouver) Up-regulation of Dopamine D1 receptors in the Central Nucleus of the Amygdala (CeA) Reduces Alcohol Consumption in C57BL/(B6) Mice.

Samson HH, Hodge CW, Tolliver GA, Haraguchi M (1993) Effect of dopamine agonists and antagonists on ethanol-reinforced behavior: the involvement of the nucleus accumbens. Brain Res Bull 30:133-141.

Sawicki DL, Sawicki SG (1993) A second nonstructural protein functions in the regulation of alphavirus negative-strand RNA synthesis. J Virol 67:3605-3610.

Schlesinger MJ, London SD, Ryan C (1993) An in-frame insertion into the Sindbis virus 6K gene leads to defective proteolytic processing of the virus glycoproteins, a trans-dominant negative inhibition of normal virus formation, and interference in virus shut off of host-cell protein synthesis. Virology 193:424-432.

Schlesinger S, Schlesinger MJ (1972) Formation of Sindbis virus proteins: identification of a precursor for one of the envelope proteins. J Virol 10:925-932.

Schlesinger S, Schlesinger MJ (2001) Togaviridae: The viruses and their replication. In: Fields Virology, vol 1 Philadelphia: Lippincott Williams & Wilkins:895-916.

Schwartz RA, Greenwald ER, Fletcher PJ, Houle S, DaSilva JN (2003) Up-regulated dopamine D1 receptor binding can be detected in vivo following repeated SCH 23390, but not SKF 81297 or 6-hydroxydopamine, treatments. Eur J Pharmacol 459:195-201.

Selbie LA, Hayes G, Shine J (1989) The major dopamine D2 receptor: molecular analysis of the human D2A subtype. DNA 8:683-689.

Senogles SE (1994) The D2 dopamine receptor isoforms signal through distinct Gi alpha proteins to inhibit adenylyl cyclase. A study with site-directed mutant Gi alpha proteins. Journal of Biological Chemistry 269:23120-23127.

Sheppard C, Kompfner, R. (1978) Resonant scanning optical microscope. Appl Opt 17:2879-2882.

Sheppard CJR, Choudhury A (1977) Image formation in the scanning microscope. Optica Acta 24:1051-1073.

Shi SH, Hayashi Y, Petralia RS, Zaman SH, Wenthold RJ, Svoboda K, Malinow R (1999) Rapid spine delivery and redistribution of AMPA receptors after synaptic NMDA receptor activation. Science 284:1811-1816.

Shippenberg TS, Elmer GI (1998) The neurobiology of opiate reinforcement. Crit Rev Neurobiol 12:267-303.

Sibley DR, Housley MD (1994) Molecular Pharmacology of Cell Regulation. Wiley and Sons, Chichester 3.

Sidhu A (1998) Coupling of D1 and D5 dopamine receptors to multiple G proteins: Implications for understanding the diversity in receptor-G protein coupling. Mol Neurobiol 16:125-134.

Smiley JF, Levey AI, Ciliax BJ, Goldman-Rakic PS (1994) D1 dopamine receptor immunoreactivity in human and monkey cerebral cortex: predominant and extrasynaptic localization in dendritic spines. Proc Natl Acad Sci U S A 91:5720-5724.

Spence DE, Kean PN, Sibbett W (1991) 60-fsec pulse generation from a self-mode-locked Ti:sapphire laser. Optics Letters 16:42-44.

Steffey ME, Snyder GL, Barrett RW, Fink JS, Ackerman M, Adams P, Bhatt R, Gomez E, MacKenzie RG (1991) Dopamine D1 receptor stimulation of cyclic AMP accumulation in COS-1 cells. Eur J Pharmacol 207:311-317.

Stoppini L, Buchs PA, Muller D (1991) A simple method for organotypic cultures of nervous tissue. Journal of Neuroscience Methods 37:173-182.

Strauss JH, Wang KS, Schmaljohn AL, Kuhn RJ, Strauss EG (1994) Host-cell receptors for Sindbis virus. Arch Virol Suppl 9:473-484.

Strauss JH, Jr., Burge B, W. , Pfefferkorn E, R. , Darnell J, E., Jr. (1968) Identification of the membrane protein and "core" protein of Sindbis virus. Proc Natl Acad Sci U S A 59:533-537.

Sunahara RK, Niznik HB, Weiner DM, Stormann TM, Brann MR, Kennedy JL, Gelernter JE, Rozmahel R, Yang YL, Israel Y, Seeman P, O'Dowd BF (1990) Human dopamine D1 receptor encoded by an intronless gene on chromosome 5. Nature 347:80-83.

Suopanki J, Sawicki DL, Sawicki SG, Kaariainen L (1998) Regulation of alphavirus 26S mRNA transcription by replicase component nsP2. J Gen Virol 79:309-319.

Suryanarayana S, von Zastrow M, Kobilka BK (1992) Identification of intramolecular interactions in adrenergic receptors. J Biol Chem 267:21991-21994.

Swanson LW, Cwan WM (1975) A note on the connections and development of the nucleus accumbens. Brain Res 92:324-330.

Tabakoff B, Hoffman PL (1979) Development of functional dependence on ethanol in dopaminergic systems. J Pharmacol Exp Ther 208:216-222.

Tabakoff B, Nelson E, Yoshimura M, Hellevuo K, Hoffman PL (2001) Phosphorylation cascades control the actions of ethanol on cell cAMP signalling. J Biomed Sci 8:44-51.

Taylor RM, Hurbut HS, Work TH, Kingstin JR, Frothingham TE (1955) Sindbis virus: a newly recognized arthropodtransmitted virus. Am J Trop Med Hyg 4:844-862.

Thomas MP, Morrisett RA (2000) Dynamics of NMDAR-mediated neurotoxicity during chronic ethanol exposure and withdrawal. Neuropharmacology 39:218-226.

Thomas MP, Monaghan DT, Morrisett RA (1998a) Evidence for a causative role of N-methyl-D-aspartate receptors in an in vitro model of alcohol withdrawal hyperexcitability. J Pharmacol Exp Ther 287:87-97.

Thomas MP, Davis MI, Monaghan DT, Morrisett RA (1998b) Organotypic brain slice cultures for functional analysis of alcohol-related disorders: novel versus conventional preparations. Alcoholism: Clinical & Experimental Research 22:51-59.

Thompson WJ (2001) Seeing is believing: GFP transgenics illuminate synapse elimination. Neuron 31:341-342.

Tiberi M, Nash SR, Bertrand L, Lefkowitz RJ, Caron MG (1996) Differential regulation of dopamine D1A receptor responsiveness by various G protein-coupled receptor kinases. J Biol Chem 271:3771-3778.

Todd RD, Khurana TS, Sajovic P, Stone KR, O'Malley KL (1989) Cloning of ligand-specific cell lines via gene transfer: identification of a D2 dopamine receptor subtype. Proc Natl Acad Sci U S A 86:10134-10138.

Trogadis JE, Ng GY, O'Dowd BF, George SR, Stevens JK (1995) Dopamine D1 receptor distribution in Sf9 cells imaged by confocal microscopy: a quantitative evaluation. J Histochem Cytochem 43:497-506.

Tsai SJ, Hong CJ (2003) Dopamine receptor hetero-oligomerization: a hypothesis for behavioral sensitization to psychostimulants. Med Hypotheses 61:18-20.

Ungerstedt U (1971) Stereotaxic mapping of the monoamine pathways in the rat brain. Acta Physiol Scand Suppl 367:1-48.

Usuda I, Tanaka K, Chiba T (1998) Efferent projections of the nucleus accumbens in the rat with special reference to subdivision of the nucleus: biotinylated dextran amine study. Brain Res 797:73-93.

Van Bockstaele EJ, Pickel VM (1995) GABA-containing neurons in the ventral tegmental area project to the nucleus accumbens in rat brain. Brain Res 682:215-221.

Vasconcelos SM, Macedo DS, Lima LO, Sousa FC, Fonteles MM, Viana GS (2003) Effect of one-week ethanol treatment on monoamine levels and dopaminergic receptors in rat striatum. Braz J Med Biol Res 36:503-509.

Ventura AL, Sibley DR (2000) Altered regulation of the D(1) dopamine receptor in mutant Chinese hamster ovary cells deficient in cyclic AMP-dependent protein kinase activity. J Pharmacol Exp Ther 293:426-434.

Vincent SL, Khan Y, Benes FM (1993) Cellular distribution of dopamine D1 and D2 receptors in rat medial prefrontal cortex. J Neurosci 13:2551-2564.

Walaas I, Fonnum F (1980) Biochemical evidence for gamma-aminobutyrate containing fibers from the nucleus accumbens to the substantia nigra and ventral tegmental area in the rat. Neurosci 5:63-72.

Wand G, Levine M, Zweifel L, Schwindinger W, Abel T (2001) The cAMP-protein kinase A signal transduction pathway modulates ethanol consumption and sedative effects of ethanol. J Neurosci 21:5297-5303.

Wang X, Wang G, Lemos JR, Treistman SN (1994) Ethanol directly modulates gating of a dihydropyridine-sensitive Ca(2+) channel in neurohypophysial terminals. J Neurosci 14:5453-5460.

Wang YF, Sawicki SG, Sawicki DL (1991) Sindbis virus nsP1 functions in negative-strand RNA synthesis. J Virol 65:985-988.

Weiss B, Geigenmuller-Gnirke U, Schlesinger S (1994) Interactions between Sindbis virus RNAs and a 68 amino acid derivative of the viral capsid protein further defines the capsid binding site. Nucleic Acids Res 22:780-786.

Weiss F, Lorang MT, Bloom FE, Koob GF (1993) Oral alcohol self-administration stimulates dopamine release in the rat nucleus accumbens: genetic and motivational determinants. J Pharmacol Exp Ther 267:250-258.

Whistler JL, Chuang HH, Chu P, Jan LY, von Zastrow M (1999) Functional dissociation of mu opioid receptor signaling and endocytosis: implications for the biology of opiate tolerance and addiction. Neuron 23:737-746.

Widmer H, Lemos JR, Treistman SN (1998) Ethanol reduces the duration of single evoked spikes by a selective inhibition of voltage-gated calcium currents in acutely dissociated supraopticneurons of the rat. J Neuroendocrinol 10:399-406.

Wise R (1996) Neurobiology of addiction. Curr Opin Neurobiol 6:243-251.

Wise RA (1984) Neural mechanisms of the reinforcing action of cocaine. NIDA Rec Mongr 50.

Wollemann M (1980) Receptors acting through adenylate cyclase in the CNS. Acta Physiol Acad Sci Hung 55:299-304.

Wong AC, Shetreat ME, Clarke JO, Rayport S (1999) D1- and D2-like dopamine receptors are co-localized on the presynaptic varicosities of striatal and nucleus accumbens neurons in vitro. Neurosci 89:221-233.

Woods JM, Ricken JD, Druse MJ (1995) Effects of chronic alcohol consumption and aging on dopamine D1 receptors in Fischer 344 rats. Alcohol Clin Exp Res 19:1331-1337.

World Health Organization (1967) Arboviruses and human disease. WHO technical Report Series 369.

World Health Organization (1975) International Statistical Classification of Diseases and Related Problems. 9th ed Geneva, World Health Organization.

Xiao X, Li J, McCown TJ, Samulski RJ (1997) Gene transfer by adeno-associated virus vectors into the central nervous system. Exp Neurol 144:113-124.

Xiong C, Levis R, Shen P, Schlesinger S, Rice CM, Huang HV (1989) Sindbis virus: an efficient, broad host range vector for gene expression in animal cells. Science 243:1188-1191.

Yang F, Moss LG, Phillips GN, Jr. (1996) The molecular structure of green fluorescent protein. Nat Biotechnol 14:1246-1251.

Yim HJ, Schallert T, Randall PK, Bungay PM, Gonzales RA (1997) Effect of ethanol on extracellular dopamine in rat striatum by direct perfusion with microdialysis. J Neurochem 68:1527-1533.

Yu S, Lefkowitz R, Haudor W (1993) beta-Adrenergic Receptor Sequestaration. The Journal of Bioloical Chemisrty 268:337-341.

Yung KK, Bolam JP, Smith AD, Hersch SM, Ciliax BJ, Levey AI (1995) Immunocytochemical localization of D1 and D2 dopamine receptors in the basal ganglia of the rat: light and electron microscopy. Neurosci 65:709-730.

Zaborszky L, Alheid GF, Beinfeld MC, Eiden LE, Heimer L, Palkovits M (1985) Cholecystokinin innervation of the ventral striatum: a morphological and radioimmunological study. Neurosci 14:427-453.

Zhang G, Gurtu V, Kain SR (1996a) An enhanced green fluorescent protein allows sensitive detection of gene transfer in mammalian cells. Biochem Biopys Res Commun 227:707-711.

Zhang J, Ferguson SS, Barak LS, Menard L, Caron MG (1996b) Dynamin and beta-arrestin reveal distinct mechanisms for G protein-coupled receptor internalization. J Biol Chem 271:18302-18305.

Zhou QY, Grandy DK, Thambi L, Kushner JA, Van Tol HH, Cone R, Pribnow D, Salon J, Bunzow JR, Civelli O (1990) Cloning and expression of human and rat D1 dopamine receptors. Nature 347:76-80.

Zhou X, Feussner, GK., and Fishman, PH. (1993) beta 1-Adrenergic and D1 Dopaminergic Receptors in Human Neurotumor Cells: Differences in Spare Receptors and Desensitization of Adenylyl Cyclase. Mol Cell Neurosci 4:74-82.

Zhou XM, Fishman PH (1991) Desensitization of the human beta 1-adrenergic receptor. Involvement of the cyclic AMP-dependent but not a receptor-specific protein kinase. J Biol Chem 266:7462-7468.

Zhou XM, Sidhu A, Fishman PH (1991) Desensitization of the Human D1 Dopamine Receptor:Evidence for Involvement of Both Cylic AMP-Dependent and Receptor-Specific Protein Kinases. Molecular and Cellular Neurosciences 2:464-472.

Vita

Laurea Marie Diaz was born in Las Cruces, NM on March 14, 1977 the daughter of Linda Diaz and John Diaz. After completing her education at Mayfield High School, in Las Cruces, NM in 1995, she entered Worcester Polytechnic Institute, Worcester, MA. There she received her degree of Bachelor of Sciences in Chemical Engineering with a concentration in Biochemistry in February 1999. She received an NIH fellowship that supported research at the University Of Massachusetts Medical School, Worcester, MA the summer of 1998. In 1999 she entered the graduate program at the University of Texas at Austin.

Permanent address: 525 Linda Vista, Las Cruces, NM 88005

This dissertation was typed by the author, Laurea Diaz.